



*The University of Sheffield*

---

# Advanced Electric Vehicle Car Park Control to Enable Grid Support

---

*A thesis submitted in partial fulfilment of the requirements for the degree of  
Doctor of Philosophy*

YingchengWANG

November 2021





*The University of Sheffield*

Faculty of Engineering

Department of Electronic & Electrical Engineering

---

# Advanced Electric Vehicle Car Park Control to Enable Grid Support

---

*A thesis submitted in partial fulfilment of the requirements for the degree of  
Doctor of Philosophy*

Yingcheng WANG

November 2021



## Abstract

Future car parks will require significant power to support electric vehicle (EV) charging as there will be both an increase in the penetration of EV chargers and a higher demand for charging power as battery packs increase in capacity and users demand short charge durations. Effective control of the charging and local storage can be installed to help avoid excessive increases in electrical feeder capacity, however, car parks will inevitably attain significant power capability in the future compared to that seen today. It is therefore proposed in this research to leverage this power capability and use vehicle-to-grid charging, under the central control of the car park operator, to act as an aggregated energy storage system to deliver grid frequency response services. In this thesis, an agent-based model of a novel smart EV car park (SECP) is presented that can incorporate detailed power models for agents whilst providing a centralised command-based control structure to support advanced power flow management. It is first used to analyse how to manage the peak power demand of the EVs through charging management with four different power management methods proposed and evaluated. These methods are demonstrated to enable the power feeder to the SECP to be constrained whilst providing an equitable EV charging service. The thesis then investigates how photovoltaic panels and a battery energy storage system can be integrated into the SECP model to support improved EV charging. A methodology to control the power flow between the elements is presented and this is demonstrated to effectively increase the available power for EV charging and maximise the use of available PV energy over the day reducing the demand from the grid. The results show how the power feeder can be then minimised with the appropriate sizing of PV and the BESS. Finally, a power flow management strategy is proposed to enable the import and export of power to the grid to provide frequency response services as a single aggregated unit. Two frequency response services used by the Electricity System Operator in GB are simulated and it is validated that the SECP can deliver to the requirements of the services. A sizing methodology is proposed for the BESS to maximise service availability and EV charging capability whilst

meeting the constraints of a power feeder limit. The research presented in this thesis transforms an EV car park from a burden on the grid to being effectively a short term energy storage system that can provide a fast power response to help balance the electrical transmission system.

## List of Publications

Parts of the work presented in this thesis have been reported in the following internationally-respected publications:

### Journal Publications

1. **Y. Wang**, D. T. Gladwin, “Power Management Analysis of A Photovoltaic and Battery Energy Storage Based Smart Electrical Car Park Providing Ancillary Grid Services,” in *Energies*, 14(24), pp.8433.

### Conference Proceedings

1. **Y. Wang**, D. T. Gladwin, “Power management of EV car parks,” in *IECON 2019 - 45th Annual Conference of the IEEE Industrial Electronics Society*, 2019, pp. 4316-4322.
2. X. Mou, R. Zhao, **Y. Wang**, D. Gladwin, “Angular Offset Analysis in Wireless Vehicle to Vehicle (V2V) Charging System,” in *IECON 2019 - 45th Annual Conference of the IEEE Industrial Electronics Society*, 2019, pp. 4293-4297.

## Acknowledgements

Firstly, I would like to express the depth of my gratitude to my supervisor Daniel Gladwin who gave me the opportunity to study at the University of Sheffield as a PhD student for the last four years. He not only taught me a lot of knowledge but also taught me how to think independently and how to conduct academic research. He is a very patient teacher, as Chinese, English is my second language, however, in the last several meetings with him, I have never felt any inconvenience in communication and understanding. He always explains things to the extent that I can easily understand. He is also a person who cares about his students, His encouragement warmed my heart during the worst period of the epidemic in the UK. He is also a friendly person, we have had many happy conversations, the days of drinking in the pub of Lisbon and Red Deer are my most precious memories.

Many thanks to my groupmates, Thomas L.Fantham, Matthew J.Smith, Zhuo Wang, Rui Zhao, Xiaolin Mou, it is lucky to work with you in the lab and thank you very much for your help over the years. I must also make a note of thanks to Rhys Munden who has helped proofread my work.

I would like to thank my parents for their support, encouragement and understanding throughout my study.

Finally, I would like to thank the University of Sheffield for providing such an enjoyable learning environment and a lot of convenience for staff and students during the epidemic. I am so proud to be part of it.

# Contents

<b>Abstract</b>	<b>i</b>
<b>List of Publications</b>	<b>iii</b>
<b>Acknowledgements</b>	<b>iv</b>
<b>Nomenclature</b>	<b>xii</b>
<b>List of Symbols</b>	<b>xiv</b>
<b>1 Introduction</b>	<b>1</b>
1.1 Background & Motivation . . . . .	1
1.2 Thesis Contributions . . . . .	4
<b>2 Literature Review</b>	<b>6</b>
2.1 The useful EV information . . . . .	6
2.1.1 EV types . . . . .	6
2.1.2 Battery state estimation . . . . .	7
2.1.3 EV charging infrastructure . . . . .	11
2.2 PV . . . . .	15
2.2.1 PV modelling . . . . .	16
2.3 Smart EV charging (SEC) . . . . .	17
2.3.1 The disadvantages of EV grid integration . . . . .	17
2.3.2 The definition of SEC . . . . .	20
2.3.3 EV charging load modelling . . . . .	20
2.3.4 Optimisation of EV charging station . . . . .	27
2.4 Conclusion . . . . .	39
<b>3 SECP model</b>	<b>40</b>
3.1 Introduction . . . . .	40
3.2 The parameters of EVs and SECP with their setup . . . . .	41
3.2.1 Daily driving distance of an EV ( $L_d$ ) . . . . .	41

3.2.2	Daily energy consumption of an EV ( $E_d$ ) . . . . .	42
3.2.3	The initial SoC of EV ( $SoC_{initial}$ ) . . . . .	45
3.2.4	EV types . . . . .	46
3.2.5	EVs charging power . . . . .	47
3.2.6	EVs charging period ( $T_p$ ) . . . . .	50
3.2.7	The penetration of DC fast charging ( $R_p$ ) . . . . .	53
3.3	EV load model and results . . . . .	54
3.4	Conclusion . . . . .	59
<b>4</b>	<b>Power management of SECPs</b>	<b>60</b>
4.1	Introduction . . . . .	60
4.2	Simulation of power management . . . . .	60
4.2.1	The first power management method by recovering the shortfall power based on proportional power . . . . .	62
4.2.2	The second power management method by recovering the shortfall power based on SoC proportion . . . . .	62
4.2.3	The third power management method by sharing the available power based on SoC proportion . . . . .	63
4.2.4	Simulation results . . . . .	64
4.2.5	Fourth method on power management based on the results of Method 3 . . . . .	69
4.3	Cases study of the provided four methods . . . . .	70
4.4	Conclusions . . . . .	73
<b>5</b>	<b>The integration of BESS and PV</b>	<b>75</b>
5.1	Introduction . . . . .	75
5.2	The BESS based SECP . . . . .	76
5.2.1	The structure of the BESS based SECP . . . . .	77
5.2.2	Modelling the BESS based SECP . . . . .	79
5.2.3	Cases study of the BESS based SECP . . . . .	80
5.2.4	Sensitivity analysis of power feeder limit and the ca- pacity of BESS based on the cases study . . . . .	82
5.3	The BESS and PV based SECP . . . . .	86
5.3.1	The structure of the BESS and PV based SECP . . . . .	86
5.3.2	Model of the BESS and PV based SECP . . . . .	89
5.3.3	Cases study of the BESS and PV based SECP . . . . .	91
5.3.4	Sensitivity analysis of power feeder limit and the capac- ity of BESS based on the case study with PV integrated . . . . .	93
5.4	Conclusion . . . . .	98

<b>6</b>	<b>SECP for providing ancillary grid services</b>	<b>99</b>
6.1	Introduction . . . . .	99
6.2	DFFR and DC modelling . . . . .	100
6.3	Energy flow between the system components . . . . .	105
6.4	DFFR results . . . . .	107
6.5	DC results . . . . .	113
6.6	The Pareto front of availability vs average increasing SoC of EVs based on GA optimisation . . . . .	118
6.7	Conclusion . . . . .	120
<b>7</b>	<b>Conclusions &amp; Further Work</b>	<b>123</b>
7.1	Conclusions . . . . .	123
7.2	Further Work . . . . .	128
7.2.1	Improvements of the ABM of SECP . . . . .	128
7.2.2	Research on hardware aspects . . . . .	129
7.2.3	A remote centralized management system for multi-locations EV charging . . . . .	130
	<b>References</b>	<b>131</b>

# List of Figures

1.1	Global EVs stock 2010-2020 [1]. . . . .	2
1.2	Global slow and fast EV chargers stock in public area 2015-2020 [2]. . . . .	3
2.1	EVs' types. . . . .	8
2.2	On-Board charger and off-board charger. . . . .	12
2.3	Unidirectional and bidirectional charger and power flow. . . . .	12
2.4	Schematic framework of the solar-PV system . . . . .	16
2.5	Possible cases of vehicle state transitions at time t [3] . . . . .	26
2.6	The aggregator functions and collaboration with other grid systems [4] . . . . .	28
2.7	AC-connected system and DC-connected system . . . . .	34
3.1	PDF of daily mileage . . . . .	43
3.2	CDF of daily energy consumption . . . . .	44
3.3	Charging power vs SoC of tested EV brands . . . . .	46
3.4	SoC vs time charging profile of tested EV brands . . . . .	49
3.5	Charging power vs time of tested EV brands . . . . .	49
3.6	Charging Power vs SoC by adjusting the charging power of the DC fast charging points to a maximum of 7.68kW . . . . .	50
3.7	The traffic flow of the car park in 24 hours on a weekday . . . . .	51
3.8	PDF of traffic flow (Hainault Station in London) . . . . .	51
3.9	CDF of traffic flow (Hainault Station in London) . . . . .	52
3.10	The comparison of real park occupancy and one random simulated occupancy . . . . .	53
3.11	Diagram of EVs' load procedure of SECP . . . . .	54
3.12	EVs power load vs time . . . . .	55
3.13	The comparison of fast charging and slow charging and total EVs occupancy . . . . .	56
3.14	Distribution of EVs' increasing SoC . . . . .	56
3.15	The comparison of EVs load of $R_p=80\%$ and $R_p=100\%$ . . . . .	58

4.1	Diagram of the four EV charging management methods' procedure of SECP . . . . .	61
4.2	The results without applying any power management method	64
4.3	The simulation results of applying Method 1 . . . . .	65
4.4	The simulation results of applying Method 2 . . . . .	66
4.5	The simulation results of applying Method 3 . . . . .	68
4.6	The simulation results of applying the Method 4 . . . . .	71
5.1	The BESS based SECP. . . . .	77
5.2	The energy flow of BESS based SECP. . . . .	78
5.3	System response for EV load . . . . .	81
5.4	Sensitivity analysis result of SECP with BESS. . . . .	84
5.5	The BESS and PV based SECP. . . . .	86
5.6	The energy flow of the BESS and PV based SECP . . . . .	88
5.7	The PV power generation based on the 80 charging spaces . .	90
5.8	The response of PV-BESS based SECP to the various EV load	92
5.9	Sensitivity analysis result of SECP with BESS and PV on 01/01/2019. . . . .	95
5.10	Sensitivity analysis result of SECP with BESS and PV on 01/07/2019. . . . .	96
6.1	DFFR droop curve for a provider (blue line) . . . . .	101
6.2	DC droop curve for a provider (blue line) . . . . .	101
6.3	The energy flow in the LFZ . . . . .	104
6.4	System response for DFFR - one day simulation . . . . .	108
6.5	Key DFFR operating behaviours during a day . . . . .	109
6.6	The SoC of the BESS for one day DFFR simulation . . . . .	110
6.7	System response for DC - one day simulation . . . . .	114
6.8	Key DC operating behaviours during a day . . . . .	115
6.9	The SoC of BESS for one day DC simulation . . . . .	116
6.10	The Pareto fronts of SECP with a 500kW BESS in summer .	121
6.11	The Pareto fronts of SECP with a 500kW BESS in winter . .	122

# List of Tables

2.1	Current and voltage level in SAEJ1772, IEC62196, and IEC61851 [4] . . . . .	13
2.2	The key feature of each Lithium-ion battery [5] . . . . .	15
3.1	Annual mileage of cars in England and energy consumption . .	42
3.2	EVs battery capacity and their registration number . . . . .	46
3.3	The parameters of SECP for EVs charging load . . . . .	55
3.4	Analysis with various penetration of fast charging points . . .	57
3.5	$SoC_a$ value with various $R_p$ when all EVs arrive with $SoC_{initial} = 10\%$ . . . . .	59
4.1	The calculation details of $R$ . . . . .	69
4.2	Comparison of the simulation results of the provided four methods and the result without a power limit . . . . .	70
4.3	The parameters of the simulated SECP . . . . .	72
4.4	The average increasing SoC of four power management methods	72
5.1	The parameters of BESS based SECP . . . . .	80
5.2	Data points as shown in Figure 5.3 . . . . .	81
5.3	The parameters of EV based charging load for sensitivity analysis	83
5.4	Sensitivity analysis results of Method 1 . . . . .	83
5.5	Sensitivity analysis results of Method 2 . . . . .	85
5.6	Sensitivity analysis results of Method 3 . . . . .	85
5.7	Sensitivity analysis results of Method 4 . . . . .	85
5.8	The parameters of BESS and PV based SECP . . . . .	90
5.9	Data points as shown in Figure. 5.8 . . . . .	92
5.10	The parameters of PV-BESS based SECP for sensitivity analysis	94
5.11	Sensitivity analysis result: average increasing SoC on 01/01/2019 . . . . .	97
5.12	Sensitivity analysis result: PV energy utilization on 01/01/2019	97
5.13	Sensitivity analysis result: average increasing SoC on 01/07/2019	97
5.14	Sensitivity analysis result: PV energy utilization on 01/07/2019	98

6.1	The main parameters of the simulation . . . . .	107
6.2	Data points as shown in Figure. 6.4 . . . . .	108
6.3	The main parameters of the sensitivity analysis for simulating DFFR and DC . . . . .	111
6.4	Analysis with 25% initial SoC of BESS for DFFR . . . . .	112
6.5	Analysis with 50% initial SoC of BESS for DFFR . . . . .	112
6.6	Analysis with 75% initial SoC of BESS for DFFR . . . . .	112
6.7	Data points as shown in Figure. 6.7 . . . . .	114
6.8	Analysis with 25% initial SoC of BESS for DC . . . . .	116
6.9	Analysis with 50% initial SoC of BESS for DC . . . . .	117
6.10	Analysis with 75% initial SoC of BESS for DC . . . . .	117
6.11	GA settings for 100% availability . . . . .	119
6.12	GA results for 100% availability . . . . .	119
6.13	GA parameters for the Pareto front of a 500kW BESS for providing DC service . . . . .	121
6.14	The points from Pareto fronts from summer simulation . . . . .	122
6.15	The points from Pareto fronts from winter simulation . . . . .	122

# Nomenclature

**ABM** Agent Based Model.

**AEV** All-electric Vehicles.

**ASoC** Absolute SoC.

**BESS** Battery Energy Storage System.

**BEV** Battery Electric Vehicle.

**BMS** Battery Management System.

**CDF** Cumulative Distribution Function.

**DC** Dynamic Containment.

**DFFR** Dynamic Fast Frequency Response.

**DSO** Distribution System Operator.

**EM** Electric Motor.

**EV** Electric Vehicle.

**FCEV** Fuel Cell Electric Vehicle.

**GA** Genetic Algorithm.

**GENCO** Generation System Operator.

**HEV** Hybrid Electric Vehicle.

**HFZ** High-Frequency Zone.

**ICE** Internal Combustion Engine.

**Lead acid** Pb-acid.

**LFZ** Low-Frequency Zone.

**Li-ion** Lithium-ion.

**LSE** Load Serving Entity.

**NaNiCl** Sodium Nickel Chloride.

**NGESO** National Grid Electricity System Operator.

**NiCd** Nickel-Cadmium.

**NiMH** Nickel-Metal-Hydride.

**PDF** Probability Density Functions.

**PHEV** Plug-in Hybrid Electric Vehicle.

**PV** Photo-voltaic.

**RSOC** Relative SOC.

**SEC** Smart EV Charging.

**SECP** Smart EV Car Park.

**SoC** State of Charge.

**SoH** State of Health.

**TSO** Transmission System Operator.

**V2G** Vehicle to Grid.

# List of Symbols

$C_{rated}$  The rated capacity of the battery.

$P_{MPV}$  Maximum power generation of a PV panel.

$L_d$  Daily driving distance of an EV (mile).

$E_{ev}$  Average energy consumption of different brands of EVs (kWh/mile).

$SoC_{ll}$  SoC of EV on its last departure.

$C_{remaining}$  The remaining capacity of the battery.

$T_C$  The battery cell temperature.

$E_d$  Daily energy consumption of an EV.

$SoC_d$  Daily SOC drop of an EV.

$P_{Bmax}$  Charging power demand controlled by the EV's BMS.

$C_{faded}$  The capacity of faded battery.

$G$  Irradiance.

$L_a$  Average yearly mileage of an EV.

$SoC_{initial}$  Initial SoC of EV.

$P_{Amax}$  EV charging power.

$C_t$  Measured capacity of a battery.

$f(x)$  The PDF of daily energy consumption of each EV.

$E_{cev}$  Capacity of the EV battery.

$P_{Umax}$  Maximum charging power of an EV set by the EV user.

$P_{Cmax}$  Maximum output power of an EV charger.  
 $P_{Smax}$  Maximum charging power allocated to each EV by an aggregator.  
 $SoC_R$  The SoC of an EV at this time slot.  
 $\alpha$  Charging efficiency of an EV charger.  
 $T_p$  EVs charging period.  
 $T_{in}$  The time when an EV arrives SECP.  
 $T_{out}$  The time when an EV departs SECP.  
 $R_p$  Penetration of DC fast charging.  
 $N_f$  Number of fast charging EVs.  
 $N_s$  Number of slow charging EVs.  
 $N_p$  Number of EVs which are charging in the SECP.  
 $C_m$  SECP capacity/charging spaces.  
 $SoC_a$  Average increasing SoC of all EVs.  
 $P_a$  Average maximum daily EVs' load.  
 $N$  Total number of EVs charged in the SECP.  
 $P_{Smaxi}$  Power which is allocated to the  $i$ th EV.  
 $P_{Bmaxi}$  The maximum power demand of the  $i$ th vehicle in this minute.  
 $P_L$  Power limit of power feeder.  
 $SoC_{Rit}$  SoC of the  $i$ th EV at the time  $t$ .  
 $V_t$  Variance of SoC in a given minute.  
 $\mu_t$  Mean of all EVs'  $SoC_{Rt}$ .  
 $AV$  Average SoC variance for the entire working time.  
 $AS$  Average SoC of all EVs.  
 $F$  Hysteresis factor of the method 4.  
 $R$  Ratio factor of the method 4.

$P_{BESS}$  Charging power of BESS.

$P_{EV}$  Total EVs load.

$SoC_{BESS}$  SoC of BESS.

$E_{cBESS}$  Capacity of BESS.

$T_s$  Time of start charging/discharging BESS.

$T_e$  Time of stop charging/discharging BESS.

$SoC_{T_s}$  SoC of BESS when the charging/discharging process starts.

$P_{Grid}$  Grid power/local power feeder power.

$P_{Cpv}$  Capacity of PV panel.

$P_{pv}$  PV power utilization.

$Z(t) \frac{P_{pvUK}(t)}{P_{CpvUK}}$ .

$P_c$  Contracted power, the response power that the provider has tendered.

$P_{AFR}$  Actual power required by DFFR based on the grid frequency.

$F(t)$  Real-time grid frequency.

$P_{ADC}$  Actual power required by DC based on the grid frequency.

$SoC_{min}$  Minimum SoC of EV battery.

$AVA$  Availability to evaluate the quality of the DFFR/DC service.

$T_Z$  Period of DFFR/DC.

$T_F$  Period of DFFR/DC when failure happens.

$GP$  Grid power.

$EVP$  EVs power.

$PVP$  PV power.

$BSCP/BSDP$  Available power of the BESS for charging/discharging.

$f_G$  Grid frequency.

$SoC_{BESSi}$  Power from BESS to grid.

**PV2EV** Power from PV to EVs.

**PV2BESS** Power from PV to BESS.

**Grid2BESS** Power from grid to BESS.

**Grid2EV** Power from grid to EV.

**BESS2EV** Power from BESS to EV.

**BESS2Grid** Power from BESS to grid.

# Chapter 1

## Introduction

### 1.1 Background & Motivation

With the increasing concerns about climate change, massive emission of greenhouse gases, noise generation, the price, and the depletion volatility of fossil fuels, electric vehicle (EV) as competitive green transportation has attracted a lot of attention. In a recent survey, the environmental benefits such as reduced pollution was the most common response, followed by more economical benefits, quieter driving, and reduced on-the-road costs (tax, fuel) [6]. Meanwhile, the EV also has the advantage in control performance, such as accurate and quick torque generation, quicker torque measurement, and the motor can be installed for each wheel [7].

Recent research on the scale of EVs has revealed that the EVs will play a vital role in the future. Figure 1.1 shows global plug-in hybrid EV (PHEV) and battery EV (BEV) stock in the period 2010-2020. Globally, EVs exceeded 5.1 million in 2018 with this number doubling by 2020 to over 10 million. The UK government announced in November 2020 that the phase-out date for new petrol and diesel vehicles and vans would be pushed back to 2030, with all new vehicles and vans being entirely zero-emission at the tailpipe by 2035 [8]. The predicted trend in growth of EVs is based on two scenarios: the New Policy Scenario, which introduces the impact of announced policy ambitions and it illustrates that in 2030, global EV sales will

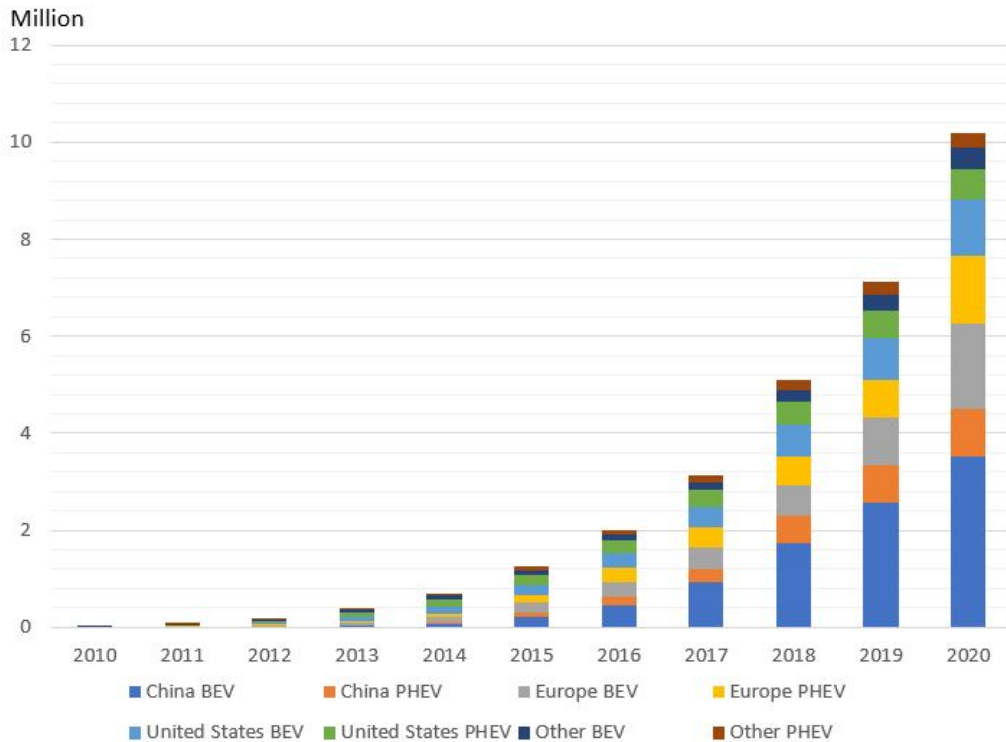


Figure 1.1: Global EVs stock 2010-2020 [1].

reach 23 million and the stock will exceed 130 million EVs. Another scenario, the EV30@30 Campaign is organized by Clean Energy Ministerial, and sets a collective aspirational goal to reach 30% sales share for EVs by 2030, it forecasts that EV stock and sales will nearly double in 2030 with roughly 250 million of EV stock and 43 million sales [9].

The number and distribution of EV chargers in an area are vital factors for customers who consider purchasing an EV. The research in [2] classified EV chargers into two types: slow chargers (with charging below 22kW) and fast chargers (with charging over 22kW). The number of slow and fast EV chargers' stock in the worldwide public area in the period of 2015-2020 is shown in Figure. 1.2. From the figure, the public accessible EV chargers reached 1.3 million in 2020, which is almost 7 times more than the numbers in 2015, and almost 30% are fast chargers. The installations in 2020 increased by 45%. Meanwhile, according to [10], as of 1 October 2019, there were 15,116 public EV charging devices available in the UK, an increase of 312%

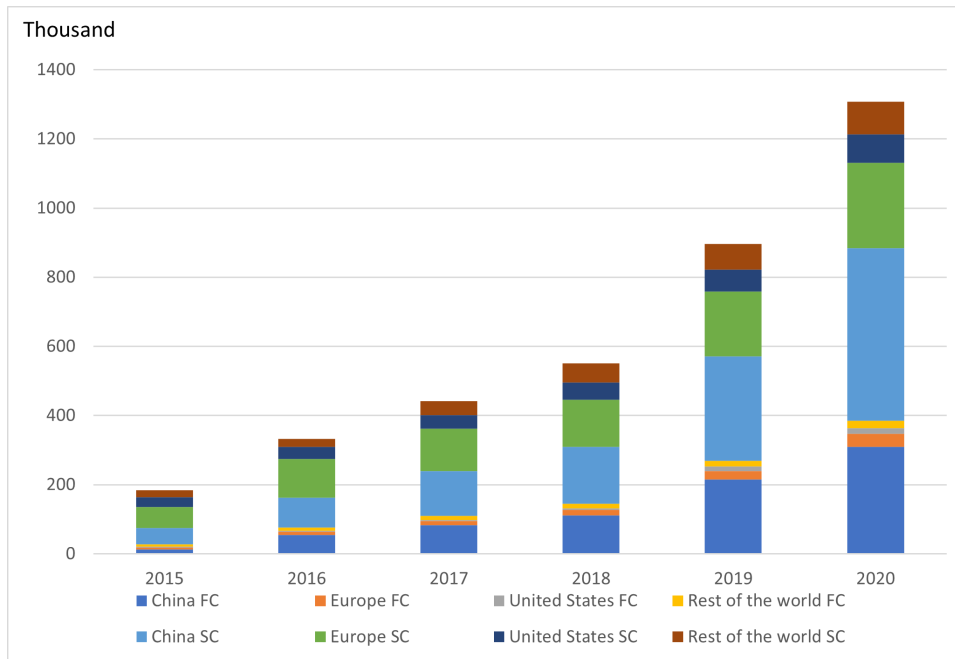


Figure 1.2: Global slow and fast EV chargers stock in public area 2015-2020 [2].

since 2015. Of these, 2,495 were fast chargers. Fast chargers have also grown quickly, rising by 260%, in the same period.

EV charging speeds are increasing sharply, the entry AC Level 1 charging speed was set below 2kW, whereas AC level 2 chargers can achieve 10kW and DC fast charging already has reached 120kW. Some research has developed Extreme Fast charging, which could charge an EV in excess of 350kW [11]. Taking an example of an EV park with 100 spaces, if 20% of those spaces are installed with a DC fast charger, the total potential maximum power requirement will be 2,400kW; such massive instantaneous power demand would be a burden on the local power supply, if available at all in some locations.

Many research projects have started to investigate how the power grid system is impacted by EV charging, and how to manage EVs charging to reduce these impacts. Overall, these impacts can be summarized as load demand increase, component overloading, phase and voltage unbalance, harmonics injection, and power loss and stability [4]. Research uses power management

methods to shift EV peak load to other periods, or integrated PV and BESS into EV charging to reduce these impacts of EV charging on the grid.

Meanwhile, in order to maintain the quality of electricity supply across Britain's transmission system and balance demand and supply, Britain's national grid provides services for generators/storage providers to participate in, such as frequency response service, reserve service and reactive power services. Some of these services require a significant capacity of BESS. The battery in EVs can be considered as energy storage unit when connecting with grid via a bi-directional charger. EVs can therefore both import and export electricity energy from/to the grid, this is also known as V2G technology.

## 1.2 Thesis Contributions

The literature has presented research in distributed charging on the electrical grid whereby chargers are installed at our homes and workplaces, however, car parks have had less attention, particularly when considering them as a single large storage asset with the potential to both import and export power to support the grid through frequency response services. In this thesis the car park is considered as such, whereby, all the parked EVs that are connected to chargers can both import and export power under the central control of the car park operator. Ultimately, the car park would be viewed by the grid as a standalone grid connected battery yet still provide a satisfactory charging service to the EV users. To achieve this there needs to be

- an understanding in how to manage the peak power demand of the EVs through charging management
- an evaluation of how renewable energy sources such as PV and additional energy storage can support EV charging to reduce the demand from the grid
- the development of power management strategies in the car park to enable grid services to be supported effectively

Therefore, the aim of this thesis is to model a novel smart EV car park (SECP) that can then be used to research the above points and validate whether the burden on the grid can be minimised and grid frequency response services provided.

The contributions can be summarised as:

1. Introducing a novel agent-based model (ABM) of an SECP that can both incorporate detailed power models for each agent whilst providing a centralised command-based control structure to support advanced power flow management. (Chapter 3)
2. Four novel charging power management methods that allow the peak power feeder requirements to be constrained. These are evaluated and the effect on the charging to the EVs is quantified demonstrating the need for additional power. (Chapter 4)
3. Introducing how PV and a BESS can be integrated into the SECP model to support EV charging. A methodology to control the power flow between the elements is presented and this is demonstrated to effectively increase the available power for EV charging and maximises the use of available PV energy over the day. The results show how the power feeder can be minimised with the suitable sizing of PV and the BESS. (Chapter 5)
4. Simulating two frequency response services based on the National Grid Electricity System Operator (NGESO) in GB and developing the effective power flow strategies for the services. It is validated that a PV-BESS based SECP can provide these services and a sizing methodology is proposed for the BESS to maximise service availability and EV charging capability. (Chapter 6)

# Chapter 2

## Literature Review

This review has been divided into three sections. In the first section, the review is concentrated on introducing some concepts about EV and EV parameters. The second section focuses on PV, which will be used in SECP concept. In the third section, the objective of the work is first to introduce the disadvantage of EV load, and the work aims to reduce the EV load. Hence the review has concentrated on analysing the previous research on EV total charging load prediction for an EV car park and the optimisation of SECP which includes EV load management, integration of PV and control of BESS. The end focus is on exploring the use of SECP for providing grid ancillary services.

### 2.1 The useful EV information

#### 2.1.1 EV types

There are three types of EVs: hybrid electric vehicles (HEVs), plug-in hybrid electric vehicles (PHEVs), and all-electric vehicles (AEVs). HEVs are powered by an electric motor (EM) and an internal combustion engine (ICE). Based on EM or ICE supporting the drive train, HEV can be further classified as the parallel hybrid, the series hybrid, and the power-split hybrid. For the parallel hybrid, ICE and EM are both connected to the drive train. The series hybrid uses ICE as a generator to support battery and EM, and EM is

the only power source support for the drive train. For the power-split hybrid, the ICE can directly power the drive train or support the EM to power the drive train, HEV equipped with a battery, however, can only be charged by regenerative braking and ICE. PHEVs are very similar to HEVs, however, the battery of PHEVs can also be charged by connecting with an electrical charger. AEVs only have EMs, these are further divided into battery electric vehicles (BEVs) and fuel cell electric vehicles (FCEVs). BEVs do not have an ICE, which means there is no fuel tank, no exhaust pipe, and no emissions from driving. The EM directly connects with the drive train, the battery supporting the EM is charged by regenerative braking or EV charger. FCEVs are powered by EM, but there is no need for an external charging system with a FCEV. Figure. 2.1 shows the details of EV types. Therefore, the EV charging points in the market only provide charging services to PHEV and BEV. In this thesis, EV mainly refers to BEV, or PHEV and BEV.

## 2.1.2 Battery state estimation

Batteries in the vehicles need to be considered for modelling and simulation. In literature, there are some important concepts to this, in particular, the state estimation of the battery.

### 2.1.2.1 Measuring the SoC

SoC refers to the battery charge level. SoC is divided into two types. The first one is absolute SoC (ASoC) as indicated in Equation 2.1 [12], which always focuses on a new battery. The second is relative SoC (RSoC) for a faded battery since charging and discharging a battery repeatedly leads to significant damage to its behaviors and life, which is shown in Equation 2.2 [13]. Voltage method, Coulomb Counting and Hydrometer measurement [13, 14] have been employed in the SoC estimation.

$$ASoC = \frac{C_{remaining}}{C_{rated}} \times 100\% \quad (2.1)$$

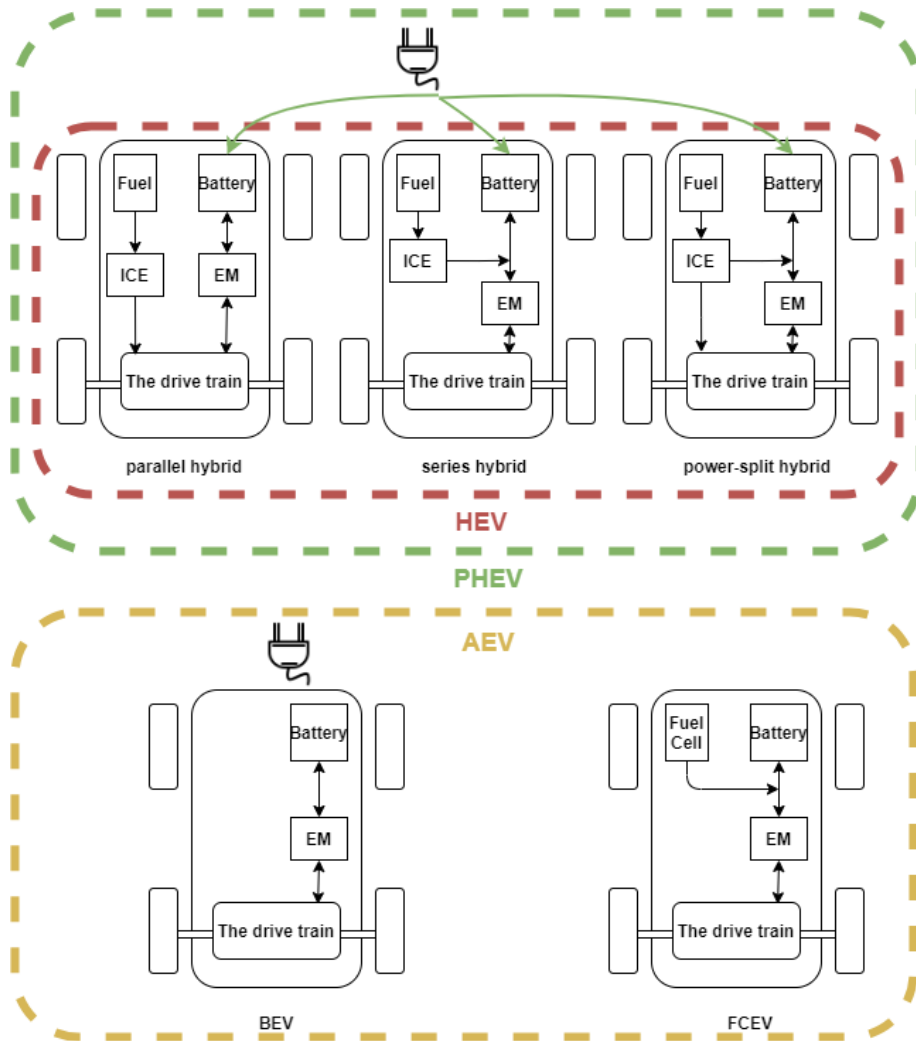


Figure 2.1: EVs' types.

$$RSoC = \frac{C_{remaining}}{C_{faded}} \times 100\% \quad (2.2)$$

where the  $C_{rated}$  and  $C_{faded}$  represent the rated capacity of the battery and the capacity of the faded battery respectively.  $C_{remaining}$  is the remaining capacity of the battery in the current situation. The unit of capacity depends on the measurement methods, such as Wh or Ah.

Voltage is a straightforward way to measure state-of-charge, although

it might be incorrect due to cell materials and temperature. The battery must rest in the open circuit condition for at least four hours to acquire reliable measurements; battery manufactures recommend 24 hours for lead-acid batteries [14].

Coulomb counting is used to estimate SoC by measuring the in-and-out-flowing current. The energy losses are a significant problem of coulomb counting, which results in the electricity available in the battery at the end always being less than the electricity that had been put in. If the Ah capacity is used, the change of ASoC and RSoC from time  $t_0$  to  $t$  can be expressed as [13]:

$$ASoC = ASoC(t) - ASoC(t_0) = \frac{\int_{t_0}^t i(t)dt}{C_{rated}} \times 100\% \quad (2.3)$$

$$C_{faded} = \int_{t_1}^{t_2} i(t)dt \quad (2.4)$$

$$RSoC = RSoC(t) - RSoC(t_0) = \frac{\int_{t_0}^t i(t)dt}{C_{faded}} \times 100\% \quad (2.5)$$

Where  $i$  is the battery current,  $C_{faded}$  is defined as the maximum total electrical charge which a faded battery can deliver from the fully charged state (SoC of 100%) at time  $t_1$  to a fully discharged state (SoC of 0%) at time  $t_2$ .

The hydrometer is another way to measure the SoC of flooded lead-acid batteries. The principle of this method is when the lead-acid battery is charged, the concentration of sulfuric acid increases, and the specific gravity increases, so the SoC will increase. SoC can be estimated to build the connection between the average specific gravity and approximate SoC. However, specific gravity might vary with battery applications and temperature.

The Kalman Filter is a nonlinear estimation algorithm, which was firstly proposed by R.E Kalman. It can estimate the state of dynamic systems from a series of incomplete measurements which contain noise. Kalman filter

on SoC estimation can be seen from [14–18]. Other methods include, a neural network scheme which is used to build a prediction model for SoC estimation [15,19–21]. Fuzzy logic methods employ a fuzzy rule set to analyse the observed data of complex and nonlinear systems. Fuzzy logic is employed to estimate SoC in [22].

### 2.1.2.2 Measuring the SoH

SoH is a tool to provide the general condition of a battery. It can be used as an indicator to the condition of a battery and potentially the remaining life of the battery. There are three main SoH indexes of a battery, which are capacity, internal resistance, and self-discharge. Generally, a battery is considered to reach its end of life when the battery capacity fades to 80% of its initial value [23]. Unlike SoC, SoH does not have an absolute definition over the last few years, the measurement of SoH may depend on different indicators and will have various methods. In [24], they classify SoH estimation with four approaches: The direct assessment approach, the Adaptive approach, the data-driven approach, and others. Therefore capacity loss alone is commonly used as a measure of battery degradation, where it is referred to as the SoH of the cell, which is generally defined as:

$$\text{SoH}(t) = \frac{C_t}{C_{rated}} \times 100\% \quad (2.6)$$

where  $C_t$  is the measured capacity at time  $t$  and  $C_{rated}$  is the rated capacity of the battery.

Coulomb counting is also used to calculate the SoH. The discharge value which the battery has been discharged to a SoC value of 0 is divided by the rated capacity to calculate SoH. The open-circuit voltage method is provided to estimate SoH by using the relationship between SoH and open-circuit voltage which is tested in the laboratory. SoH can also be determined via impedance spectroscopy, which employs a wide frequency spectrum with which to measure the impedance over [25].

A Kalman filter can accurately estimate battery SoH, its application can be seen from [26, 27]. The particle filter method is provided for nonlinear

non-Gaussian system state estimation. The Particle filter algorithm selects a set of random samples for state approximation with the least amount of estimation variance. In [28, 29], the researchers applied the particle filter on SoH estimation.

The Fuzzy logic and Neural network application of SoH estimation are similar to SoC, which can be seen in [30, 31] and [32, 33] respectively. A Probability Density Function (PDF) is also used to calculate SoH based on the history data of battery capacity [24].

## **2.1.3 EV charging infrastructure**

### **2.1.3.1 EV charger protocols**

The increasing number of EVs requires more EV charging points to meet the high customer demand. Usually, EV batteries are DC systems, any devices with AC input or output requirements, such as a BESS, will require an AC/DC converter. EV charging also requires DC/DC converter to achieve different voltage levels. EV charger equipped with AC/DC and DC/DC functions can be classified into the on-board charger and the off-board charger, where the on-board charger is installed inside the actual EV, and the main function is to convert AC power from the grid to DC power. The off-board charger is an outside charger that directly provides a DC output power. Both of them are shown in Figure 2.2.

Because of the weight and cost constraints and the limitation of space and cooling system, on-board chargers are limited in the amount of energy they can transfer [34]. Due to the limiting power ratings of on-board chargers, off-board chargers, normally rated at 50 kW and, more recently, at 350 kW, have been developed. EV chargers are frequently designed for use as off-board arrangements because of their large size and weight resulting from the required inductors, capacitors, cooling system, and eventual isolating transformer [35]. Despite the higher cost of an off-board charger, they offer some promising features such as decreasing the weight of the EV; charging at high power levels; faster charging capability; less heating issues; and proper communications between utility companies and owners of commercial sites for

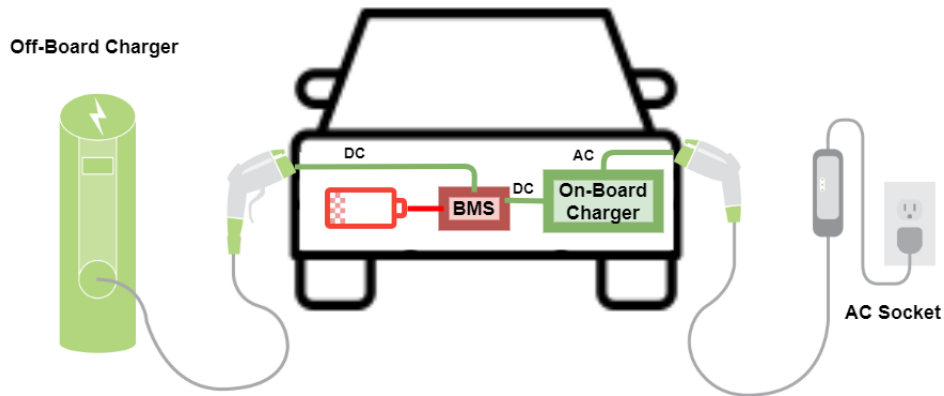


Figure 2.2: On-Board charger and off-board charger.

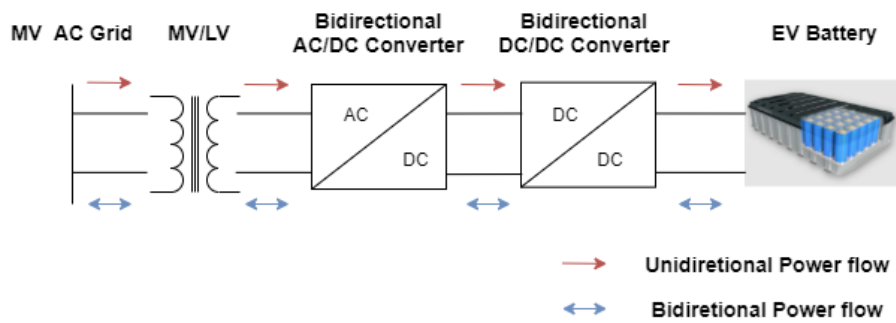


Figure 2.3: Unidirectional and bidirectional charger and power flow.

creating charging situations to provide better congruence [34]. On the other hand, the use of EV chargers with an on-board arrangement would allow battery charging at any time, given the availability of the supply grid [35].

Meanwhile, EV chargers can also be classified as unidirectional and bidirectional, where Figure. 2.3 shows their electricity flow. The unidirectional charger has benefits such as simplification of interconnection, fewer Components needed [36]. By contrast, the bidirectional charger can provide the opportunity of integrating an EV with grid for ancillary services. The research of bidirectional chargers on on-board [37–39] and off-board versions [40, 41] designs are vital topics in V2G technology.

### 2.1.3.2 Classification of EV charging

EV charging can be classified into AC and DC charging. The charging speed of an EV can be classified as either slow charging (level 1 and level 2) or fast charging (level 3 and DC charging). There are some EV charging standards available to give the exact value of different charging levels, but different countries follow different charging standards. USA uses SAE and IEEE, whereas IEC is widely used in Europe, and China has Guobiao (GB/T) as standard for AC and DC charging. The AC charging part of GB/T is similar to IEC standard. The details can be seen in Table. 2.1.

Levels 1 and 2 charging stations can be put in a private site, whereas, Level 3 charging stations require dedicated electrical connections and transformers, and are typically installed at public charging stations, so require permission from grid companies. DC fast charging is faster than AC charging and usually has a higher charging power capacity at the same voltage level. The most common DC fast charging points can charge at a power of 50 kW using CHarge deMOve (CHAdeMO), Combined Charging System (CCS) or GB/T standard connectors. Tesla was the first to provide 120kW charging points (Tesla Superchargers) equipped with custom connectors. The

Table 2.1: Current and voltage level in SAEJ1772, IEC62196, and IEC61851 [4]

Standards	AC/DC	Level/Mode	Max Current (A)	Voltage (V)	Power (kW)
SAEJ1772	AC	Level 1	16	120	1.92
	AC	Level 2	32–80	240	7.68-19.2
	DC	Level 1	80	200–450	16-36
	DC	Level 2	200	200–450	40-90
IEC62196	AC	Mode 1	16	120	1.92
	AC	Mode 2	32	240	7.68
	AC	Mode 3	32–250	250	8-62.5
	DC	Mode 4	400	600	240
IEC61851	AC	Mode 1	16	120	1.92
	AC	Mode 2	80	240	19.2
	DC	Mode 4	80	200–450	16-36

North American CCS 1, the European CCS 2, the CHAdeMO (a standard established by China and Japan) and the Tesla Super Charger are the four main charging connectors that have been launched.

In 2017, Porsche first installed two 350kW CCS chargers which is the highest power rating permitted by CCS in Berlin [42]. The UK's first 350kW EV charging station was opened in Kent in 2019, however, no current electric vehicles were capable of fully benefiting from such a fast charging rate until the Porsche Taycan, which can be charged at 350kW [43]. In December 2018, BMW and Porsche in collaboration with Siemens presented a CCS charging station with an output of up to 450 kW in Bavaria, Germany. At this new charging station, a Porsche research vehicle with a net battery capacity of around 90 kWh reached a charging power of more than 400 kW, allowing charging periods of less than 3 minutes for the first 100 km range [44]. China and Japan have been making a push on a new global EV charging standard in which the maximum charging power is tentatively set at 900kW. This allows large vehicles such as earthworks, buses, trucks and helicopters to be charged faster [45]. DC fast charging reduces the range anxiety of EV customers, and can help to enable rapid growth of the EV market by minimising vehicle downtime [46].

The progress of the EV charger can not always lead to a high-speed charge. It also depends on the specification of the EV battery, the cable and the environmental conditions [47, 48]. High charging current requests larger diameters cable to avoid overheating. Meanwhile, high environment temperature causes the high temperature of the battery, which may slow down charging and reduce the lifetime of the battery. Most batteries can be charged in the temperature range of 5°C to 45°C. DC fast charging has been known to reduce energy efficiency and cause accelerated capacity and power fade and generate massive heat. Further information of EV Lithium-ion battery DC fast charging can be seen in [47, 49], and the converter typologies of DC fast charging of EV charging station is in [50–53].

An EV battery, known as a traction battery, is a battery used to power the EMs of a BEV or HEV. Lithium-ion batteries are presently the most widely used traction battery in EVs, due to its high energy density and en-

Table 2.2: The key feature of each Lithium-ion battery [5]

Chemistry	NMC	LFP	NCA
Specific Energy (Wh/kg)	150–220	90–120	200-260
Cycle life (ideal)	1000–2000	1000–2000	500
Thermal runaway (°C)	210	270	150

hanced power per mass battery unit, which has enabled the development of various types of batteries with decreased weight and dimensions at competitive prices [54]. The most popular Lithium-ion battery for the traction battery are lithium-iron phosphate battery (LFP battery) and lithium nickel manganese cobalt oxides battery (NMC or NCM battery) and lithium nickel cobalt aluminium oxides battery (NCA). LFP is a type of lithium-ion battery using lithium iron phosphate as the cathode material, and a graphite carbon electrode with a metallic backing as the anode. The difference with LFP battery is that NMC mixed metal oxides of lithium, nickel, manganese and cobalt as the cathode material and NCA mixed metal oxides of lithium, nickel, aluminium, cobalt oxides as the cathode material [55]. The specific energy and the cycle life of the three types of battery have been shown in Table. 2.2, NCA has the highest specific energy (200-260Wh/kg), NMC and LFP have similar cycle life (1000–2000), while LFP batteries has the highest thermal runaway and can stand high voltage for extended periods of time which means LFP has lower risk of electric shortages and possibly fires [56].

## 2.2 PV

A solar panel, also known as a PV module, is an installation of PV cells arranged in a framework. PV generates direct current electricity using sunlight as a source of energy. PV as a renewable energy has been applied in many areas, such as domestic and commercial generation, and grid support. According to the PV deployment [57], there are 1,088,027 solar equipment installations in the UK with a total capacity of 13,530 MW by the end of June 2021. By contrast, in January 2012, there were only 244,322 solar equipment

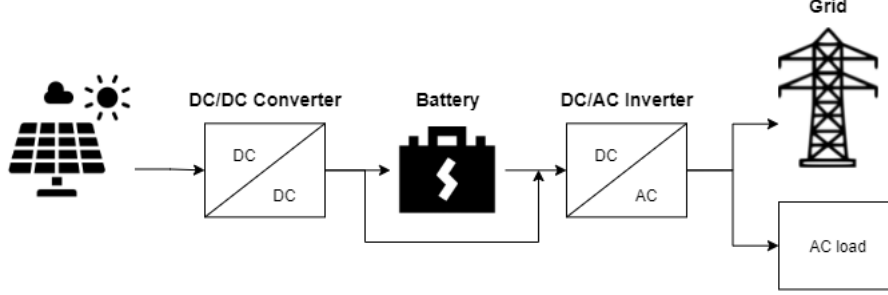


Figure 2.4: Schematic framework of the solar-PV system

installations in the UK with a total capacity of 1027.2 MW. The time data shows large capacity step changes in March for the years 2013 to 2017.

### 2.2.1 PV modelling

Figure 2.4 shows a normal framework of a PV system. PV performance modelling is essential to anticipate energy yield and rate the performance of the running plant. The relationship of maximum power generation of a PV panel  $P_{MPV}$  and operating conditions [58] can be expressed by the equation below:

$$P_{MPV} = P_{MPV}(G, T_C) \quad (2.7)$$

where  $G$  and  $T_C$  represent the irradiance and the cell temperature respectively. The standard test condition (STC) of a PV (the irradiance is  $1000W/m^2$ , the spectrum is AM 1.5, the cell temperature equals to  $25^\circ C$ ) is employed to get the rated power of a PV generator. Various studies on the modelling of PV technology have been provided. In [59], the author calculates generated PV power  $P_j$  in time slot  $j$  based on the equation:

$$P_j = P_{MPV} \frac{G_j}{1000} [1 - \beta_{PV}(T_{Cj} - T_{CRj})] \quad (2.8)$$

$$P_{jR} = \eta_{conv} \rho_{PV} \eta_{MPPT} P_j \quad (2.9)$$

where  $G_j$  is the solar irradiance in the  $j$ th time slot,  $\beta_{PV}$  is the coefficient of temperature for the PV module's efficiency, and  $T_{CRj}$  is the rated cell temperature.  $P_{jR}$  is the output power which includes efficiency of the converter ( $\eta_{conv}$ ) and maximum power point tracking ( $\eta_{MPPT}$ ), and derating factor of PV panel ( $\rho_{PV}$ ).

## 2.3 Smart EV charging (SEC)

### 2.3.1 The disadvantages of EV grid integration

Overall, the negative impacts of EV grid integration can be classified into six aspects which are load demand increase, component overloading, phase and voltage unbalance, harmonics injection, power loss, and stability [4].

#### 2.3.1.1 Load demand increase

Along with the increasing number of EVs, the capacity of batteries continues to grow and the demand for public EV fast charging points is higher than ever before. Research in [60] finds that the number of fast charging stations per 1000 vehicles for EVs will be similar to the fuel station network in the future. Car parks have to increase EV charging points to meet the high customer demand. Research in [61] states that according to information from Germany, before 2030, EV growth is likely to result in slight increases in power demand, which will likely add around 1% to the total and require roughly 5 GW of additional generation capacity. By 2050, that percentage might rise to over 4%, necessitating an additional 20 GW of capacity. These results focus on a country, however, high densities in large cities will become early EV adoption hot spots, increased local grid support requirements for significant EV populations will probably emerge.

Estimated data shows that globally EVs consumed 58 TWh of electricity in 2018, which is equal to the electricity demand of the whole of Switzerland in 2017. In the New Policies Scenario, worldwide EV fleet electricity demand is expected to reach over 640 TWh in 2030, which is the same as France and Spain's combined total electricity consumption in 2016. The larger worldwide

EV fleet in the EV30@30 Scenario results in 1110 TWh of electricity demand in 2030, nearly double that of the New Policies Scenario [62]. EVs will bring a significant increase in power demand on the grid, especially during the high-power demand period, which might be a big problem without any management.

### **2.3.1.2 Component overloading**

The analysis in [61] found that a typical residential feeder circuit of 150 dwellings with 25% local EV penetration would see a 30 percent increase in local peak power load, they also anticipate that if nothing is done, the total cost of grid investment will be several hundred Euros per EV. Massive electricity demand will be a burden on the local grid and the local transformers in the substation will eventually be overloaded. A case study in Toronto [63] chose the two most loaded distribution transformers (OT1 and OT2) rated at 100 kVA to model the impact of EV chargers on the distribution substation. In this study, 35 houses are using the transformers, three hours in a random day are selected which are 4:00–5:00, 12:00–13:00, and 20:00–21:00. The basic load without EVs in this period are 31.833, 44.566, and 60.904 kVA respectively. The EVs are using 6.6 kW chargers with a penetration rate of 33%, 66%, and 100%. The results reveal that a 6.6 kW charger creates potential system overloading even under low EV penetration. This case just uses a 6.6 kW EV charger, if it were upgraded to a DC fast charger supplying 50kW or over, the transformer can easily exceed the capacity limit. In [64], to quantify transformer ageing under both unmanaged and smart charging situations, the author employs a Monte Carlo simulation of a 25kVA distribution transformer with ambient temperature data from Burlington, VT and Phoenix, AZ. The data show that AC Level 2 charging causes more significant ageing than AC Level 1. Smart charging, where the power level of charging is dynamically controlled, has the potential to greatly reduce these side effects.

### **2.3.1.3 Phase and voltage unbalance**

[65–67] reveal that that as the penetration level of EV charging or discharging increases, the voltage imbalance will grow. EVs also have an impact on the voltage imbalance at the feeder’s end, if EVs connect to a low load phase of the system which is operating in the discharging mode, voltage unbalance at the end of the feeder may exceed the regulatory limits, if PEVs are connected to a heavily loaded phase and operate in charging mode, similar results are expected. When the charging rate of EVs is raised, the voltage unbalances between the phases will increase. Furthermore, if EVs charge or discharge when the grid system is under a high demand period, the voltage unbalance will increase.

### **2.3.1.4 Harmonics injection**

The total harmonic distortion of the grid current must be less than 5%, and the individual harmonic components must be tightly regulated [68], high harmonic current distortion in charging systems can result in secondary distribution line and transformer de-rating, as well as quality of service issues, the main source of EV charging related harmonics is the interface circuit architecture that connects to the grid network [69]. Unidirectional chargers are used in electric vehicles to transfer energy in one direction and might inject harmonic current into the grid network [70]. [71] reveals that an EV penetration level of 45 percent can produce a significant voltage drop in the system, and voltage total harmonic distortion with a current total harmonic distortion of 17.4 % is over the permissible limit of 8%.

### **2.3.1.5 Power loss and stability**

Power loss in an electricity network can be caused by a variety of factors, such as faults in power plants, damage to electric transmission lines, substations, or other sections of the distribution system. The higher power demand resulting from the increasing EVs leads to the growth of power loss. Research in [72] demonstrates that with 62% of EV penetration, up to 40% power loss increment can occurs when considering two large-scale real distribution areas.

EV loads are nonlinear and require a huge amount of power in a short period of time, causing power system instability [4]. In [73], the author simulated results reveal fast charging of several EVs can put excessive stress on the components of power grids, which leads to voltage instability and shortened life.

### **2.3.2 The definition of SEC**

The management of EV charging is necessary along with the increase of the EV penetration and their charging speed, SEC as a hot research topic gets a lot of attention. SEC entails changing charging to a different time of day, such as overnight when electricity demand is lower or during periods of significant renewable energy generation. According to [8], the smart charging point can be described as:

1. Send and receive information
2. Respond to this information by increasing or decreasing the rate of electricity flowing through the charge point; and changing the time at which electricity flows through the charge point.

According to the UK government response to SEC [8], the UK government proposed four objectives to support smart charging policy: consumer uptake, innovation, grid protection and consumer protection. For achieving SEC, the Automated and Electric Vehicles Act 2018 gives the UK government the power to require all EV charging points sold and installed in the UK to have smart functionality and meet minimum device-level criteria through secondary legislation. In 2021, the UK government intends to impose a minimum set of regulations to promote the early SEC market.

### **2.3.3 EV charging load modelling**

In order to develop SEC strategies, the EV charging points or the EV charging park need a power management system which integrate the information of each devices and manage these devices. there are a lot of parameters in

the system that need to be studied, the EV charging load model is one of the most complex parts as it is related to many complex factors, such as people behaviour which is affected by external and internal environments. It is challenging to predict people's actions without massive and long term behaviour captures and analysis. Hence, most research will transfer these questions to small parts in some particular cases. For example, how long and how often an EV owner would like to charge their EV can be divided into how far the EV owner drive every day, what model of EV they have (battery capacity/charge capability), and the parameters of this EV, the charging speed of the charging point, etc. Many factors affect EV charging load, this can be classified to indirect factors which are benefit, market, policy and environment; and direct factors which are infrastructure, user and technology [74], where the infrastructure includes the capacity of power supply from the power conversion system and the distribution of EV charging facilities etc; The user factors include the user behaviour such as driving time, charging performance, EV size etc; The technology includes the power supply level, battery characteristics, cooling system for facilities, battery management system (BMS) development.

### **2.3.3.1 Introduction of probability density function (PDF) and cumulative distribution function (CDF)**

For estimating the EVs load and solving some probability problems, PDF and CDF are normally used.

The link between observations and their probability is defined as a probability density. Some random variable outcomes will have a low probability density, while others will have a high probability density. A probability distribution is the general shape of the probability density, while a PDF calculates probabilities for distinct outcomes of a random variable. A random variable  $x$  has a PDF  $f(x)$  [75].

The cumulative distribution function (CDF)  $F(x)$  describes the probability that a random variable  $x$  with a given PDF will be found at a value less

than or equal to  $M$  [76]. This CDF is given as:

$$F(M) = \int_{-\infty}^M f(x)dx \quad (2.10)$$

Meanwhile, CDF also has the following properties:

$$\lim_{x \rightarrow -\infty} F(x) = 0 \quad (2.11)$$

$$\lim_{x \rightarrow \infty} F(x) = 1 \quad (2.12)$$

### 2.3.3.2 The application of queuing theory and the Poisson process on load modelling

When analysing the consequences of consumers randomly arriving and being serviced by a system, queuing theory is typically applied. In [77], A EV charging station equipped with AC chargers and DC chargers is modelled to provide the charging services for connecting EVs. This research presumes that fast charging leads to battery degradation. Hence, this charging station process allows EV owners to consider short charging duration, long battery lifetimes or both of them. However, the service unavailability rate might increase when most EV owners prefer one type of charger. Hence, the author presumes EV owners are price sensitive, then uses an optimal pricing scheme to guide the selection of EV owners. The author uses the queuing theory for modelling EV charging load. The implications of consumers arriving at random and being served by a system are often theoretically analysed using queuing theory since the chargers are limited to customers. The research uses queuing theory to analyse a specific case and to design a balanced system that serves customers quickly and efficiently but does not cost too much to be sustainable. The basic queuing theory includes an analysis of arrivals at a facility, and an analysis of the processes currently in place to serve them. In queuing theory the possibility of the numbers of EVs arriving in at a time slot follows a Poisson process, this can also be seen in [78, 79], the probability of  $n$  EVs arriving at the EV charging station during the time slot  $t$  ( $P(n)$ ) can be expressed by

$$P(n) = \frac{e^{-\lambda_t} * \lambda_t^n}{n!}, n = 0, 1, 2, 3... \quad (2.13)$$

where  $\lambda_t$  represents the average number of EVs arriving during this t time slot. In [78, 80], the charging time requested by an EV is transferred to an exponential distribution, [78] divides the charging period into exponential distribution in the daytime and a log-normal distribution in the night-time. The probability density function of an exponential distribution for n EVs' the charging duration time  $t_d$  of EVs can be expressed by

$$P(t_d) = \alpha * e^{-\alpha t_d}, \quad (2.14)$$

where  $\alpha$  is the average EV charging duration. The probability density function of log-normal distribution for the charging duration  $t_d$  is

$$P(t_d) = \frac{1}{t_d \sigma \sqrt{2\pi}} * e^{-\frac{\ln t_d - \mu}{2\sigma^2}} \quad (2.15)$$

where  $\mu$  is the average charging duration time,  $\sigma^2$  represents the variance of all EVs' charging duration. The charging duration is related to the travel distance of an EV, as a longer travel distance might lead to more energy demand. EV customers with more energy demand might request a longer charging period to feed the EV battery.

For the travel distance, a lot of papers use the normal distribution or exponential distribution or Poisson distribution, however, in some cases, these distributions can not reflect the actual as the travel distance might contain multiple regions with high probability mass. A mixture model is a probabilistic model for expressing the sub-populations within a larger population which does not require an observed data set to determine the sub-population to which an individual observation belongs. In [80], the mixture model-based technique is used to analyse for more general outcomes. The mixture model

can be express as

$$P(x|\theta) = \sum_{k=1}^K \eta_k l_m(x|\theta_k) \quad (2.16)$$

In this function,  $\theta$  is the parameters of this PDF,  $K$  is the PDF numbers.  $\eta_k$  represents the probability that the  $x$  belongs to the  $k$ -th selected PDF,  $l_m(x|\theta_k)$  is the  $k$ -th PDF. The mixture model simulates random variables by combining some significant PDFs.

### 2.3.3.3 The application of neural networks and deep learning on load modelling

A neural network is a set of algorithms that attempts to recognise underlying relationships in a batch of data using a method that mimics how the human brain works. In the [81], three types of the EV charging load forecasting model for the EV charging station are established by using neural networks and the Grey model, which are the BP neural network, RBF neural network, and GM(1,1) model. The idea is to analyse the data of a forecasting day, the same type of days in the past weeks will be chosen as the inputs to the forecasting model to predict the daily load curve of the forecasting day, then the result will be acquired based on the flexible factors and EV driver action. A selection of training databases is extracted from the preceding 70 days before the forecasting day in this paper.

Deep learning algorithms, which are aided by an unprecedented ability to learn from large amounts of data, offer novel approaches to solving difficult predicting problems. [82] provides a comparison of deep learning algorithms for forecasting PHEV super-short-term stochastic charging load by using long-short-term memory which is also used in [83] for building energy load prediction. In [80], the traffic flow around an EV charging park is predicted by using a deep learning based convolution neural network. The data from the M42 motorway between J5 and J6 in England for the first two months of each season are employed as the training data-set for the convolution neural

network model. Then the arrival rate at time  $t$  can be predicted by

$$\delta_t = \beta * P_t * f_t \quad (2.17)$$

where the  $f_t$  is the traffic flow around the EV charging park,  $\beta$  is the penetration of EVs,  $P_t$  is the probability that the EVs travelling around will choose to charge in the charging park.

#### 2.3.3.4 The application of the Markov Chain on load modelling

In [84], the author uses Markov Chain to represent variations in battery SoC by using three decision-making behaviours: driving, charging, and neither charging nor driving during the entire day of an EV owner's journey. The Markov chain model is a type of stochastic dynamic system that describes a system with a random state at each time and a state transition probability from one time to the next time that is only connected to the current state and its transition probability which is defined. In this model, the random state is the SoC of EVs, EVs have corresponding transition probabilities based on different decision-making behaviours. It is worth noting that the author classifies the chargers into fast and slow chargers. The decision is made based on the long statistics, hence the charging load can be predicted by using the coulomb counting and the SoC of EVs in the different time periods and their decisions.

In [3], Markov Chain is employed to represent the EV state transition from 'driving' (D), 'parking at home' (H), 'parking at workplace' (W), and 'parking at commercial areas' (C). Figure. 2.4 shows all the state transitions that could happen in the system. All state transitions have their corresponding possibility at each time slot based on imperial PDF Monte Carlo simulation. Based on that, the author could calculate the driving time, the charging time and the initial SoC of the EVs. In the model, the charging profile of BMW i3 in 2013 is employed as the charging data. The result shows that the initial SoC of EVs are 100% and those EVs are recharged back to 100% by the end of the day.

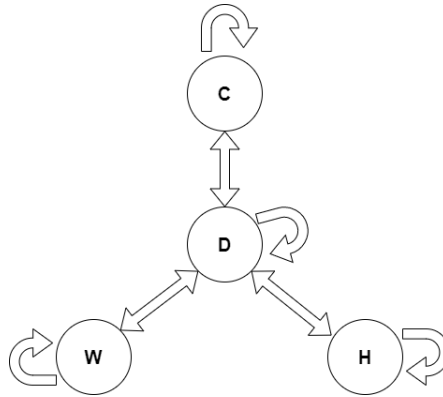


Figure 2.5: Possible cases of vehicle state transitions at time  $t$  [3]

### 2.3.3.5 The application of ABM on EV load modelling

Many papers discuss the EV charging load based on ABM as this method can show the details of each EV. In [85], each EV agent represents an EV driver and its vehicle. There are two other agents which are the electricity retailer agent and the EV aggregator agent, they are able to set the electricity price and manage the EVs' charging time to reduce the electricity price. In the provided system, the EV agents have their own EV model such as Nissan Leaf or BMW i3, etc. the main parameters of EV agents include the number of the daily trips based on a Poisson distribution function, travel distance per trip, destination, velocity, driving time and period, and social variables which contain a lot of different charging variables. The main advantage of ABM in [85] are:

1. Individual components that are independent and different which can be viewed as an EV model and mobility pattern for each EV owner.
2. The system is adaptable, EV's charging demand can be managed.
3. Location influence: the impacts of the charging point's position in the power network is considered.
4. Social interaction representation: different sorts of EV owners may have varied effects on the overall system.

[59] employs an agent-based methodology with NetLogo software. NetLogo is a multi-agent programmable modelling environment that allows agents to communicate, making it ideal for complex systems research. Thousands of agents can receive instructions and act autonomously at the same time. The author classifies the parameters of the agents (EVs) to the micro-level parameters and macro-level parameters. The micro-level includes: a category of EV which includes private and commercial EV; Range anxiety and battery capacity; Initial SoC and final SoC of EVs which are the SoC when an EV is arriving and leaving respectively; Mode of charging which includes fast and slow charging; charging time; parking duration; range anxiety and driver experience, the range anxiety refers to the fear of the battery being empty before arriving at the destination, the fear is influenced by the driver experience. The macro-level parameters are: the availability of the slots in the charging stations, velocity of EVs, number of EVs, type of day, purpose of travel, and charging cost.

### **2.3.4 Optimisation of EV charging station**

In brief, SEC can be divided into two types of control: decentralised and centralised. Decentralised control divides computation effort to individual EV charging sites [86], making it easier to operate and install for private use. However, due to a lack of global coordination, decentralised charging cannot attain system-wide optimal performance. A centralised system, on the other hand, uses aggregators to connect electricity markets, vehicle owners, and charging data of EVs, which is enabled by managing charging power across a large population of EVs [87, 88]. According to an EV owners' preferences, an EV aggregator groups EVs to provide new economic prospects in the electricity market, therefore, the market contribution of individual EVs can be improved.

#### **2.3.4.1 EV charging station aggregator**

Figure. 2.6 shows the potential activities aggregators can do, where the GENCO is responsible for providing the capacity of electricity generation

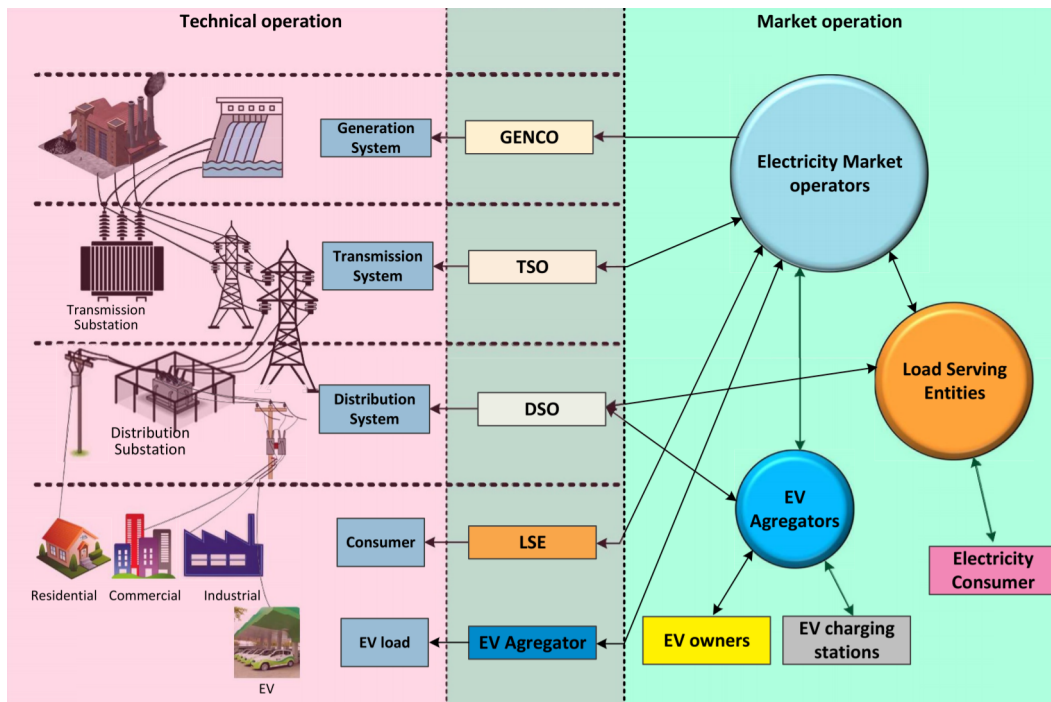


Figure 2.6: The aggregator functions and collaboration with other grid systems [4]

and ensures lucrative power generation; TSO is responsible for the transmission system's operation security as well as system service procurement such as operational reserve and frequency control; The businesses responsible for distributing and managing energy from generation sources to supplier or retailer agent are known as the DSO. LSE and aggregators are retailer agents which sell the electricity to end-user and bidding for electricity from GENCO. To EV owners, aggregators provide the real-time charging price and the number, and the locations, of available EV charging points, and the optimised EV charging curve for a limited power feeder. Aggregators could also estimate power demand behaviour for the next day and prepare their buy/sell prices for EVs. To the grid side or EV charging park owner, aggregators buy electricity from the market at lower prices and could sell them during daily peak power consumption period or use them to provide other ancillary grid services by taking advantage of their clients' EV storage capability through the link of the aggregators with the TSO.

### 2.3.4.2 Decentralised EV charging

Many papers discuss EV charging management from decentralised and centralised methods. In decentralised control, EV owners do not need to provide information of EVs such as SoC or the capacity of the battery, meanwhile, EV owners are able to choose their charging schedules based on the electricity price or other information from the upper level of the grid system such as the aggregator. The decentralised strategy achieves "valley-filling" in [89–91], which flattens the load profile by filling valleys in load curves, for example, scheduling EV charging from daylight to midnight to cover the nighttime valley in power demand. Decentralized charging might require the increased computation capability of EV chargers as the charger might be required to seek the best charging period for EVs based on the information from upper level. [92] provides a probability transition matrix which allows EV charging loads to be scheduled to fill the nightly load valley while still fulfilling the EV owners charging demand. The transition probability of transferring a EV charging load from time  $j$  to time  $i$  is represented by the elements of the probability transition matrix at the  $i$ th row and  $j$ th column. The aggregator calculates the probability transition matrix, EVs will upload their charging schedule based on the probability transition matrix and EV owner requirements such as preferring charging period, then aggregator calculated the total power demand of all EVs in new schedule, if the total power demand is still higher than the limit, the new probability transition matrix will be calculated repeatedly until all the EVs can be scheduled with total power demand lower than power feeder limit. A distributed algorithm is developed in [93] to tackle the decentralized EV charging problem and achieve the maximizing user convenience. Same with [92], each EV is only required to upload its power demand to the aggregator, and EVs only have two charging options which are charging or not charging. For the situation where the aggregator provides the same optimization instructions to all EVs, and EVs decides the charging power individually based on the instructions and individual parameters, this control also called distributed control [94].

In [94], the author provides a fully decentralized EV charging strategy

without communication among the aggregator and EVs, this method is an autonomous stochastic charging control strategy that employs power management control from the on-board charger. To achieve that, the on-board charger management system has to acquire a baseload profile (non-EV load) by analyzing historical load data on the power grid, and the daily baseload variations must be very small. However, from a practical perspective, the variations of daily base load are not always minimal, if the base load profile is not updated frequently for on-board charger or the way of analyzing historical load is not very accurate, valley filling by the method might be invalid. References [95, 96] provide a decentralised charging approach that optimises charging profiles for the following day through a negotiation process between the grid and EVs based on the grid's inelastic base load profile (non-EV load) forecast. The optimised charging profiles are then utilised the next day to plan EV charging with the goal of keeping the overall load curve flat (base load plus aggregate EV load). However, the optimisation requires extremely precise load profile prediction and all data of EV charging demand must be known before their arrival [97].

Decentralised charging control around frequency regulation is proposed in [98, 99], where EVs function as producers or energy receivers, preventing the grid frequency from decreasing or growing through bi-directional power transfer. The technical drawback of this technique is that the total combined EV power is unknown (decentralised scenario), which makes balancing the system more difficult for the electrical grid operator.

Reference [64] introduces two decentralised charging strategies for EVs charging management with a limited transformer power to reduce the ageing of a transformer. Method one first calculates whether there is enough capacity of the transformer to facilities the charging through receiving the EVs charging demand information from each EV, if there is enough, the EV charging park will provide charging on a first come first served for all EVs, otherwise, the charging request will be denied. The second method builds the connection of charging cost with the charging urgency level, along with the charging urgency increasing, the price of electricity rises, assuming the customer accept this method, EV owners may choose to receive more charge

urgently. If the EV has a high priority charging requirement, there will be a higher chance of obtaining a charge than if the EV requires charging less urgently.

Building an EV charging station consumes a lot of time to work with the power grid, since there is a lot of infrastructural work and planning that goes into such projects, meanwhile, the local grid must be taken into account. Volkswagen and a developer E.ON [100] provided a solution that directly integrated BESS with an EV charger, and the charger called Drive Booster draws power from a standard power outlet found in any supermarket, like a soda machine. The charger can charge two EVs at once at speeds of up to 150 kW. The battery has a capacity of 193.5 kWh and is charged between charging sessions and at night, during off-peak hours. The aim of the Drive Booster is to make fast EV charging stations easier for anywhere without the need for major infrastructure construction.

#### **2.3.4.3 Centralised EV charging**

In a centralised architecture, a central aggregator is employed to collect data from EVs, and process it centrally, and deliver a globally optimal solution that takes into account all user constraints and grid information to deliver a smoothing aggregated electric load profile in a region and minimise system-wide electricity cost. The advantage of centralised EV charging compared with decentralised charging is centralised charging provides the guarantee to reach the global optimal solution for the overall system, but individual EV users might have peaks in their charging profiles resulting in high costs or longer charging periods [4, 101].

Conventional centralised EV charging research mainly focuses on the optimisation of power management methods to achieve "valley-filling". In [102], a double-layer optimal charging method is introduced to minimise EV charging load variance, in the first layer, the central control allocates electricity sources to each charging station. In the second layer, the electricity allocated from the first layer is planned to each EV charging device which is connected to the same node transformer, by doing this, the large-scale computing re-

quirements are converted to several small groups, but this method might not be a sensible strategy for global optimisation. Another double-layer smart charging strategy is proposed in [102], the first layer help EVs to reach the most suitable charging station by considering transformer power demand, transformer capacity and charging station status, the shortest way algorithm is used to guide EVs to charging stations. The function of the second layer is to reduce the charging cost by considering the dynamic pricing and minimising peak demand. A receding horizon control framework is proposed in [103], RHC is a general-purpose control scheme that makes a decision on EV charging strategies for each time step (e.g. every 10 minutes) by using the prediction of the non-PEV load profile and charging demands of EVs connected inside this system within the pre-set prediction time horizon (e.g. 24h) and the information of current charging demands. In this framework, a two-stage hierarchical optimisation is introduced to calculate the energy constraints by utilising the charging information to reduce the computation complexity, however, lots of forecasted data might bring uncertainties. Time-of-use pricing has been widely adopted in the electricity market, in [104], the difference of the retail electricity price and the market price is employed to seek the balance between the profit of EV park owners and the satisfaction of customers. Customers specify their charging requirement when they arrive in the EV charging park, an admission control mechanism is introduced to guarantee all admitted EVs can be charged to the target SoC before their departure. EVs are refused entry if the algorithms calculate that their charging requirement will unbalance the current charging strategy and/or reduce potential profit. In [105], quality of service is provided to measure user satisfaction, the capacity of an EV charging station and the type of chargers are optimised to achieve the minimum investment cost of the EV charging station for its owner and meet a certain quality of service for EVs by using the chance-constraints method. The quality of service in this paper is defined based on the various charging delay levels and the satisfaction of EVs charging demand.

#### **2.3.4.4 Renewable energy integrated centralised and decentralised EV charging**

Significant PV penetration can result in a number of drawbacks, including component overloading and voltage fluctuations, adding EV charging load with PV can improve PV self-consumption and reduce EV loads on a distribution network [106]. The research incorporates PV and BESS into centralised EV charging to reduce the loads in high power demand periods of the power grid.

The local distribution network among multiple chargers, PV, and BESS can be AC or DC transmission. Figure. 2.7 shows the AC-connected system and DC-connected system. For the AC-connected system, the number of conversion stages between the distribution network and the DC port of the EV, PV or BESS is greatly increased with this strategy, which leads to an increase in the system's complexity and reduces the system efficiency. The advantages of using the AC bus include well-established standards and the maturity of related electrical equipment such as rectifiers and inverters, by contrast, a DC-connected system has fewer conversion stages, higher system efficiency and lower system installation cost, however, the DC protection, DC metering, and standards are issues for this method [50].

To reduce the load variability resulting from PV generation and EV charging loads, [106] investigates the PV integrated EV charging and household electricity consumption at residential buildings from a decentralised and a centralised EV smart charging system. For the decentralised charging, EV energy demand, the electricity consumption of a single household, and PV power generation, EV arrival and departure time are the input of the optimisation formulation, to describe load variability, the population variance equation was employed and it could be minimised by adjusting the charging rate and charging time. For the centralised charging management, instead of using data from a single household, the elements in the population variance equation are considered from multi-users levels such as the electricity consumption of all households and PV power generation, the centralised charging management would minimise the load variability of the whole res-

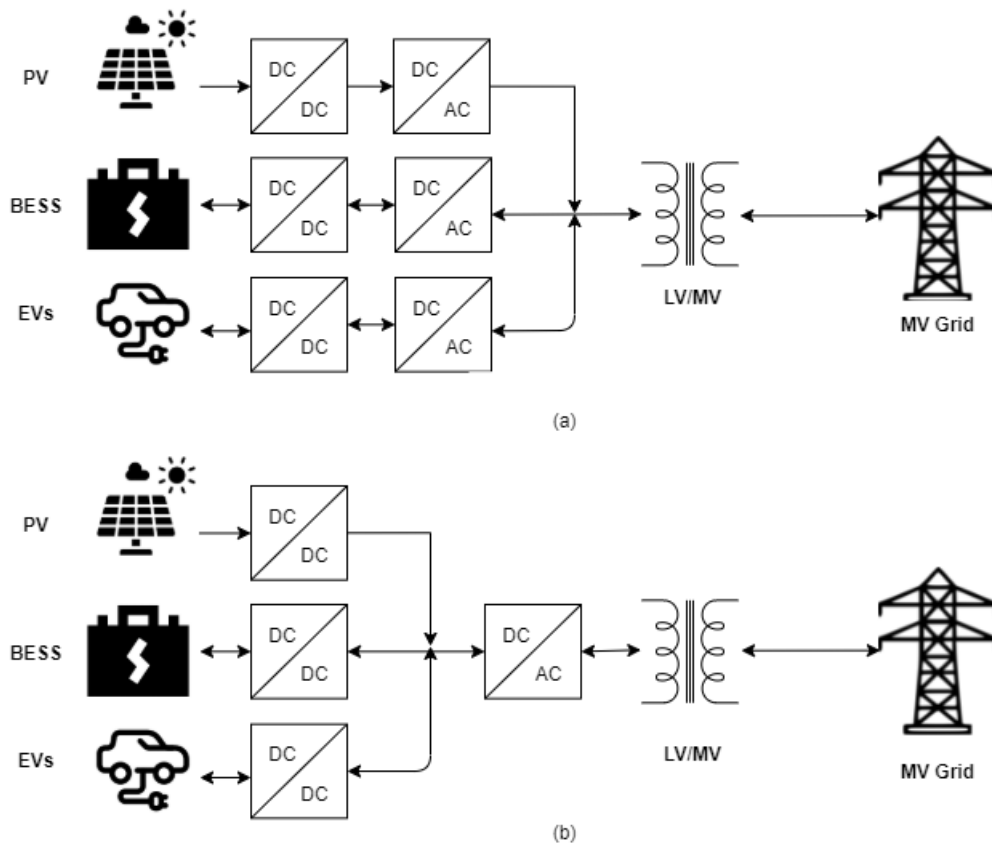


Figure 2.7: AC-connected system and DC-connected system

idential buildings. The results reveal that from multi-users, the centralised EV charging has better performance on reducing load variability.

In [107], the authors introduced an EV charging park with renewable energy and non-renewable energy supply, a group of EVs with an EV leader is considered as an EV platoon coming into the charging park, A queuing system including first-come-first-serve and random selection are employed to pick up platoons to charge from the waiting EV platoon lists. In the model, renewable energy is the main energy source to supply the EVs, if the EVs power demand exceeds the generated renewable power, the difference will be provided by a non-renewable feeder. However, PV power depends highly on the weather and season, once the EV power demand is far higher than the real-time PV power generation, this method has limited success in reducing

the load on the grid.

The research [108] adds an additional BESS for storing energy with power transferring modes presented to address the energy flow among the facilities, which are PV to EV, BESS to EV, PV to BESS, Grid to EV, and PV to Grid. The BESS exports energy to EVs when PV is insufficient for EVs charging, and be charged by PV when there is surplus PV energy after supporting EVs.

In [109], the author presents storing the energy in the BESS from the grid based on the pricing on the electricity market in Singapore. When the real-time electricity price is lower than a defined price, and the surplus PV energy cannot fill the BESS, the energy will be imported from the grid to the BESS, this energy will be further used to charge EVs. This method enables the BESS to supply more energy directly to EVs to reduce electricity demand from the grid in high load periods.

The above papers provide the methods of utilisation of renewable energy in EV charging stations, [110] proposes a novel method to design the power generation planning of renewable energy in EV charging stations. The author firstly uses HOMER® Pro software to generate a list of different configurations for the system by inputting the local renewable resources and EV charging station demand and then performs a new multi-criteria analysis to assess them to get the most suitable renewable energy power generation planning for EV charging station based on economic, environmental and technical parameters.

EV charging parks containing many EV charging points provide an opportunity to manage the power flow compared to unmanaged isolated charging points. Centralised control of all EV charging points can support control for power-limited electricity feeders and can provide V2G services. This centralised charging coordination can provide SEC and ancillary services such as frequency response to the grid. [49]

#### 2.3.4.5 The concept of V2G and its economics

Kempton and Letendre first proposed V2G [111]. V2G is considered a beneficial technology for vehicle owners and the grid, it provides profit for the vehicle owners when they feedback electricity energy to the grid under certain conditions. These services may include regulation (second by the second balancing of demand and supply), spinning reserve, and peak power provision, load levelling and reactive power compensation [112].

The concept of V2G is that every EV can be seen as a mobile power source, which stores electricity from the grid. However, this stored electricity may not be used when the grid is in high demand condition, so V2G technology will return this unused electricity to the grid when it is in high demand condition and will store electricity in vehicle batteries when the power grid is in low demand condition. According to [113], there could be 90% of EV vehicles available for V2G at any given time. Meanwhile, the research on fast charging and battery has become very popular. The development of these advanced technologies provides a huge potential for V2G. The faster EV charging speed, the higher the flexibility in the EV charging period. The larger capacity of EVs batteries can meet higher demands from the grid and EV owners. Reference [114] summarises that V2G offers benefits to the grid including both the TSO and the DSO. The most popular topic of V2G for TSO services was providing auxiliary services, frequency regulation; The other two topics, dealing with grid intermittency on the grid and peak shaving, were frequently addressed together. For DSO services, V2G is utilised to resolve local electricity congestion and reduce the cost on upgrading the local transformers, electrical cables.

For the economic benefits of the vehicle to grid, V2G revenues are estimated to be about 900 Danish kroner (€120) per month based on the income potential of the pilot project in Denmark [114]. V2G economic data was analysed in [115] in three U.S. cities, authors use hourly electricity prices to calculate the daily profit, the battery degradation was considered as the economy loses. The results show that the maximum annual profit could be \$142-249 without considering the losses of battery degradation, and \$12-118

with the cost of the battery degradation. [116] analyses price data of the V2G experiment that was held in New York City area from 2010 to 2014 by using the Tesla Model S and Chevrolet Bolt. The author finds that the one-way power efficiency and battery lifetime have a significant impact on the economics of V2G. The extra cost might lead to low economic benefits for electric vehicle owners to sell electricity back to the grid. Especially, if it results in higher battery degradation. Therefore, V2G might not be attractive for EV owners given the current economic benefits. However, the potential economic benefits of V2G technology have shown a positive trend over the last few years. Carbon dioxide tax to the normal vehicles will promote V2G adoption, which provide additional opportunities for V2G economics. Along with the development of smart grid technology and market, V2G services will have more opportunities to seek profits in different areas such as lifesaving by providing electricity to hospitals when the grid suffers a power outage.

V2G can be used to do frequency regulation for the grid. The number of researchers investigating frequency regulation using V2G are minimal, although some papers named their paper as frequency regulation, it is actually valley filled grid service.

For a system, the frequency deviation is mainly caused by the mismatch between the load and generation. [117] calculates mismatch power based on the grid frequency and the area control error, and gets the required regulation power based on PI control and calculated mismatch power. The grid frequency is divided into three zone by two trigger points, in the range between two trigger points, the grid does not request any response. In other zones, aggregators will allocate the required regulation power for EVs by sending global control signal. When EVs respond to the global control signal, their original charging schedules and preferred charging requirements are disrupted in order to achieve frequency regulation. [117] also provided a state recovery strategy to reduce the disturbance of regulation service to EVs' charging preferences, the strategy controls EVs back to their charging schedule with conventional generator power supporting when the grid does not request any response, the authors also set the upper/lower boundary for EVs power to reduce the disturbance of frequency regulation. In [117],

the power regulation cases mainly focus on the frequency deviation resulting from the local wind generator, in the real-world, the frequency deviation might be caused by several reasons such as the fluctuation of PV power and market power demand. Responding to the grid frequency might request more power from EVs, hence a threshold of maximum regulation power with the grid is necessary to prevent EVs deep discharging even with power support from a conventional generator. In addition, EVs can not always provide the required power due to reaching SoC limits, if there is no other electricity storage system, the power capacity of frequency respond will have significant change over time, which is not preferred by the grid.

[118] provides a method that using EVs to provide frequency response, the service in Great Britain (GB) is called dynamic frequency response. The EV charging/discharging power is regulated using a droop control mechanism in response to the frequency signal. To ensure that adequate energy in the EV battery for user travel at the plug-out time, a forced-charge boundary and a forced-charge area are proposed. However, providing the dynamic frequency response in GB might request a contracted maximum power, the dynamic EV numbers in the charging station might not meet the this requirement at all times.

[119] develops an energy management system to integrate V2G technology in a residential scale micro-grid which includes PV and BESS, EVs in this research only provide frequency regulation when the SoC of the EV battery exceeds a user-defined threshold, the frequency is also divided three parts by two trigger points, the regulation power from EV changes along with the grid frequency, the maximum regulation power is set as the maximum EV charging/discharging power when the grid is under the maximum frequency deviation. However, in the developed system, BESS is only for domestic load, which means the EV owner has to reserve a minimum SoC level for frequency regulation, even though, the EV charging status might jump between normal charging and V2G mode. However, the grid prefers a stable frequency regulation unit, but not an uncontrollable unit, and EV owners may find it conflicting to choose a reasonable and expected SoC threshold for self-use and V2G service.

## 2.4 Conclusion

In this chapter, the background and presented research for this thesis have been provided. The first section describes the fundamental information of EV, such as EV classification and trend and charging parameters, a conclusion of the necessity of SEV is drawn based on the background. The second section introduces some basic knowledge of PV. In the third section, several EV charging load model strategies and parameters are introduced. Meanwhile, this section provides popular researches on how to optimise EV charging to shift EV peak load, and reduce the capacity of the power feeder. In the end, some basic knowledge of the V2G concept and the application are provided.

# Chapter 3

## SECP model

### 3.1 Introduction

A SECP model requires the calculation of the EV charging load to be driven by a specific modelling strategy and the parameters. It has been discussed in Chapter 2 that the parameters of the EV charging load can be classified into indirect factors and direct factors, to further sort these parameters, queuing theory, neural networks, Markov Chain and ABM have been introduced. In this chapter, an ABM method is employed to simulate SECP and calculate EV charging load. A system is modelled as a collection of independent decision-making units called agents in ABM. Each agent analyses its circumstances independently and takes decisions based on a set of rules. ABM is characterised by repetitive competitive interactions between agents [120]. The bottom-up method replicates the system by coupling all of the agents. In this chapter, each EV is considered to be an agent and autonomously decides its parameters, such as EV brand (including charging power, capacity of battery), charging time, charging period, energy consumption, etc. The decisions are based on some rules acquired by the Monte Carlo method.

The advantages of using ABM for SECP are:

1. The details of each agent charging process in each time slot can be observed. Then a relevant optimisation can be applied to the model accordingly to achieve a better charging performance.

2. ABM can produce some events which have a low probability of occurrence in real life; these events will help us face emergencies in advance and propose corresponding solutions.
3. ABM allows for competitive interactions between agents. For an SECP with a limited power feeder, the total power demand of EVs in different time slots might exceed the power capacity of the SECP feeder. ABM gives us a chance to allocate power for these EVs based on various algorithms.

Many papers which build EV charging load models concentrate on the distribution of EV charging points in some particular areas such as commercial or residential places. In this research, a SECP including fast and slow chargers is modelled to explore the relationships between the SECP, EV owners and the grid. Different from a gas station, vehicles leave quickly once their requests are met, a SECP provides chargers for EV charging and allows EVs to park for long periods of time. Longer duration parking gives SECP a chance to utilise their batteries as energy storage units to import/export electricity and provide grid services (the details are introduced in Chapter 5).

The ABM of SECP is simulated in MATLAB. The real-time total charging power requirement of the SECP depends on the number of connected EVs, the charging power profile of each EV and its current SoC. Therefore, simulation of SECP traffic flow and the SoC of each EV is required. The main parameters include EVs' and SECP's.

## **3.2 The parameters of EVs and SECP with their setup**

### **3.2.1 Daily driving distance of an EV ( $L_d$ )**

$L_d$  represents the mileage of an EV in a day, a longer driving distance of EVs results in more electricity demand. Hence, in a SECP, daily driving distance is a vital parameter related to the charging period of an EV in a certain

charging power level. The daily driving distance mainly connects to the EV owners' commuting distance and driving experience.

Table 3.1 shows the vehicle mileage and occupancy in 2017 in the UK, which is reported by the UK Department of Transport [58]. The median value of each range of annual mileage in Table 3.1 is chosen to represent the average yearly mileage of an EV ( $L_a$ ) for each range, where the daily drive distance is calculated by:

$$L_d = \frac{L_a}{365} \quad (3.1)$$

In this case, the probability density function (PDF) of daily driving distance is then directly expressed in Figure 3.1 based on the Monte Carlo method.

### 3.2.2 Daily energy consumption of an EV ( $E_d$ )

Daily energy consumption of an EV is limited by a few parameters, such as driving experience. For example, varying driving speed leads to more

Table 3.1: Annual mileage of cars in England and energy consumption

Annual Mileage (Miles)	Percentage (%)	Average Daily Energy Consumption (kWh)
0-499	1	0.208
500-999	1	0.623
1000-1999	5	1.245
2000-2999	6	2.075
3000-3999	8	2.905
4000-4999	7	3.736
5000-6999	22	4.981
7000-8999	16	6.641
9000-11999	17	8.716
12000-14999	8	11.207
15000-17999	4	13.697
18000-20999	3	16.188
21000-29999	1	21.168
30000+	1	24.904

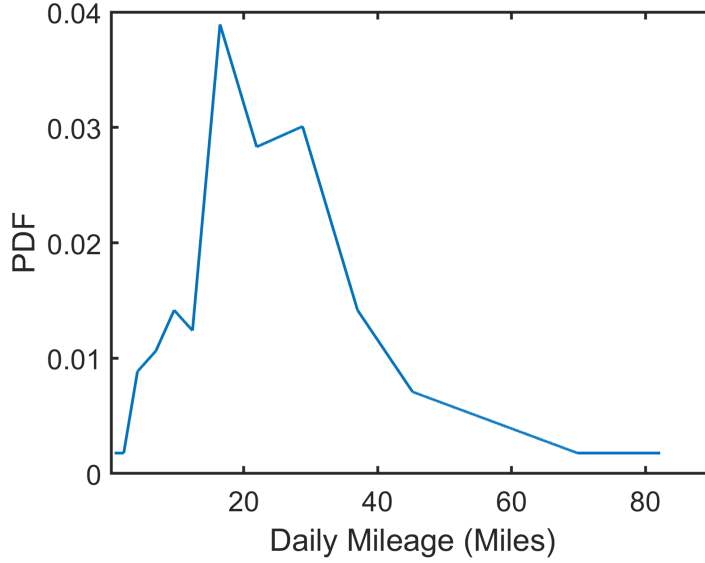


Figure 3.1: PDF of daily mileage

energy consumption compared with constant driving speed. Meanwhile, most modern EVs are equipped with regenerative braking systems, which is an energy recovery device that slows down a moving EV by transforming its kinetic energy into a form that may be utilised right away or stored into a battery for later use, which increases the efficiency of EVs, however, this makes the prediction of the energy consumption of EVs more difficult from technical analysis. Hence, the energy consumption is predicted based on the historical experience data.

The daily energy consumption of an EV in this research is transferred using the Equation below:

$$E_d = L_d * E_{ev} \quad (3.2)$$

In this equation,  $E_d$  is the average daily energy consumption for an EV (kWh), and  $E_{ev}$  is the average energy consumption of different brands of EVs (kWh/mile). Based on  $E_{ev}$  of 0.304 kWh/mi of EVs in 2019 [48] and Equation 3.2, the  $E_d$  is then calculated and shown in the third column in Table 3.1.

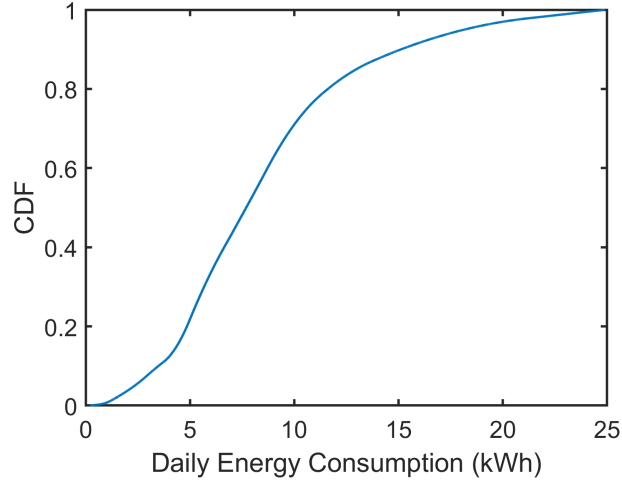


Figure 3.2: CDF of daily energy consumption

The PDF of daily energy consumption of each EV ( $f(x)$ ) could be generated based on the PDF of daily drive distance and Equation 3.2. The CDF of daily energy consumption,  $F(E_d)$ , can be calculated using the function:

$$F(E_d) = \int_0^{E_d} f(x)dx \quad (3.3)$$

The result is shown in the Figure. 3.2. Inverse transform sampling method is then used to generate random daily energy consumption based on Figure. 3.2. Inverse transform sampling is a method for randomly selecting sample numbers from any probability distribution by using its inverse CDF.  $E_d$  is generated by:

$$U = Unif(0, 1) \quad (3.4)$$

$$E_d = F(U)^{-1} \quad (3.5)$$

where  $Unif$  represents the uniform distribution,  $U = Unif(0, 1)$  means generating an independent random variable  $U$  between 0 and 1 based on a uniform distribution.  $F(U)^{-1}$  is the inverse CDF of daily energy consumption.

tion. This can also be used to understand that a daily energy consumption with a higher probability in PDF is likely to occupy a longer x-axis in the inverse CDF, random numbers generated from 0 to 1 have an increased chance to fall into this area.

### 3.2.3 The initial SoC of EV ( $SoC_{initial}$ )

In AMB of SECP,  $SoC_{initial}$  represents the SoC of an EV at the moment of connection to a charger. In reality,  $SoC_{initial}$  might be impacted by a lot of factors, such as EV owners' working time, or charging habits. Although there are some probability distributions that describe how  $SoC_{initial}$  EV owners prefer to manage the SoC of their EVs, these probability distributions are obtained via end-user surveys. They might vary in different areas where the penetration of EVs or the charging habits are determined.

In this research, the daily SoC drop of an EV ( $SoC_d$ ) can be expressed as:

$$SoC_d = \frac{E_d}{E_{cev}} \times 100\% \quad (3.6)$$

where  $E_{cev}$  is the capacity of the EV battery in kWh.  $E_d$  is generated for each EV based on the PDF of daily drive distance

Subsequently,  $SoC_{initial}$  can be represented as:

$$\begin{aligned} SoC_{initial} &= SoC_{ll} - SoC_d \\ &= \left( \frac{E_{cev} * SoC_{ll}}{E_{cev}} - \frac{E_d}{E_{cev}} \right) \times 100\% \\ &= \frac{E_{cev} * SoC_{ll} - L_d * E_{ev}}{E_{cev}} \times 100\% \end{aligned} \quad (3.7)$$

where  $SoC_{ll}$  represents the SoC of EV on its last departure.  $L_d * E_{ev}$  is a random value based on the previous section.

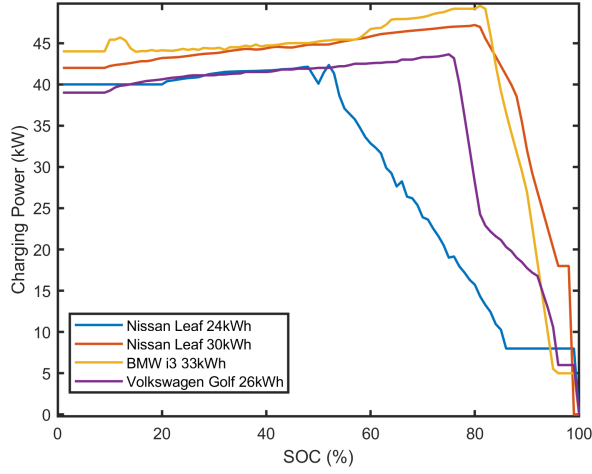


Figure 3.3: Charging power vs SoC of tested EV brands

### 3.2.4 EV types

Different EV brands might lead to various battery capacities and charging curves when EVs connect with the same charger and charge with the same charging level. In the model, 4 types of EV are considered, which are two types of Nissan Leaf, BMW i3, and Volkswagen Golf; the proportion of them in the SECP are based on their registration for the first time in GB during 2019 [121], and their details are provided in Table 3.2. The Nissan Leaf is the most popular EV type with the highest registration number in 2019 of 53,000, followed by BMW i3 and Golf being 41,000 and 38,000 respectively. The EV brand of an EV in the model is randomly generated corresponding to their registration number by using the inverse transform sampling method. How their charging power changes with time can be seen from Figure. 3.3, the

Table 3.2: EVs battery capacity and their registration number

EV Types	Battery Capacity (kWh)	Registration Number
Nissan Leaf	24kWh/30kWh	53,000
BMW i3	33kWh	41,000
Volkswagen Golf	26kWh	38,000

charging power is controlled by the EV's BMS based on DC CCS standard ( $P_{Bmax}$ ). The SoC vs  $P_{Bmax}$  profiles for the different EV types are obtained from sources that experimentally measure this relationship in [122]. Most of the experiments end the charging at approximately 90% SoC, according to [123], when SoC is greater 90%, the charging power of EVs show slight changes until about 99% SoC. Hence, in this model, we use this assumption to plot the entire charging curve from 0% to 100% SoC where the last 10% is slightly lower than the last experimental data point. From the graph, we can see the charging power at the beginning shows a slight uptrend. Nissan Leaf 24kWh starts decreasing sharply at the end of 55% SoC, then the other three drop significantly at about 80%. The charging power for all of these vehicles drop to 0 kW as the SoC of the vehicle approaches 100%.

### 3.2.5 EVs charging power

The real-time total charging power requirement (also called total EV load) of the SECP depends on the number of connected EVs, the charging power profile of each EV and their current SoC. In this section, EV charging power is investigated.

Research [124] proposes that the EV charging power ( $P_{Amax}$ ) could be represented by:

$$P_{Amax} = \min\{P_{Umax}, P_{Cmax}, P_{Bmax}\} \quad (3.8)$$

where  $\min$  means choosing the minimum value from  $P_{Umax}$ ,  $P_{Cmax}$ , and  $P_{Bmax}$ .  $P_{Umax}$  is the maximum charging power of an EV set by the EV user and  $P_{Cmax}$  is the maximum output power of an EV charger.

In the ABM of SECP, EV users are not allowed to choose  $P_{Umax}$  as forecasting  $P_{Umax}$  requires large amounts of customer data. Therefore, the system maximum charging power ( $P_{Smax}$ ) is used to replace the  $P_{Umax}$  and  $P_{Cmax}$ .  $P_{Smax}$  is the power allocated to each EV by an aggregator in a fair way for each customer based on some charging management methods (these methods will be introduced in chapter 4). For an SECP, the total EV charging power requirement could be very high, taking an example of 50 EVs, with the

maximum charging power individually being 50kW, the total EV load of the SECP could reach 2.5MW. For a given SECP location, there is likely to be a limit on electrical capacity due to local electrical network constraints, and upgrade through re-enforcement is often physically complicated with long lead times and costly. Furthermore, on the GB grid, connections are subject to a fixed capacity charge based on £/MW/Day at the maximum potential power requirement regardless of actual usage. Controlling  $P_{Smax}$  can reduce the peak power demand and therefore reduce the overall power requirements from the local power feeder thus reducing this cost. Equation 3.8 is then transferred to:

$$P_{Amax} = \min\{P_{Smax}, P_{Bmax}\} \quad (3.9)$$

where  $P_{Bmax}$  can be acquired by matching the real-time SoC of an EV ( $SoC_R$ ) with the charging profile of SoC vs  $P_{Bmax}$  [124]. The charging profiles of the four types of EV are shown in Figure. 3.3. For instance, a BMWi3 at 75% SoC will demand  $P_{Bmax}$  of 49kW at that instant.

In applications where energy transferred to/from the battery is measured in kWh, the integration of the terminal voltage multiplied by battery current is required, which is useful in cases where the real power transmitted between system assets is critical [13].

According to [13],  $SoC_R$  is given as :

$$SoC_R = \frac{\alpha * \int_{T_{in}}^T P_{Amax}}{E_{cev}} \times 100\% + SoC_{initial} \quad (3.10)$$

$T$  is the current time, and  $\alpha$  represents the charging efficiency. According to Figure 3.3 and Equation 3.10, when  $P_{Amax} = P_{Bmax}$ , the relationship of SoC from four types of EV vs time and corresponding charging power vs time are calculated and shown in Figure. 3.4 and Figure. 3.5 respectively. From Figure. 3.4 we can see that the Nissan Leaf 30kWh is the first EV reaching 100% SoC at 45 minutes, followed by the Volkswagen Golf 26kWh at 54 minutes, BMW i3 33kWh at 65 minutes, and Nissan Leaf 24kWh at

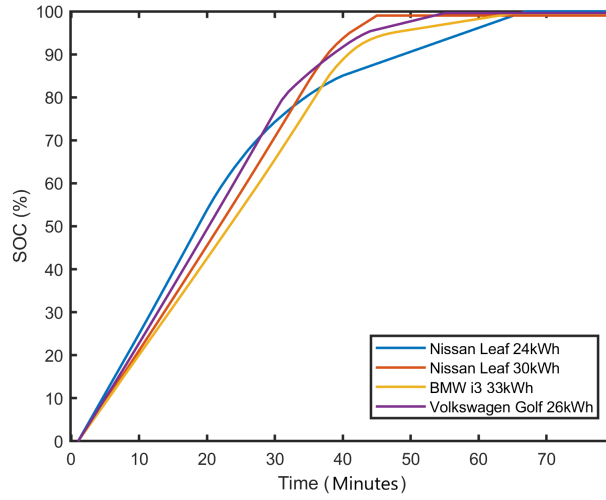


Figure 3.4: SoC vs time charging profile of tested EV brands

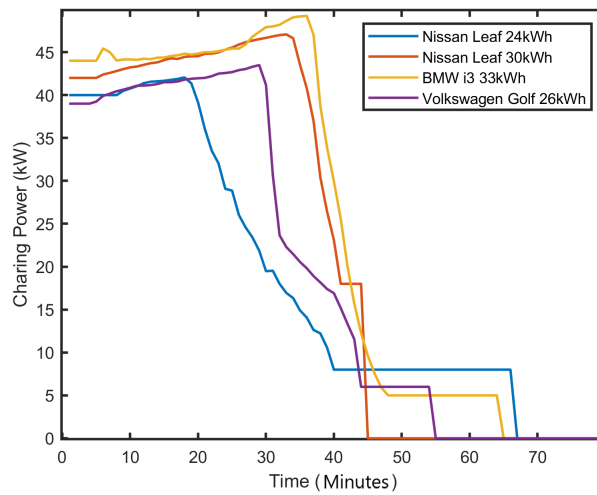


Figure 3.5: Charging power vs time of tested EV brands

67 minutes. According to Figure. 3.5, the charging power of the Nissan Leaf 24kWh decreases after 18 minutes, followed by the Volkswagen Golf 26kWh reducing after 28.5 minutes, whilst the Nissan Leaf 30kWh is lower after 34 minutes and the BWM i3 after 36 minutes.

EV drivers might choose to charge their EVs with lower power to minimise the degradation of the battery [125]. Based on mode 2 in the IEC62196

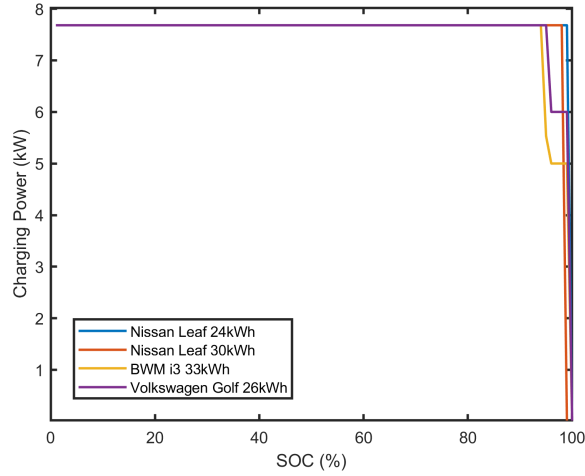


Figure 3.6: Charging Power vs SoC by adjusting the charging power of the DC fast charging points to a maximum of 7.68kW

protocol from Table. 2.1, the maximum slow charging power ( $P_s$ ) is 7.68kW, this protocol is widely employed in the UK. To simulate this, the charging power from the DC fast charging points are scaled to a maximum of 7.68kW once customers request slow charging. We can then plot the charging power profile vs SoC for four types of EV as shown in Figure. 3.6. The slow charging power is supported by DC fast charging points in this model, hence the charging profile is still modelled by using the fast charging equation based on Figure. 3.3 and Equation. 3.10. The result might be different with mode 2 AC charging.

### 3.2.6 EVs charging period ( $T_p$ )

An EV charging period can indirectly affect the EV charging load since EV charging power varies with charging time. Occupying a charging point for a long time might result in no charging points left for other EVs. In this model, we also need to consider that an EV might be requested to provide ancillary grid services where the EV charging period can be used to estimate the period when the EV could provide ancillary grid services. The charging period of each EV is directly related to SECP traffic flow.

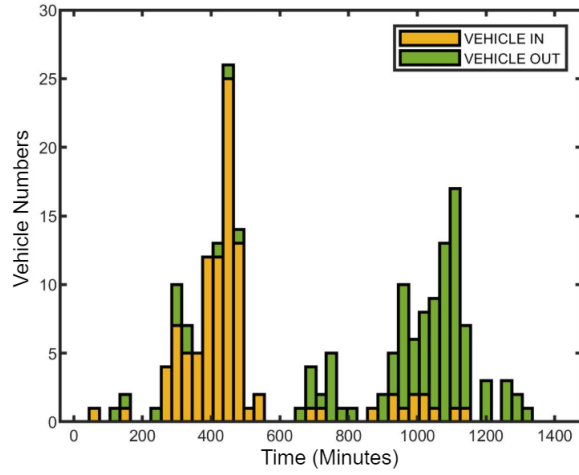


Figure 3.7: The traffic flow of the car park in 24 hours on a weekday

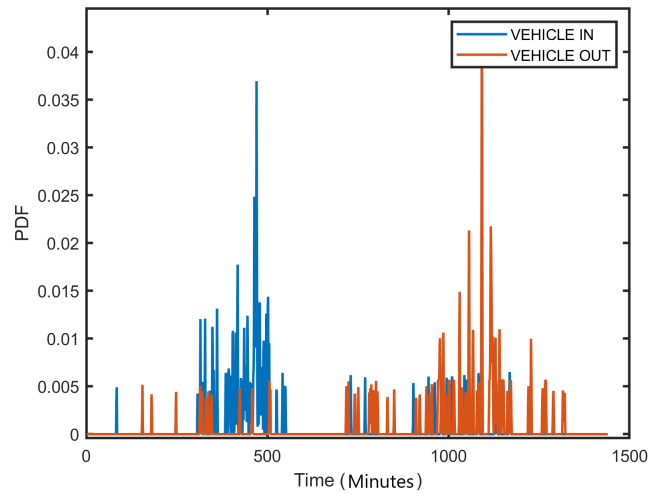


Figure 3.8: PDF of traffic flow (Hainault Station in London)

To formulate  $T_p$ , real-world car park data (Hainault Station in a commercial area of London) is acquired from Transport for London, seen in Figure. 3.7.  $T_p$  can be represented as:

$$T_p = T_{out} - T_{in} \quad (3.11)$$

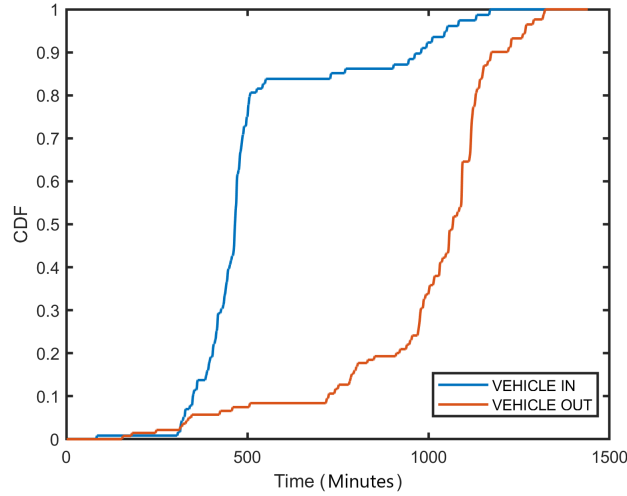


Figure 3.9: CDF of traffic flow (Hainault Station in London)

$T_{in}$  and  $T_{out}$  are the time when an EV arrives and departs the SECP. A PDF, a CDF and inverse transform sampling method is employed again to generate  $T_{in}$  and  $T_{out}$  randomly for each EV based on the vehicle park in Figure. 3.7. For example, from Figure. 3.7, at around 450 minutes, the highest number of vehicles arrives at the real-world car park, so  $T_{in}$  has the highest probability of being equal to 450 minutes in the traffic flow simulation. The PDF and CDF of traffic flow are indicated in Figure. 3.8 and Figure. 3.9 respectively. The process of generating  $T_{in}$  and  $T_{out}$  is similar to the steps to produce  $E_d$ .

$T_p$  of each EV is then calculated based on Equation. 3.11. The simulation results of  $T_p$ ,  $T_{out}$  and  $T_{in}$  of all EVs have been demonstrated to be a good approximation of the original EVs' traffic flow in Hainault Station. Figure. 3.10 shows the comparison of real park occupancy and one random simulated occupancy.

The model is configured with the capacity of the SECP. During the simulation, the number of EVs leaving and entering is managed to ensure that the model maintains the number of available spaces and ensures that the number of EVs entering the SECP does not exceed the capacity.

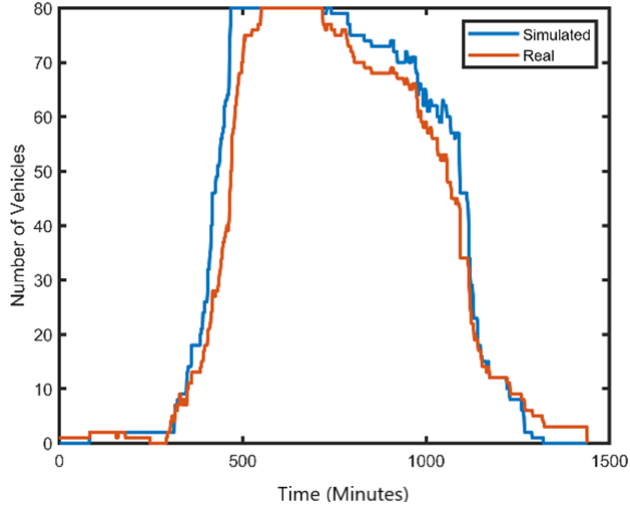


Figure 3.10: The comparison of real park occupancy and one random simulated occupancy

### 3.2.7 The penetration of DC fast charging ( $R_p$ )

In the simulated SECP, it is presumed that every charging point is equipped with DC charging facilities, however, EV users are allowed to charge their EVs with slow charging power ( $P_s$ ) if their charging needs are not urgent and slow charging might prolong their EV battery life [125]. It is clear that the total EV charging load will vary depending on the mix (penetration) of fast and slow charging. The estimation of the EV load under different penetration levels of DC fast and slow charging can also help the SECP owner to estimate if the power range of the local feeder can supply the total EV load, if not, the SECP owner can reduce the penetration (allowable number of fast charger selections by the user) or the charging spaces.  $R_p$  is represented as Equation. 3.12. The number of fast charging EVs ( $N_f$ ) and slow charging EVs ( $N_s$ ) are indicated in Equation. 3.13 and Equation. 3.14 respectively.

$$R_p = \frac{N_f}{N_p} \quad (3.12)$$

$$N_f = N_p * R_p \quad (3.13)$$

$$N_s = N_p * (1 - R_p) \quad (3.14)$$

where  $N_p$  is the number of EVs charging in the SECP.

### 3.3 EV load model and results

In this section, the EV load model is introduced using the parameters presented in the previous section to simulate the charging loads of the EVs. A sensitivity analysis is carried out to investigate the load of the SECP on the grid and the EV charging behaviour as the penetration of fast charges is increased. Figure. 3.11 shows the model of the EV load calculation for each time slot by the provided parameters. It should be noted that before the time loop, all traffic flows and EV initial conditions have already been generated, the details of how to generate these parameters have been well introduced above. The loop only checks the space availability and calculates the required outputs.

The proposed model is simulated for a weekday over a 24 hour time period from 12:00 midnight to 11:59pm. All the parameters of the SECP are

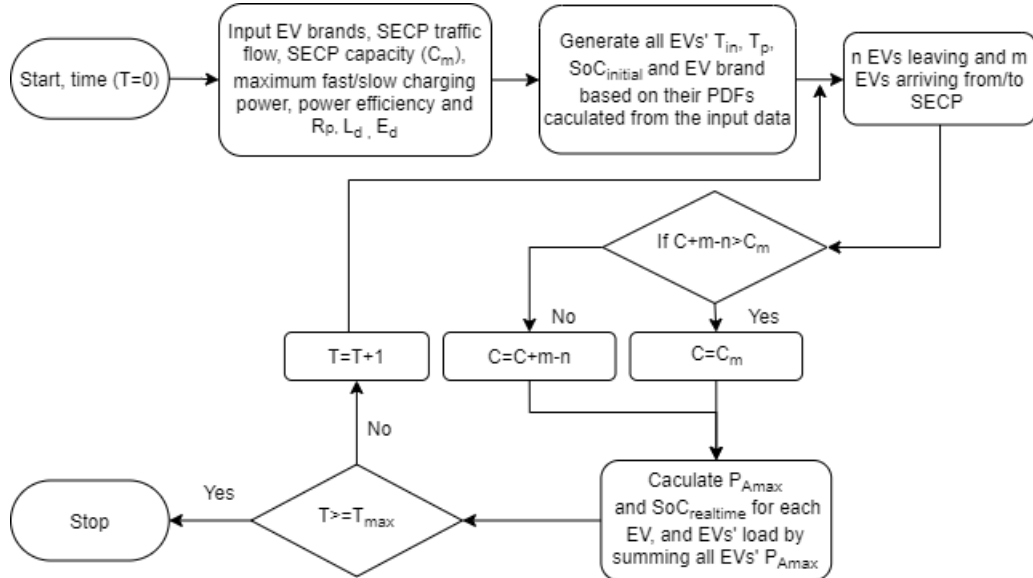


Figure 3.11: Diagram of EVs' load procedure of SECP

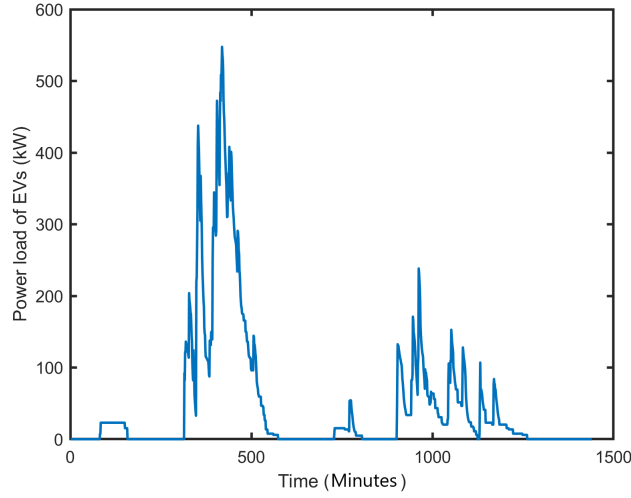


Figure 3.12: EVs power load vs time

indicated in Table 3.3.

Figure. 3.12 shows the total EV power load on a weekday. From the figure we can see that the charging power of the first wave increases from 81 to 84 minutes. According to Figure. 3.13, from 81 to 84 minute, three EVs come into the SECP and charge with slow chargers, the total charging load reaches the maximum charging power of 23.04kW in this wave. The total EV power load drops back down to 0kW at 158 minutes, and the three EVs have already fully charged since Figure. 3.13 shows the three EVs remain

Table 3.3: The parameters of SECP for EVs charging load

Parameters	Details
EV brands	4
Traffic Flow	Hainault Station (London)
Simulation time	one day
$R_p$	50%
$C_m$	80
Maximum fast charging power	50kW
Maximum slow charging power	7.68kW
Power efficiency	97%

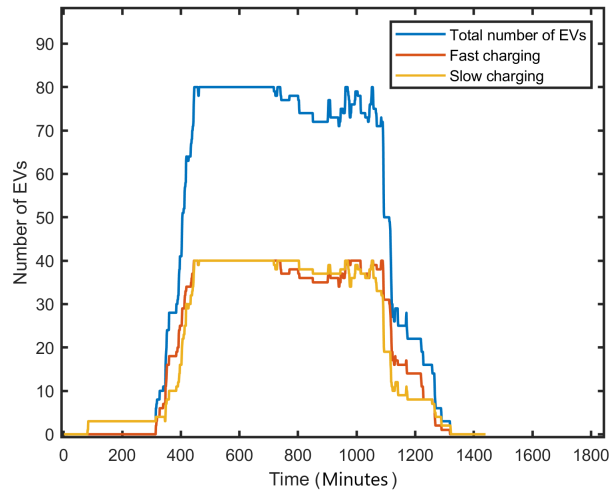


Figure 3.13: The comparison of fast charging and slow charging and total EVs occupancy

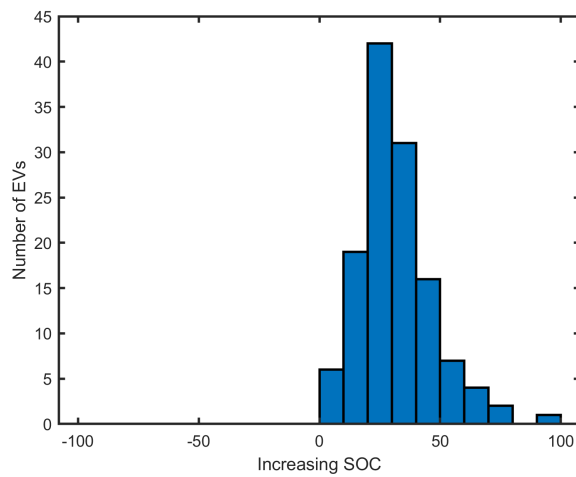


Figure 3.14: Distribution of EVs' increasing SoC

Table 3.4: Analysis with various penetration of fast charging points

$R_p(\%)$	$P_a(kW)$	$SoC_a(\%)$
0	401.70	30.74
20	415.97	31.30
40	512.20	31.58
60	770.16	31.69
80	818.59	31.96
100	802.16	32.57

in the SECP. The second wave starts from 314 minutes, and the charging power has a sharp increase. After a few significant fluctuations, the charging power demand finally reaches its highest point (547.7kW at 419 minutes) for the whole day, and the SECP is fully occupied at 446 minutes. Then most EVs are gradually charged fully, and there are no more spaces left for other EVs to park, hence the total EV power load reduces to 0kW at 574 minutes; meanwhile, SECP is still fully occupied until 718 minutes. The last wave of total EV load starts from 728 minutes and reaches its highest point at 962 minutes with 238.3kW. For this wave, the previous EVs gradually leave, while other EVs have a chance to park in; the total parked EVs remain with slight fluctuations until 1089 minutes and then decrease significantly. At 1262 minutes total EV load reduces back to 0kW, and at 1322 minute all EVs have left the SECP. Figure. 3.14 represents the value of the increase in SOC referring to the number of EVs. The SoC of most EVs increases by 10-50%, whereas the average increasing SoC of all EVs ( $SoC_a$ ) is 31.7% which is calculated by the equation:

$$SoC_a = \frac{\sum_{i=1}^N SoC_i}{N} \quad (3.15)$$

Where  $N$  is total number of EVs which are parked in the SECP, and  $SoC_i$  represents the increasing SoC of the  $i$ th EV.

In order to observe the impact of the penetration of fast charging on the SECP, a sensitivity analysis on the penetration of fast charging is provided for a week long time period, where the outputs are average maximum daily

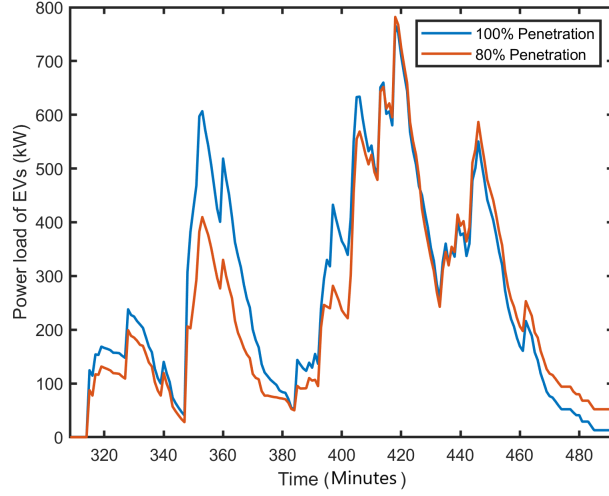


Figure 3.15: The comparison of EVs load of  $R_p=80\%$  and  $R_p=100\%$

EVs' load ( $P_a$ ) and  $SoC_a$  in the week where  $SoC_a$  could reflect the behavior of SECP in EVs charging and  $P_a$  could reflect the maximum power requirement of SECP to local power feeder.  $P_a$  can be calculated by finding the daily maximum total EV load for the week and calculating their average value.

From Table. 3.4 we can see that with the penetration of EV fast charging rising, the  $P_a$  has a significant increase and reaches its highest point 818.59kW from 401.70kW. From 80% to 100% penetration.  $P_a$  slightly decreases from 818.59kW to 802.16kW, which can be explained by Figure. 3.15, as we can see that from 315 minutes to 412 minutes, the charging power of 100% penetration is always higher than 80% penetration. This directly leads to most EVs having being fully charged before the peak of EVs load at 418 minutes, and hence  $P_a$  of 100% penetration is slightly lower. However, the maximum charging power of 100% penetration in this week is still the highest value of 1038kW.  $SoC_a$  in the days simulated show a gradual increase from 30.74% to 32.57%.

The penetration of fast charging has a clear impact on  $SoC_a$  when all EVs arrive with a very low level of  $SoC_{initial}$ . It is worth noting that most EVs arrive in this SECP with high  $SoC_{initial}$  which is about 68%, since we presume that they come here and get charged every day, hence most EVs

Table 3.5:  $SoC_a$  value with various  $R_p$  when all EVs arrive with  $SoC_{initial} = 10\%$

$R_p(\%)$	$SoC_a(\%)$
0	77.06
20	80.77
40	82.36
60	83.34
80	84.70
100	86.84

can be fully charged, however, in reality, some EV owners might prefer to charge their EVs when their EVs are under very low level  $SoC_{initial}$ . Charging EVs with low level  $SoC_{initial}$  allows  $SoC_a$  to increase more. Hence, we set  $SoC_{initial} = 10\%$  for all EVs and calculate  $SoC_a$  with various  $R_p$ . The one day simulation results could be seen from Table. 3.5,  $SoC_a$  increases from 77.06% to 86.84% when  $R_p$  rises from 0% to 100%.

### 3.4 Conclusion

In this Chapter, an ABM of SECP and the parameters are introduced as the basic model to produce EV load. The higher penetration of fast charging is a trend across the world, and it also requires more investment on the grid facilities and more payment on the electricity capacity for the SECP owner. The penetration of fast charging has a significant impact on peak EV load. To observe the impact, a sensitivity analysis of  $R_p$  is applied, the results show that as the  $R_p$  reaches 100%, the peak EV load is nearly double under the simulation conditions, however, the average increasing SoC only has small improvement. Only when all EVs arrive with a very low level  $SoC_{initial}$ , the penetration of fast charging could have an obvious impact on the average increasing SoC. Hence, the power capacity of the local feeder is not well utilized, and some optimisations for EV charging is necessary for SECP.

# Chapter 4

## Power management of SECPs

### 4.1 Introduction

The results of Chapter 3 show that growing power requirements due to faster charging development is a burden to the grid. It is often the case that for either technical or commercial reasons, the power feed for a SECP is restricted, and it is also advantageous to manage the total EV load and avoid the on-peak charges to reduce electrical costs dynamically. In this Chapter, a SECP is modelled that contains a defined number of rapid chargers with a limited incoming power supply. This study proposes four methods to manage the charging of EVs when the power feed is limited in capacity resulting in a necessary sharing of power. Simulation results show that by controlling the charging rate of each EV the overall power limits can be met. Furthermore, it is shown that the methods chosen can be used to influence the variance in SoC across all EVs.

### 4.2 Simulation of power management

In this chapter it is considered how we manage the power limits for EVs if the sum of power demand exceeds the power capacity of the power feeder. Four methods are compared here to demonstrate how different strategies can be implemented.

The four power management methods are presented as equations for calculating the EV charging power of each EV allocated by the SECP system ( $P_{Smax}$ ), the final charging power of each EV ( $P_{Amax}$ ) then could be calculated based on Equation 3.9. Figure. 4.1 shows the model of the managed EV charging power calculation for each time slot. The part which is different with Figure. 3.11 is presented in the dashed box. In the dashed box, the system first calculates the EV power demand of each EV for the time slot ( $P_{Bmax}$ ) based on Figure. 3.3 and the  $SoC_R$  calculated from the last time slot. If the EVs' load calculated by summing all EVs'  $P_{Bmax}$  is larger than the power limit ( $P_L$ ), the EV charging power management is required to restrict the charging power, one of the four power management methods' equations is used to calculate  $P_{Smax}$ ; Otherwise, the EVs power demand can be fully supported by the power feeder, hence  $P_{Smax} = P_{Bmax}$ . Finally,  $P_{Amax}$  and  $SoC_R$  are calculated based on Equation 3.9 and Equation 3.10, respectively.

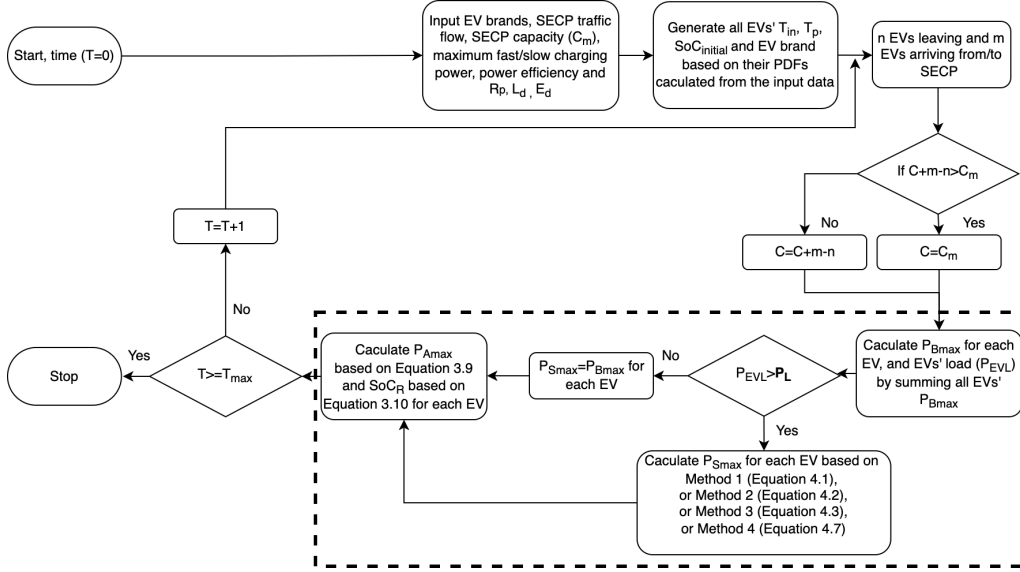


Figure 4.1: Diagram of the four EV charging management methods' procedure of SECP

### 4.2.1 The first power management method by recovering the shortfall power based on proportional power

The first method is based on proportional power where power is shared across the vehicles according to the power demand of each vehicle. The charging system calculates the real-time power demand of each EV and sums all the EVs power demand, if the total power demand is larger than the power limit, then the shortfall is treated as the total amount of power that needs to be recovered across all EVs. This amount is split per vehicle according to the proportion of charging power of each vehicle to the total charging power. The final charging power for each EV is its calculated power demand minus its share of the power shortfall. The function of the method can be represented as:

$$P_{Smaxi} = P_{Bmaxi} - \left( \sum_{N=1}^{N_p} P_{BmaxN} - P_L \right) * \frac{P_{Bmaxi}}{\sum_{N=1}^{N_p} P_{BmaxN}} \quad (4.1)$$

In this function,  $P_{Smaxi}$  represents the power which is allocated to the  $i$ th vehicle,  $P_{Bmaxi}$  is the maximum power demand of the  $i$ th vehicle controlled by BMS in this time slot,  $P_{Amaxi}$  can be calculated based on Equation 3.9,  $\sum_{N=1}^{N_p} P_{BmaxN}$  represents the total demand power of all EVs.  $P_L$  and  $N_p$  are the power limitation and the numbers of EVs in the SECP, respectively.

### 4.2.2 The second power management method by recovering the shortfall power based on SoC proportion

The second method is to share the shortfall power proportionally to the SoC of each EV. In the first method, the power to recover is split between each EV based on their real-time maximum power demand proportion, in this method, it is calculated based on the real-time SoC proportion. The relationship can

be represented as:

$$P_{Smaxi} = P_{Bmaxi} - \left( \sum_{N=1}^{N_p} P_{BmaxN} - P_L \right) * \frac{1 - SoC_{Ri}}{\sum_{N=1}^{N_p} (1 - SoC_{RN})} \quad (4.2)$$

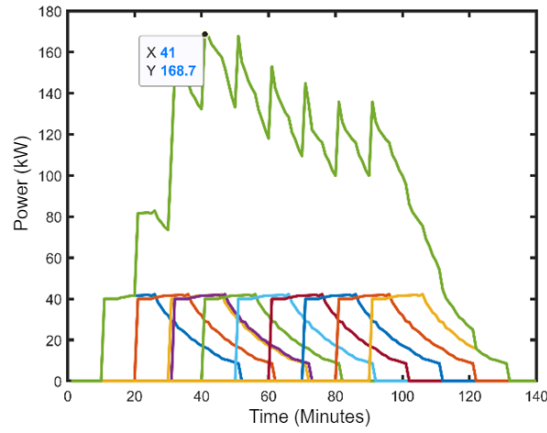
In the function,  $SoC_{Ri}$  is the SoC of the  $i$ th EV.

### 4.2.3 The third power management method by sharing the available power based on SoC proportion

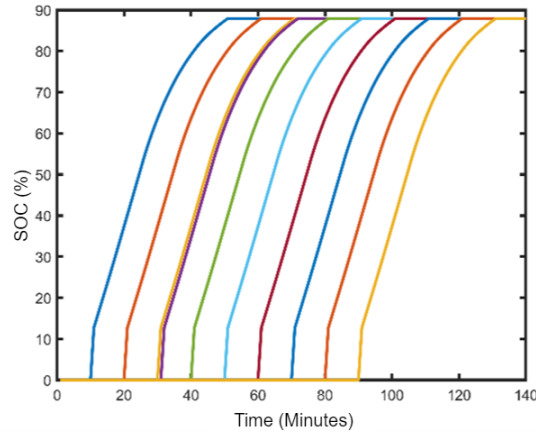
The third method is similarly based on SoC proportion, however, rather than recovering the shortfall burden across the EVs when the demand power is greater than the limit, the available power is shared proportionally according to the SoC of each EV. The relation is represented as follows:

$$P_{Smaxi} = P_L * \frac{1 - SoC_{Ri}}{\sum_{N=1}^{N_p} 1 - SoC_{RN}} \quad (4.3)$$

The practical differences between Method 2 and 3 can be explained. For a given EV in Method 2, the calculated charging power may be 0kW, this is because power demand is less than or equal to their split of the shortfall power, in this situation, the algorithm will stop charging the EV and redistribute the available power. For example, if two EVs are in an EV car park with a power limit of 20kW, one with 20% SoC and 40kW power demand and the other with 80% SoC and 5kW power, the excess power can be calculated as 25kW. According to Equation. 4.3, the calculated charging power is zero for the second EV, the system will, therefore, stop charging this EV. In Method 3, this situation will never occur, however, the allocated power could still be larger than the demanded power, in this case, the excess power is shared between the other EVs proportionally to their SoC.



(a) Power of the main feeder (green) and power for each vehicle



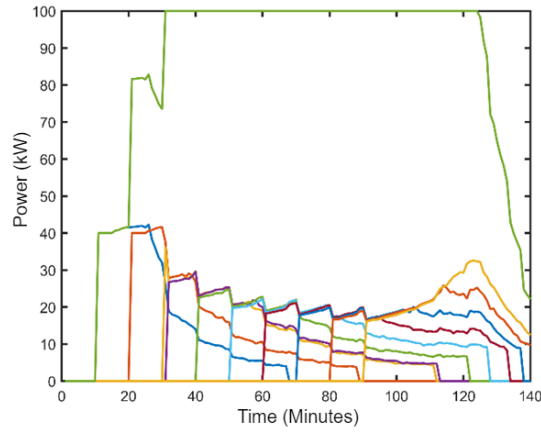
(b) SoC of each vehicle

Figure 4.2: The results without applying any power management method

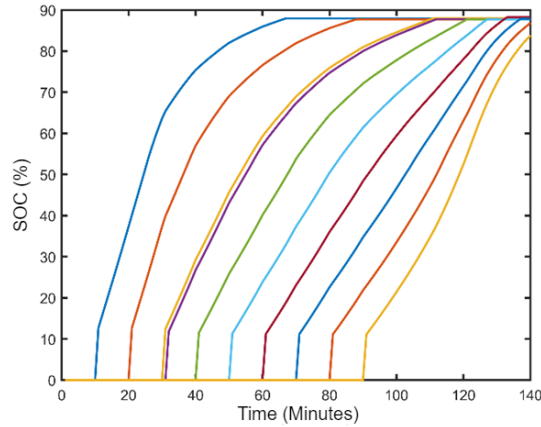
#### 4.2.4 Simulation results

To simulate and compare the three methods, the Nissan Leaf (24kWh) is used. The model is configured for 10 EVs that will arrive into the vehicle park independently with a SoC of 10% and max SoC of 95%. The car park is given a maximum power limitation of 100kW. The simulation time is 150 minutes and the arrival times of the EVs are at 10, 20, 30, 31, 40, 50, 60, 70, 80, and 90 minute. The total power demand of all vehicles is sampled each time slot. The simulation is based on Figure. 4.1

Figure. 4.2 shows the results of the simulation without applying any



(a) Power feeder capped at 100kW (green), and power for each vehicle

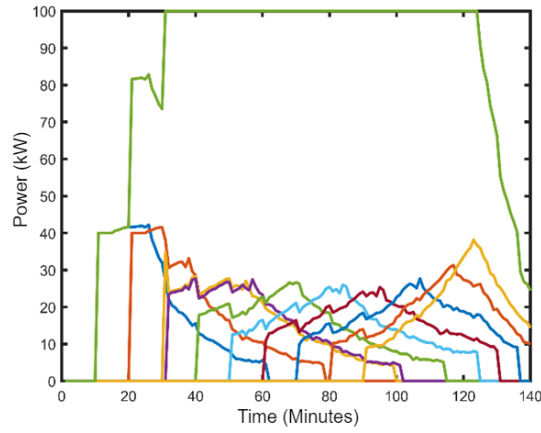


(b) SoC of each vehicle, this method has a smaller average variance than Method 2

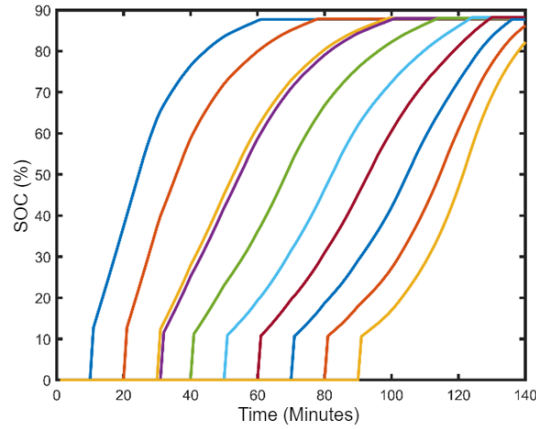
Figure 4.3: The simulation results of applying Method 1

power management method. The green line in Figure. 4.2a is the total final EVs' charging power by summing all EVs'  $P_{Amax}$  and other colours represent different EVs'  $P_{Amax}$ , it can be seen that the total power demand reaches its highest point (168.7kW) at 41 minutes and the system completes charging at 131 minutes, the energy consumption is calculated by integrating the power and is approximately 193kWh.

The results of the first, the second and the third methods are shown in Figure. 4.3, Figure. 4.4 and Figure. 4.5. From the green line in graphs



(a) Power feeder capped at 100kW (green), and power for each vehicle



(b) SoC of each vehicle

Figure 4.4: The simulation results of applying Method 2

(a), all methods limit the total final EVs' charging power below 100kW. At the end of the simulation, the total energy consumption of each method is 191.76kWh, 191.38kWh, and 192.11kWh, respectively. Compared with all methods, Method 3 could utilize more energy for the same power feeder. This means Method 3 has the highest energy utilization in the provided test conditions, followed by Method 1 and Method 2.

It is also possible to compare the average SoC variance of each solution. The average SoC variance means the difference in SoC between each vehicle

starting from the second EV. The functions are given:

$$V_t = \frac{1}{N_p - 1} \sum_{i=1}^{N_p} |SoC_{Rit} - \mu_t|^2 \quad (4.4)$$

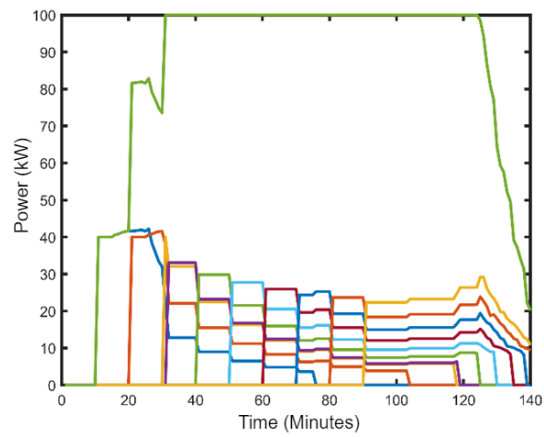
$$\mu_t = \frac{1}{N_p} \sum_{i=1}^{N_p} SoC_{Rit} \quad (4.5)$$

$$AV = \frac{1}{T_2 - T_1} \sum_{t=T_1}^{T_2} V_t \quad (4.6)$$

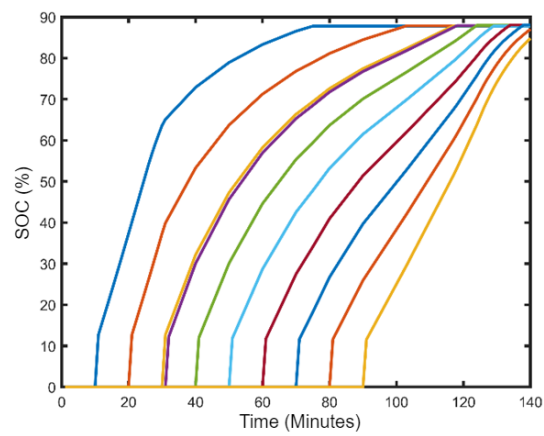
where  $V_t$  means the variance of SoC in the given time  $t$ ,  $SoC_{Rit}$  represents the SoC of the  $i$ th EV at time  $t$ ,  $\mu_t$  is the mean of all EVs'  $SoC_{Rt}$ ,  $T_1$  and  $T_2$  are start time and end time,  $AV$  is the average SoC variance for the entire working time.

If EVs tend to be at a higher SoC at the same time, the average variance is smaller. A smaller or larger average variance demonstrates whether the method is biased to provide power for EVs with lower SoC or higher SoC respectively. Observing the results for graphs (b) in Figure. 4.3, Figure. 4.4 and Figure. 4.5, it can be seen that the SoC value of each EV are much closer in Method 3 and the final EV to arrive reaches a higher SoC compared to other methods. Method 3 is reducing power to EVs with high SoC in favour of those with low SoC. The SoC variance of each method from 1 to 3 is 471.68, 562.06 and 382.72, respectively.

The SoC variance is a useful metric and depending on the situation, customers and EVs park owners might benefit from either a large or small average variance. For example, if the SECP provides grid services (explored in Chapter 6) then it might be advantageous if the SoC variance is small meaning that load sharing between EVs is more equal. Meanwhile, more customers will have higher satisfaction as their EVs will have a higher SoC when they want to leave. If these are desirable outcomes, then Method 3 should be chosen.



(a) Power feeder capped at 100kW (green), and power for each vehicle



(b) SoC of each vehicle, The SoC curve is the closest in the three methods

Figure 4.5: The simulation results of applying Method 3

Table 4.1: The calculation details of  $R$

If $SoC_{Ri} \leq AS + F$ And $Z == 1$	If $\frac{1-SoC_{Ri}}{1-AS} \geq 2$	$R_i = 2 * (1 - SoC_{Ri})$
	If $1 < \frac{1-SoC_{Ri}}{1-AS} < 2$	$R_i = \frac{1-SoC_{Ri}}{1-AS} * (1 - SoC_{Ri})$
	If $\frac{1-SoC_{Ri}}{1-AS} \leq 1$	$R_i = 1 - SoC_{Ri}$
If $SoC_{Ri} > AS + F$ And $Z == 1$	$R_i = 0, Z = 0$	
If $SoC_{Ri} \geq AS - F$ And $Z == 0$	$R_i = 0$	
If $SoC_{Ri} < AS - F$ And $Z == 0$	If $\frac{1-SoC_{Ri}}{1-AS} \geq 2$	$R_i = 2 * (1 - SoC_{Ri}), Z = 1$
	If $1 < \frac{1-SoC_{Ri}}{1-AS} < 2$	$R_i = \frac{1-SoC_{Ri}}{1-AS} * (1 - SoC_{Ri}), Z = 1$

#### 4.2.5 Fourth method on power management based on the results of Method 3

Using the results of Method 3, Method 4 is now proposed that goes further to prioritising the charging of each EV to an equal SoC (low SoC variance). The methodology is that the average SoC is calculated every time slot, if the SoC of an EV is larger than the average SoC, then the charging of the EV will be paused, if it is smaller, the charging power will be allocated based on the SoC proportion and the ratio factor ( $R$ ) in each minute. The details of the ratio factor can be seen from Table. 4.1,  $SoC_{Ri}$  is real-time SoC of the  $i$ th EV,  $AS$  represents the average SoC of all EVs,  $R$  is the ratio factor that will be used to calculate the allocated power of each EV. Meanwhile, a hysteresis band is set to reduce fluctuations,  $F$  is the hysteresis factor. For a given factor  $R$ , the power of the  $i$ th EV in each minute can be calculated from the function:

$$P_{Smaxi} = P_L * \frac{R_i}{\sum_{N=1}^{N_p} R_N} \quad (4.7)$$

In some situations,  $P_{Smaxi}$  might be larger than the  $P_{Bmaxi}$ , if so, the given EV charging power  $P_{Amaxi}$  will be  $P_{Bmaxi}$  based on Equation 3.9, and the excess power  $P_{Smaxi} - P_{Bmaxi}$  will be split to other EVs based on SoC.

Method 4 is simulated with the same parameters as in methods 1-3 with

$F=0.02$ . The results can be seen in Figure. 4.6, from the green line in Figure. 4.6a, the model remains within the 100kW limit and the system stops charging at 136 minutes, and in Figure. 4.6b, all EVs are fully charged to the target SoC almost at the same time with 201.80 average SoC variance, the maximum time gap is four minutes. Table. 4.2 shows the results of the provided four methods. Compared with the results from the previous three methods, Method 4 has the highest energy utilisation and the lowest average variance.

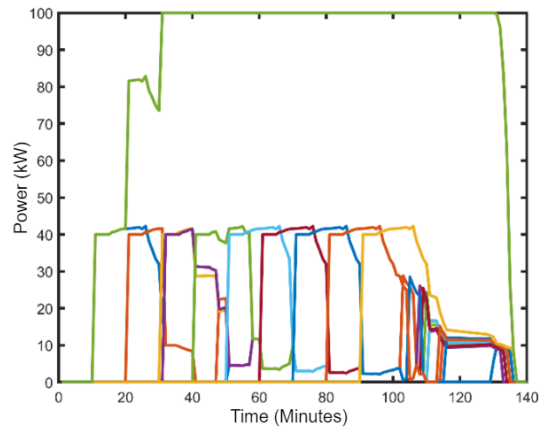
### 4.3 Cases study of the provided four methods

The previous test results are based on the ideal situations, in reality, the results might be affected by the real-world conditions. An important consideration when using these four power management methods is how they impact the increasing SoC of EVs. In this section, the proposed four methods are applied to the SECP model introduced in Chapter 3 which is closer to real-world. The aim of the case study is to find out if these four methods can allocate the charging power for all EVs with a power limited feeder and achieve a acceptable average increasing SoC. Meanwhile, a sensitivity analysis on various power limits is introduced to observe the behaviour of these four methods.

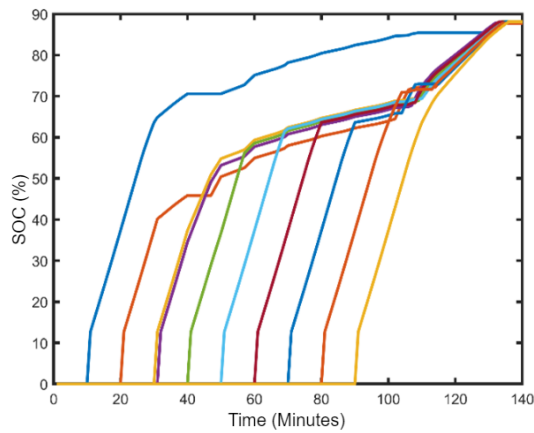
The SECP parameters are indicated in Table. 4.3, where slow charging has a very limited impact on the system, for analysing these four methods,

Table 4.2: Comparison of the simulation results of the provided four methods and the result without a power limit

Method	Energy consumption (kWh)	SoC variance
1	191.76	471.68
2	191.38	562.06
3	192.11	382.72
4	193.01	201.80
Without power limit	193.01	-



(a) Some EVs stop charging when their SoC is larger than the average SoC, Charging power for each vehicle



(b) Each EV is almost fully charged at the same time, SoC for each EV

Figure 4.6: The simulation results of applying the Method 4

it is necessary to give all the EVs in the EV charging park the same charging conditions,  $R_p$  is set to 100%. All EVs in this charging park will be connected with DC fast chargers, which means that all EVs have chances to charge with maximum charging power based on the power allocation from the four provided methods. The simulation is developed with inputs from 20kW to 200kW at 20kW increments and based on Figure. 4.1. The output is the average increasing SoC of all EVs, which is shown in Table. 4.4.

Table 4.3: The parameters of the simulated SECP

Parameters	Details
EV brands	4
Traffic Flow	Hainault Station (London)
Simulation time	one day
The probability of EV fast charging	100%
The penetration of DC fast charging	100%
SECP charging spaces	80
Maximum fast charging power	50kW
Power efficiency	97%

Table 4.4: The average increasing SoC of four power management methods

Power feeder limit (kW)	Average increasing SoC (%)			
	Method 1	Method 2	Method 3	Method 4
0	0	0	0	0
20	9.37	8.74	9.64	9.66
40	17.57	16.65	17.98	18.00
60	24.82	23.98	25.22	25.11
80	30.47	29.94	30.77	30.90
100	31.81	31.14	32.02	32.17
120	32.26	32.00	32.34	32.37
140	32.38	32.30	32.42	32.41
160	32.45	32.46	32.46	32.43
180	32.49	32.51	32.49	32.45
200	32.52	32.53	32.52	32.47
Max	32.64	32.64	32.64	32.64

From this table, we can see that the trend of four methods is for them to have a significant increase from 0kW to 80kW. Along with the rise in power feeder limit, the average increasing SoC of all four methods keeps increasing, however the increments of them decrease gradually. When the power feeder limit is 20kW, Method 4 achieves the highest average increasing SoC of all EVs (9.66%), followed by Method 3 (9.64%), then Method 1 (9.37%) and lastly Method 2 (8.74%). This ranking has been maintained until the 120kW power feeder limit. at 140kW the Method 3 has the highest value of 32.42%, which is 0.1% higher than Method 4, and then followed by Method 1 and Method 2 with 32.38% and 32.30%, respectively. From 160kW to 200kW, the average increasing SoC of Method 2 is gradually larger than Method 3 and becomes the highest value of 32.51%, and the value of Method 4 remains the minimum. Method 1 and Method 3 are same at 180kW and 200kW. The maximum average increasing SoC is 32.64% for the system without a power limit. Overall, for the same power limit, the differences of the four methods' average increasing SoC are small for the simulated SECP.

## 4.4 Conclusions

This Chapter discusses the power management strategies for SECP. Three power management strategies are introduced, one limits power based on each EV demanded power, and two use SoC of the EVs to allocate power proportionally. The Nissan leaf (24 kWh) charging profiles were used to provide the power demand data for analysing the behaviour of these strategies. The simulated results show that the power feed to the car park can be managed according to an artificial limit whilst each method has differing resulting SoC profiles for the vehicles. All three methods are based on a proposed fair method to share power for meeting the overall car park power limit. The results from Method 3 were the most significant in that they showed that the cars parked early were artificially held back from charging at higher SoC which had the effect, at the end of the simulation, of all cars being closer to the same SoC.

As discussed, this was possibly seen as desirable, therefore Method 4

was introduced to force the EVs to charge according to the average SoC of all the vehicles in the car park. This exaggerated the effect to the extent that at times vehicles were not charging at all to enable other EVs to catch up. The extreme nature of this method could be seen as unfair from a user perspective unless there were possible benefits to the user such as lower parking costs requiring further research. The simulations in this part were intentionally used with matching vehicles and initial SoC values to highlight the differences in control methods. This method also gives the SECP owner a chance to prioritize some EVs' charging by adjusting ratio factor to seek more benefits from EV owners.

In the end, the four methods are introduced to the ABM of SECP provided in Chapter 3. The cases study shows that for different EVs and initial SoC illustrated in Table. 4.3, Method 4 can achieve the highest average increasing SoC when the power limit remains at a very low level from 0kW to 80kW, which results from Method 4 seeking the lowest variance of all EVs' SoC and forcing the EVs closer to the SoC at every time slot. For example, two EVs charge with 50kW chargers and a 100 kW power feeder, so if one is fast fully charged, then the total charging power reduces to 50kW, however if both of them are keeping closer to the SoC, then the total charging power can remain at 100kW for a longer period, hence the average increasing SoC of all EVs is higher than other methods until some of EVs are charged fully. Method 1, Method 2, and Method 3 have higher average increasing SoC when the average increasing SoC is close to its highest point (32.64%) over 80kW power limit. This is because that among these situations most EVs are fully charged.

# Chapter 5

## The integration of BESS and PV

### 5.1 Introduction

Previous chapters have shown that the total EV charging peak load might reach a very high level. Simulations have modelled the situation where most EVs arrive and get charged in the same SECP every day, hence EVs have relatively high initial SoC. In real-world performance, some EVs might come with very low SoC, which results in the peak load period lasting longer for charging these EVs. Power management methods provided in Chapter 4 significantly reduce the peak charging power of the SECP, therefore reducing the equipment investment and electricity cost since the electricity capacity fee is charged based on £/MW/Day at the maximum potential power requirement regardless of actual usage in the UK. However, those methods work by extending the charging time and could result in an EV that leaves earlier than expected not having sufficient SoC and therefore does not fundamentally solve the problem of EV charging demand. Meanwhile, the small power feeder limit might lead to very limited electricity transferred to EV in the requested charging periods. For example, In Table. 4.4, EVs in the SECP with a power feeder of less than 60kW power supply do not see a significant increase in SoC.

In this chapter, the EVs' charging power are still calculated based on Figure. 4.1, the difference is the power limit ( $P_L$ ) with bold format in the dashed box is enlarged by using a BESS and PV panels.

A BESS is an energy storage system using batteries as energy storage units, hence, the BESS could be used to shift peak EV load for SECP. Different from power management methods provided in Chapter 3, the BESS shifts peak EV load by storing energy when the EV load does not exceed the power feeder limit and exporting this energy when EV load is higher than the power limit. The BESS is also widely used for ancillary services like frequency response or ramping to smooth out intermittent renewable output. The BESS is typically made up of many battery modules, a BMS, and a power conversion system.

The power generated by the PV can be used to charge EVs. Solar energy as renewable energy can be acquired easier in cities compared to other renewable energy sources and could achieve a reduction in  $CO_2$  emissions. The application of the PV in a SECP has been achieved in both theory and practice, UK's first solar-power EV car park opened in 2021 in Leeds [13]. the PV can also help EVs to shift the peak load through collaboration with the BESS, since the energy generated by the PV can be stored in the BESS or directly transferred to the EVs.

In this chapter, a BESS is first integrated into our ABM of SECP with different capacities to observe and analyse the results. The PV is then introduced with the BESS which stores the PV and grid energy and releases it when EVs need the most power.

## 5.2 The BESS based SECP

In this section, the BESS is integrated with the SECP. The BESS based SECP is first introduced from the structure of the system, followed by simulations of the system based on the ABM, then a sensitivity analysis on the capacity of the power feeder and the capacity of the BESS are provided to investigate their impacts on the average increasing SoC of EVs.

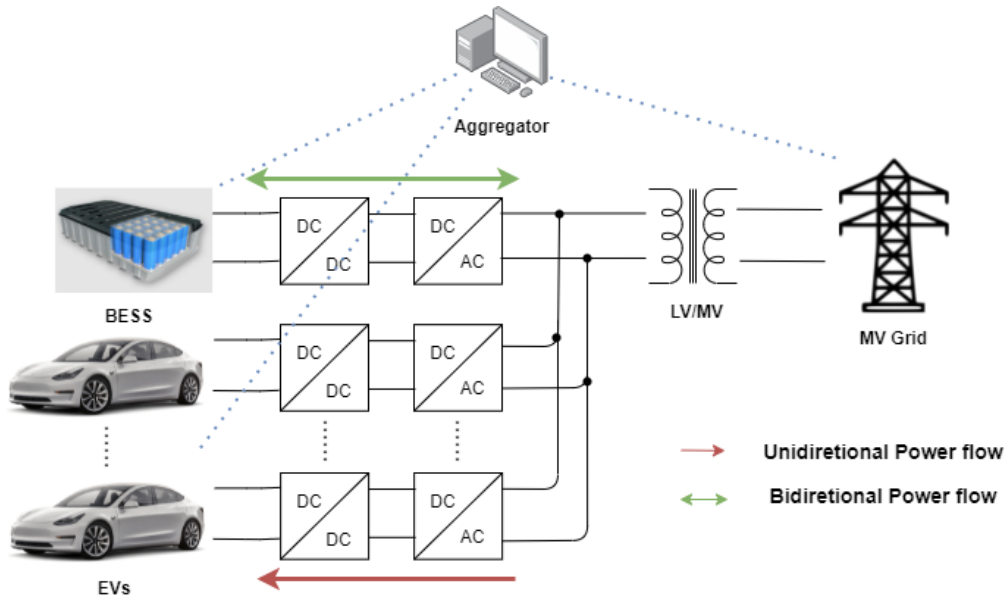


Figure 5.1: The BESS based SECP.

### 5.2.1 The structure of the BESS based SECP

The BESS based SECP is shown in Figure. 5.1. The aggregator in this stage mainly collects information from the BESS, EVs, and the grid, and sends commands to the BESS and EV chargers to manage the charging power in the system. Figure. 5.2 shows the energy flow with respect to power from the grid (GP), EVs (EVP), and BESS. BSCP and BSDP represent the available power of the BESS for charging/discharging. '2' in the middle of a word represents 'to' meaning power transfer (e.g. Grid2BESS means the power transferring from Grid to BESS). The contents inside the dashed box illustrate the energy flow between the EV, BESS, and Grid for each condition, whilst the bottom dotted box formulates the power. For the BESS, the power conversion system is bidirectional, BESS can be charged or discharged. The aggregator only requests the SoC from the BESS. Based on the SoC, local power feeder, and total EV load, the aggregator sends a power command to the BESS to either charge, discharge or do nothing (pause).

The BESS is in the charging state when the total EV load is less than the power limit of the local feeder and the BESS is not fully charged (SoC is

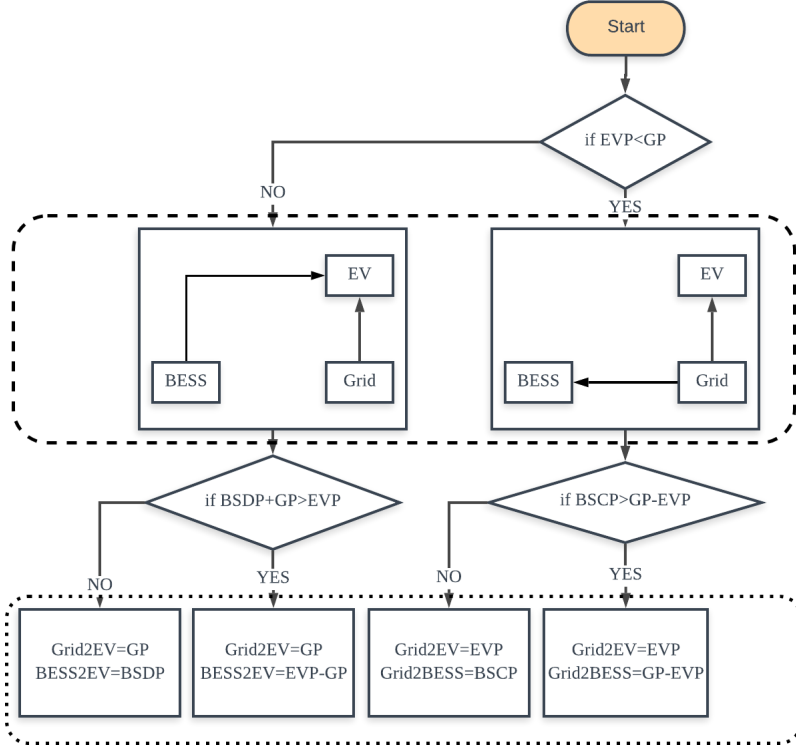


Figure 5.2: The energy flow of BESS based SECP.

less than 100%), the charging power of BESS ( $P_{BESS}$ ) is equal to the power limit of the local feeder minus the total EV load ( $P_{EV}$ ).

The BESS is in the discharging state when the total EV load is higher than the power limit of the local feeder, and there is energy stored in the BESS. The energy is transferred from the BESS to the EVs to provide the power that the the local power feeder can not provide.

The BESS remains a static state (zero power) only when the BESS is fully charged and no power request from the BESS. The function of  $P_{EV}$  and  $P_{BESS}$  is:

$$P_{EV} = \sum_{N=1}^{N_p} P_{dN} \quad (5.1)$$

where  $N_p$  is the total number of EVs.

$$P_{BESS} = P_L - P_{EV} \quad (5.2)$$

$P_{BESS}$  could be positive or negative representing the charging power or discharging power, respectively.

The aggregator collects the the real-time charging power requirement of each EV, and calculates the total EV load. According to the SoC of the BESS and local power feeder and EVs load, the charging or pause command will be sent with corresponding charging power to each EV based on the power management method.

The charging command will be sent to EVs if the power supplied by the local power feeder is higher than the EVs load, or power from the local power feeder plus BESS is higher than the EVs load. All EVs are charged with their maximum charging power.

If power from the local power feeder plus BESS is lower than the total EV load but larger than 0kW, the charging power allocated for each EV is based on the power management methods system introduced in Chapter 4.

The EVs receive pause commands only when they are fully charged or the EVs are not allocated any power based on the power management method.

For the Grid, the aggregator collects market information for the SECP operator, which was introduced in the literature review.

### 5.2.2 Modelling the BESS based SECP

Based on the structure of the BESS based SECP, the BESS is then introduced in, Equation 5.3 shows the calculation function of the SoC of BESS ( $SoC_{BESS}$ ):

$$SoC_{BESS} = \frac{\alpha * \int_{T_s}^{T_e} P_{BESS}}{E_{cBESS}} \times 100\% + SoC_{T_s} \quad (5.3)$$

where  $T_s$  and  $T_e$  represent the start time of charging/discharging and end time of charging/discharging respectively. and  $P_{BESS}$  is the charging/discharging

Table 5.1: The parameters of BESS based SECP

Parameters	Details
Power feeder limit	80kW
Capacity of BESS	200kWh
Initial SoC of BESS	100%
Power management method	Method 1

power in kW,  $E_{cBESS}$  is the capacity of the BESS in kWh.  $SoC_{T_s}$  represents the SoC of the BESS when the charging/discharging process starts.

### 5.2.3 Cases study of the BESS based SECP

We pick Method 2 as the power management strategy to observe the behaviour of the system. Because with BESS support, the power limit for all EVs is much higher than it with just a power feeder, and Method 2 have better performance in the average increasing SoC when the power limit is high based on Table. 4.4. The detail of the BESS is listed in Table. 5.1, and the other information is same as in Table. 4.3. The initial SoC of the BESS is reset to 100% every day.

The results are shown in Figure. 5.3, and where the first of four subplots show the total EV charging power ( $P_{EV}$ ), then the grid power ( $P_{Grid}$ ), where a negative value corresponds to the SECP importing energy from the feeder. The last two subplots are the BESS power and SoC of BESS, respectively, where a positive value represents the BESS charging, and discharging is expressed as a negative value. Three representative time points are chosen to refer to BESS states (grey lines) with the data shown in Table 5.2. At the first charging point (347 minutes), the BESS is operating in the charging period, where  $P_{EV}$  is 40.48kW, and the  $SoC_{BESS}$  is 82.06%. BESS is not fully charged, hence the grid not only charges EVs but also transfers the rest of the charging power to the BESS of 37.12kW with the maximum power feeder limit of 77.6kW (80kW without considering the efficiency). At the second charging point (560 minutes), the BESS is operating in the pause period. The EV power demand is far higher than the maximum power feeder

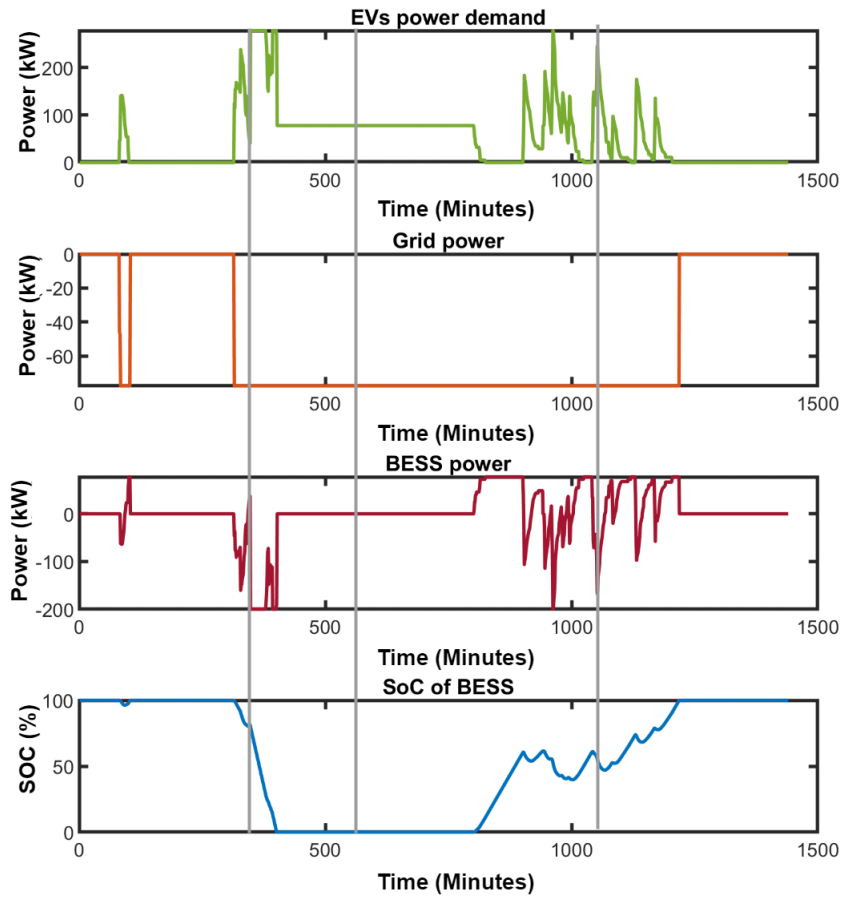


Figure 5.3: System response for EV load  
 Table 5.2: Data points as shown in Figure 5.3

Time (Min)	$P_{EV}(kW)$	$P_{Grid}(kW)$	$P_{BESS}(kW)$	$SoC_{BESS} (%)$
347	40.48	-77.6	37.12	82.06
560	77.6	-77.6	0	0
1052	244.2	-77.6	-166.6	55.75

limit of 77.6kW, hence, all the power from the grid is transferred to the EVs. Meanwhile, the BESS is already fully discharged,  $SoC_{BESS}$  is 0%, there is no more power left to export to EVs, hence  $P_{BESS}$  is 0kW, and  $P_{EV}$  is 77.6kW. The BESS is operating in the discharging period at the last charging point (1052 minutes), where the BESS still has energy stored with  $SoC_{BESS}$  of 55%, and the EV power demand is over the maximum power feeder limit, hence the BESS exports its energy to the EVs with power of -166.6kW. The  $P_{EV}$  is the power of the BESS plus the maximum grid power (244.2kW).

Overall, from Figure. 5.3 we see that, along with the power demand from the EVs increasing, the BESS starts exporting energy to the EVs at 315 minutes, and the SoC of the BESS quickly drops back to 0% from 315 minutes to 400 minutes.  $SoC_{BESS}$  and  $P_{BESS}$  remain at 0% from 400 minutes to 800 minutes. When  $P_{EV}$  can not utilize all the grid power from 800 minutes onward, the sufficient power from the grid is then transferred to the BESS, the SoC of the BESS rises gradually. After several fluctuations, the SoC of the BESS finally rises back to 100% at 1219 minutes. The average increasing SoC of the EVs is 32.53% with an 80kW power feeder which is already higher than the data in Table. 4.4 with a 200kW power feeder.

#### 5.2.4 Sensitivity analysis of power feeder limit and the capacity of BESS based on the cases study

In this part, our investigation focuses on how the average increasing SoC is affected by the power feeder and the capacity of the BESS. Increasing the investment in the power feeder and BESS can improve the average increasing SoC, SECP owners with a limited budget might want to seek the investment balance between the power feeder and BESS to get higher customer satisfaction. The simulation parameters of the sensitivity analysis are introduced in Table. 5.3, and other information is same as in Table. 4.3.

The results of the four methods are shown in Figure. 5.4. It is difficult to distinguish the behaviour of the four methods from each other by inspecting the figures, the tables of four methods are made by choosing some data points from the figures to show the results clearly, the capacity of the BESS

Table 5.3: The parameters of EV based charging load for sensitivity analysis

Parameters	Details
Power feeder limit	0-100kW
Capacity of BESS	0-500kW
Initial SoC of BESS	100%
Power management method	1-4 Method

Table 5.4: Sensitivity analysis results of Method 1

$SoC_a$ (%) \ $P_L$ (kW)	0	20	40	60	80	100
$E_{cBESS}$ (kWh)						
0	0	9.37	17.57	24.82	30.47	31.81
100	2.64	12.04	20.26	27.15	31.80	32.23
200	5.32	14.73	22.94	29.53	32.19	32.42
300	8.00	17.42	25.62	31.69	32.44	32.48
400	10.68	20.15	28.17	32.45	32.49	32.52
500	13.39	22.91	30.58	32.50	32.53	32.57

is increased from 0kW to 500kWh with 100kWh increments and the power limit is increased from 0kW to 100kW with 20kW increments, where the results are shown in Table. 5.4, Table. 5.5, Table. 5.6, and Table. 5.7. From the figures and the tables, we can see that for the four power management methods, the increase of capacity of the BESS has a significant improvement on the average increasing SoC for the same power limit. However, as the power feeder limit rises, the improvement decreases gradually. For example, from 0kWh to 500kWh BESS, the  $SoC_a$  of Method 1 increases by 13.54% with a 20kW power feeder, the increment is reduced to 0.76% with a 100kW power feeder. The maximum increment for the four methods from 0kWh to 500kWh are 13.54% , 13.29% for Method 1 and Method 2 with a 20kW power limit respectively, and 13.73%, 13.75% for Method 3 and Method 4 where there is no power feeder (off-grid).

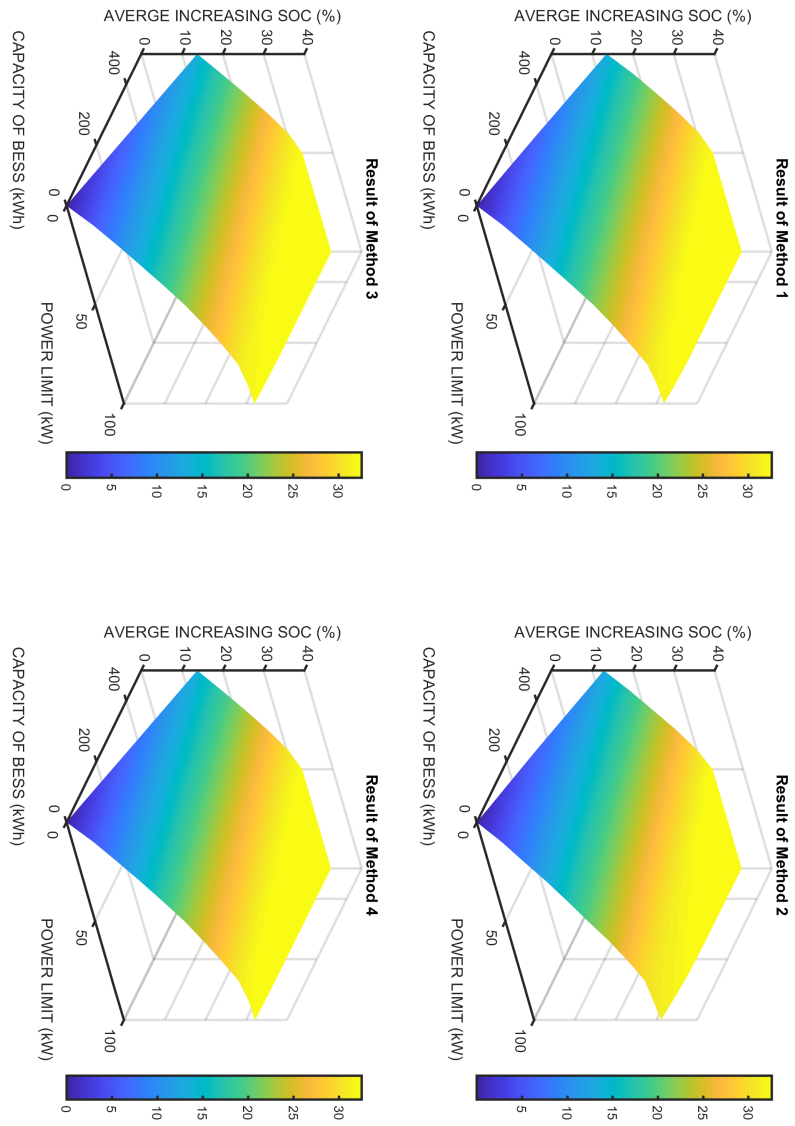


Figure 5.4: Sensitivity analysis result of SECP with BESS.

Table 5.5: Sensitivity analysis results of Method 2

$SoC_a$ (%) \ $P_L$ (kW)	0	20	40	60	80	100
$E_{cBESS}$ (kWh)						
0	0	8.74	16.65	23.97	29.94	31.14
100	2.50	11.48	19.13	26.52	31.13	31.98
200	4.97	14.03	21.85	29.10	31.83	32.41
300	7.56	16.53	24.66	31.27	32.44	32.51
400	10.18	19.21	27.79	32.40	32.52	32.53
500	12.83	22.03	30.03	32.52	32.54	32.59

Table 5.6: Sensitivity analysis results of Method 3

$SoC_a$ (%) \ $P_L$ (kW)	0	20	40	60	80	100
$E_{cBESS}$ (kWh)						
0	0	9.64	17.98	25.22	30.77	32.02
100	2.71	11.95	20.40	27.45	31.95	32.34
200	5.47	14.59	22.96	29.65	32.32	32.45
300	8.24	17.28	25.55	31.68	32.46	32.49
400	10.98	19.96	28.10	32.45	32.50	32.52
500	13.73	22.64	30.40	32.50	32.53	32.54

Table 5.7: Sensitivity analysis results of Method 4

$SoC_a$ (%) \ $P_L$ (kW)	0	20	40	60	80	100
$E_{cBESS}$ (kWh)						
0	0	9.66	18.00	25.11	30.90	32.17
100	2.72	12.00	22.44	27.35	32.15	32.37
200	5.49	14.66	22.98	29.40	32.37	32.42
300	8.27	17.36	25.52	31.68	32.43	32.45
400	11.03	20.02	28.00	32.43	32.45	32.47
500	13.75	22.68	30.35	32.46	32.48	32.49

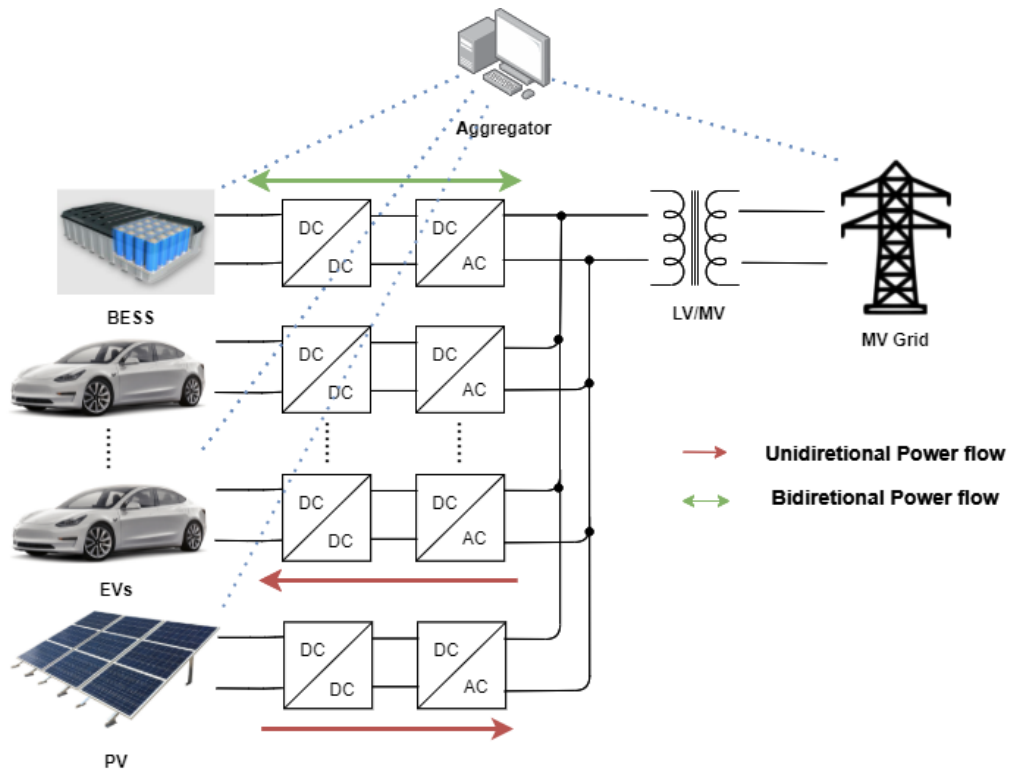


Figure 5.5: The BESS and PV based SECP.

### 5.3 The BESS and PV based SECP

In this section, the BESS and PV are integrated with the SECP to further reduce the power demand to the power grid. The BESS and PV based SECP is firstly introduced from the structure of the system which includes the PV power calculation, followed by the application of BESS and PV system based on the ABM of SECP, then a sensitivity analysis on the battery size is provided to investigate the impact of the capacity of the power feeder and the size of the BESS on average increasing SoC of EVs and the utilization of the energy generated by the PV for the SECP system.

#### 5.3.1 The structure of the BESS and PV based SECP

The BESS and PV based SECP is shown in Figure. 5.5. The functions of the aggregator in this stage are almost the same as the BESS base SECP, where

the differences are that the aggregator also needs to collect generating data from the PV, and send commands to the PV to decide if the PV transfers power to the SECP or the grid or both of them. The PV will be on all the time. Figure. 5.6 shows the energy flow respecting to power from the grid, EVs, BESS and PV (PVP).

For the BESS, based on the information from the SoC of the BESS, the power feeder, the EVs' load, and PV power, the aggregator sends the charging or discharging or pause command with the corresponding charging and discharging power.

The BESS is charging when the EVs' load is less than the power limit of the local feeder plus PV power ( $P_{PV}$ ) and the BESS is not fully charged (the SoC is less than 100%). The charging power of the BESS ( $P_{BESS}$ ) is equal to the power limit plus PV power minus total the EV power load ( $P_{EV}$ ).

The BESS is discharging when the total EV power load is higher than the power limit of the power feeder plus PV power, and there is energy stored in the BESS, then power is supplied from the BESS to the EVs to make up the difference that the power feeder and PV cannot provide.

The BESS remains in the static state only when the BESS is fully charged or discharged and no power is requested from or sent to the BESS.

$P_{BESS}$  in this section is represented as:

$$P_{BESS} = P_L + P_{PV} - P_{EV} \quad (5.4)$$

For the EVs, the aggregator sends the charging or pause command with corresponding charging power for each EV based on the power management methods.

If the power supplied by the local power feeder plus PV and BESS power is higher than the EVs' load, then the charging command will be sent, and the maximum charging power is allowed for all EVs.

If power from the local power feeder plus BESS and PV power is lower than the total EV power load but larger than 0kW, then the charging power allocated for each EV is based on the power management methods.

An EV receives the pause command only when it is fully charged or the

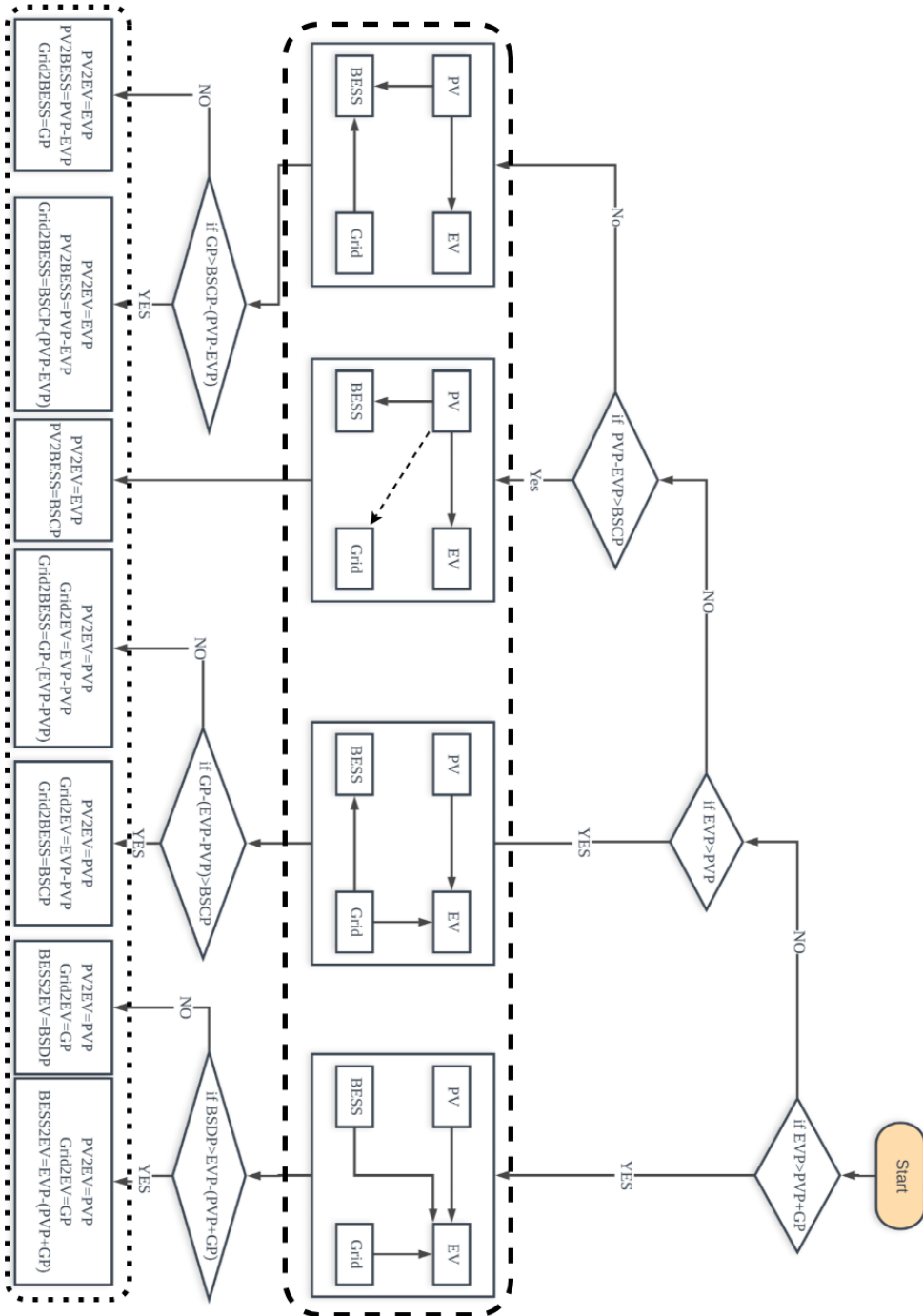


Figure 5.6: The energy flow of the BESS and PV based SECP

EV is not allocated any power based on the power management method.

For the PV, the aggregator sends commands to decide if the power generated by PV is outputted to the SECP, or the grid, or both of them with corresponding power value.

The PV power is considered as the priority power source to charge the EVs. The PV will export all its power to the EVs with any excess being delivered to the BESS according to the SoC strategy and the remaining surplus exported to the grid. In the case where the SECP power demand is 0kW, the PV will receive the command to directly output the power to the grid. SECP owners can benefit by exporting PV power to the grid through an export tariff [126].

### 5.3.2 Model of the BESS and PV based SECP

In [127], the capacity of the PV panel ( $P_{Cpv}$ ) is approximately 150Wp/m<sup>2</sup>-200Wp/m<sup>2</sup>. In this work,  $P_{Cpv}$  is set as the median value 175Wp/m<sup>2</sup>. PV power ( $P_{pv}$ ) output varies with solar irradiance, and normally can not reach  $P_{Cpv}$ . For example, [128], shows that the recorded installed capacity of PV in the UK was 13.08GWp in June 2021, and achieved a peak PV power of 9.68GW.  $Z(t)$  represents the relation between the installed capacity of PV ( $P_{CpvUK}$ ) and PV power in the UK ( $P_{pvUK}(t)$ ) which changes with time:

$$Z(t) = \frac{P_{pvUK}(t)}{P_{CpvUK}} \quad (5.5)$$

In the model, the PV canopy is over the car park spaces and the SECP only has a single floor. The area of the PV panel could be equal to the parking area which does not include the space between the car park spaces. The UK standard single car park space size is 11.52m<sup>2</sup>.  $P_{pv}$  of SECP changing with the time (t) is then given as:

$$P_{pv}(t) = Z(t) * P_{Cpv} * C_m * 11.52 \quad (5.6)$$

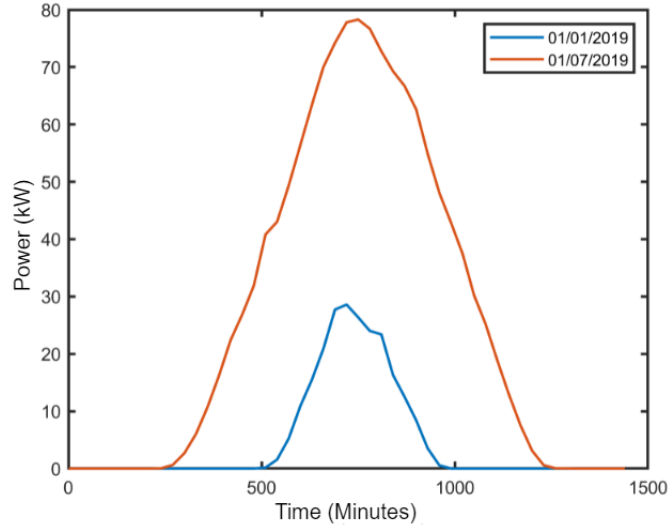


Figure 5.7: The PV power generation based on the 80 charging spaces

Table 5.8: The parameters of BESS and PV based SECP

Parameters	Details
Power feeder limit	80kW
Capacity of BESS	200kWh
Initial SoC of BESS	100%
Power management method	Method 1
Simulation date	01/01/2019
Power of PV panel	$175Wp/m^2$

where  $C_m$  is the number of parking spaces,  $Z(t)$  ranges from 0 to 1 calculated every minute based on the historical GB PV data supplied by NEGSO [128]. According to the capacity of the SECP with 80 charging spaces shown in Table. 4.3, and using PV data from 01/01/2019 and 01/07/2019 to represent winter and summer, the PV power in the SECP is shown in Figure. 5.7. No matter the duration or the power generation, the PV power generation on 01/07/2019 is obviously longer and higher than on 01/01/2019, which is because 01/01/2019 is a normal day of winter, and 01/07/2019 is a normal day of summer, the solar irradiance in the UK is much higher in the summer than in other seasons, and it is also related to the weather conditions.

### 5.3.3 Cases study of the BESS and PV based SECP

The second power management method is chosen to observe the behaviour of the system. The details of the BESS are listed in Table. 5.8, where other information is same as in Table. 4.3.

The results are shown in Figure. 5.8, where the first three subplots show the total EV power demand ( $P_{EV}$ ), grid power ( $P_{Grid}$ ), and PV power  $P_{PV}$ . The last two subplots show the BESS power ( $P_{BESS}$ ) and the SoC of BESS power ( $SoC_{BESS}$ ) respectively. In the PV power subplot, the blue line represents the maximum PV power the system can generate, the PV2EV line (the orange line) is the power sent from the PV to the EVs, and the PV2BESS line (the yellow line) represents the PV power transferred to the BESS, the power sold to grid are not shown since the results focus on the power flow in the SECP.

Four representative time points were chosen to refer to PV states (grey lines) with the data shown in Table 5.9. At the first charging point (600 minutes),  $P_{PV}$  is 10.86kW, which is lower than the total EV power demand, hence, all PV power is transferred to the EVs, therefore, PV2EV is 10.86kW and PV2BESS is 0kW. The rest of the power is supported by the local power feeder of 77.6kW, and  $SoC_{BESS}$  is 0%, therefore, the BESS has no energy to export,  $P_{EV}$  is 88.46kW which is  $P_{PV}$  plus  $P_{Grid}$ . For the second time point (794 minutes),  $P_{EV}$  (5kW) is smaller than  $P_{PV}$  (23.72kW), and PV2EV is then set to 5kW. Meanwhile,  $SoC_{BESS}$  is only 31.12%, and the BESS is not fully charged, part of the PV power is transferred to the BESS, and PV2BESS (18.72kW) is  $P_{PV}$  minus PV2EV. The power from the feeder is also sent to the BESS, so  $P_{BESS}$  (96.32kW) is PV2BESS plus  $P_{Grid}$  (77.6kW). For the third point (853 minutes), there is no power demand from the EVs, and BESS is not fully charged, hence, all power from the PV and the feeder are injected to  $P_{BESS}$  (92.28kW), which is equal to  $P_{Grid}$  (77.6kW) plus  $P_{PV}$  (14.68kW). For the last time point (895 minutes), although the maximum PV power generation is 9.108kW, there is no power demand in the SECP system, hence, the PV receives command to output power to grid.

Overall, from Figure. 5.8 we can see that the power from the PV is utilized

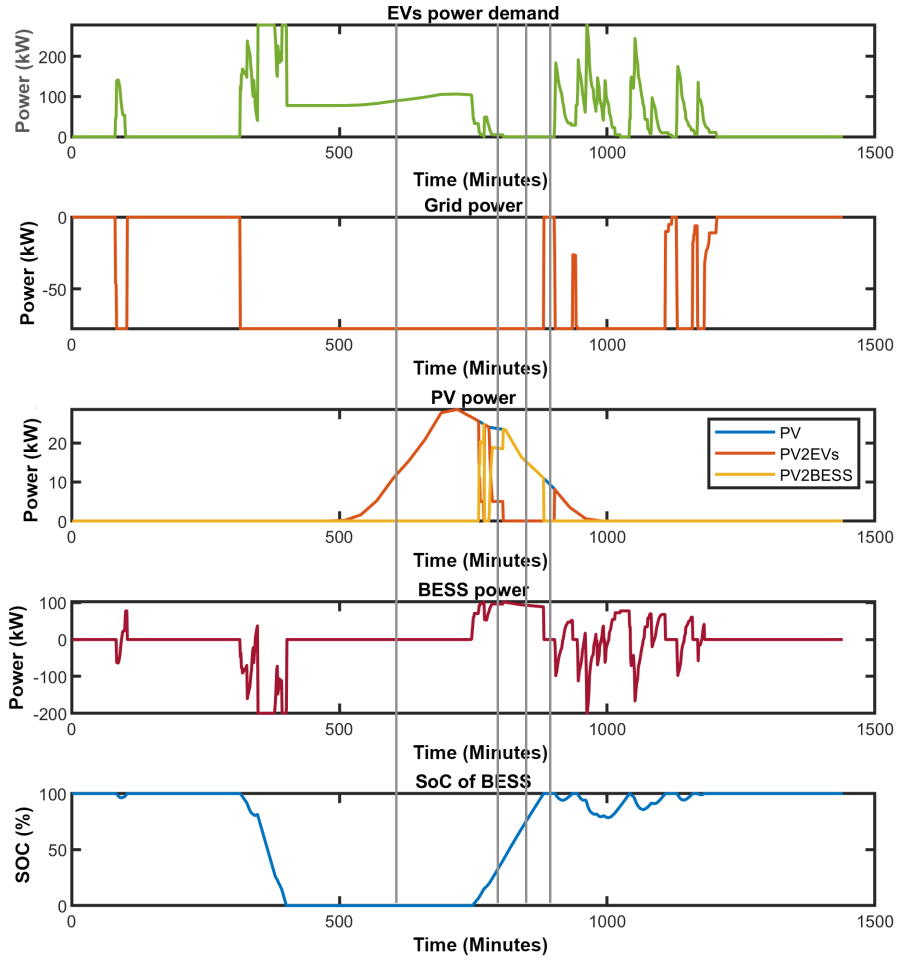


Figure 5.8: The response of PV-BESS based SECP to the various EV load

Table 5.9: Data points as shown in Figure. 5.8

Time (Min)	$P_{EV}(kW)$	$P_{Grid}(kW)$	$P_{PV}(kW)$	$P_{PV2EV}(kW)$	$P_{PV2BESS}(kW)$	$P_{BESS}(kW)$	$SoC_{BESS} (%)$
600	88.46	-77.6	10.86	10.86	0	0	0
794	5	-77.6	23.72	5	18.72	96.32	31.12
853	0	-77.6	14.68	0	14.68	92.28	78.57
895	0	0	9.108	0	0	0	100

efficiently for the SECP system in the whole working period. Only from 882 minutes to 901 minutes, the BESS and EVs are fully charged, and the PV power is exported to the grid. The average increasing SoC of the EVs is 32.56kW which is higher than it would be without the PV, meanwhile PV-BESS based SECP requests less energy from the power feeder than BESS based SECP by comparing the grid power from Figure. 5.8 and Figure. 5.3. Also  $SoC_{BESS}$  in the PV-BESS based system reminds at 100% for longer period.

### 5.3.4 Sensitivity analysis of power feeder limit and the capacity of BESS based on the case study with PV integrated

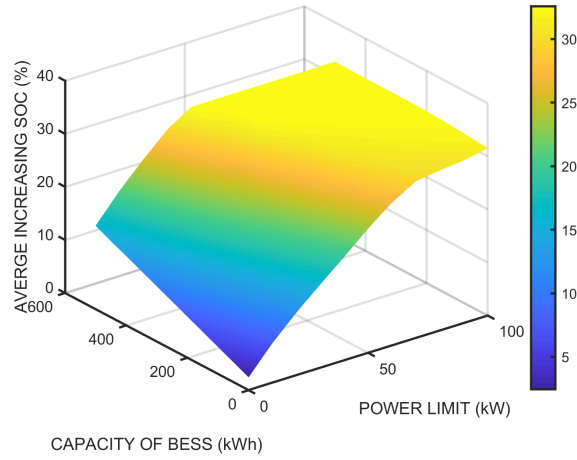
In this subsection, various power feeder limits and capacities of the BESS are employed to analyse how the average increasing SoC is affected by the PV and the BESS. The PV power usage for the SECP system is bonded with the capacity of the BESS, since the BESS can improve the utilisation rate of the PV for the SECP system by storing the energy generated from the PV and exporting this energy when needed. Meanwhile, the collaboration between the PV and the BESS can improve the average increasing SoC when the power limit is at a low level. Two test days are picked from two seasons shown in Figure. 5.7, since the PV behaviour has a huge difference between the two seasons. The outputs of the sensitivity analysis are the average increasing SoC ( $SoC_a$ ), and the PV energy utilization for the SECP system ( $E_{PV}$ ) in kWh. The PV energy utilization for the SECP system does not include the power exported to the grid. This investigation could assist SECP owners to schedule the investment to seek the cost balance of infrastructures of the power feeder and the BESS and the PV to get higher customer satisfaction. The simulation parameters of the sensitivity analysis are introduced in Table. 5.10. From Figure. 5.4, we see that the different methods have limited impact on the average increasing SoC than the BESS, adding the PV could further reduce this impact, hence Method 2 is chosen as the only power management method for the rest research. The other parameters are

Table 5.10: The parameters of PV-BESS based SECP for sensitivity analysis

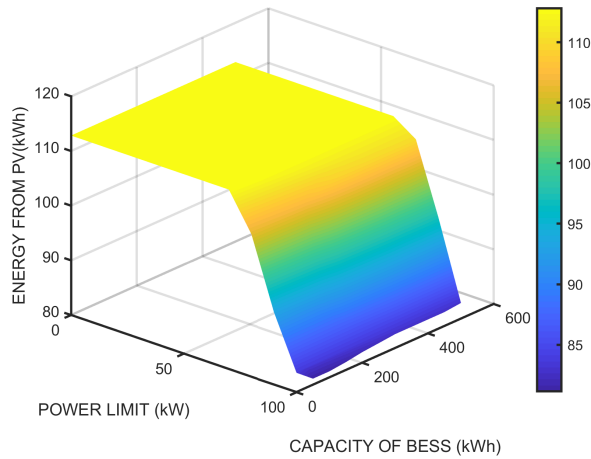
Parameters	Details
Power feeder limit	0-100kW
Capacity of BESS	0-500kW
Initial SoC of BESS	100%
Power management method	Method 2
Simulation date	01/01/2019&01/07/2019

the same as in Table. 4.3.

The results on 01/01/2019 are shown in the Figure. 5.9a and Figure. 5.9b which show the average increasing SoC and PV energy utilization for SECP system, respectively. For better observation, some of the data points are picked and shown in Table. 5.11 and Table. 5.12. The results on 01/07/2019 are shown in Figure. 5.10a and Figure. 5.10b with certain data points shown in Table. 5.13 and Table. 5.14. The capacities of BESS are increased from 0 to 500kWh with 100kWh increments and the power limits are selected from 0kW to 100kW with 20kW increments. Comparing with Figure. 5.4, Figure. 5.9a and Figure. 5.10a and their data profiles, we can see that as the PV power generation increases, the slopes of the three figures get steeper, the average increasing SoC could exceed 30kW with a 100kW power limit without PV power; or with an 80kW power limit and the PV energy generated on 01/01/2019; or with only a 60kW power limit and the PV energy generated on 01/07/2019. Meanwhile, based on Figure. 5.9b and Table. 5.13, the maximum PV energy utilization for the SECP system is 112.82kWh for most situations when the power limit is lower than 80kW. Increasing the 80kW power limit causes the PV energy usage for the SECP to decrease sharply, however, for the same power limit, as the capacity of the BESS rises, the PV energy utilization for the SECP increases slightly. According to Figure. 5.10b and Table. 5.14, the maximum PV energy utilization for the SECP is 650.42kWh, however, as the power limit increases, the PV energy utilization for the SECP decreases gradually from 0kW to 20kW power limit, and the decrease becomes sharp from 20kW to 100kW power limit.



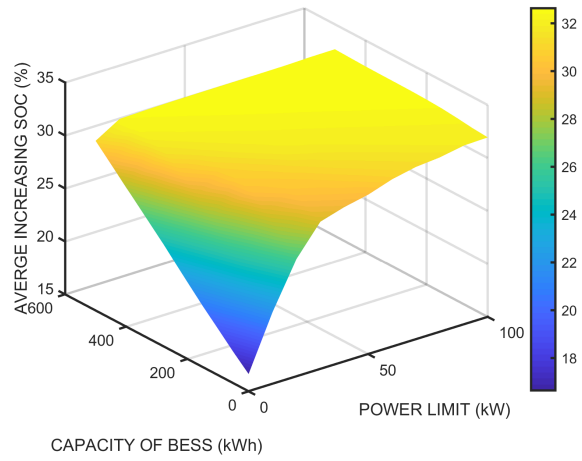
(a) Average increasing SoC



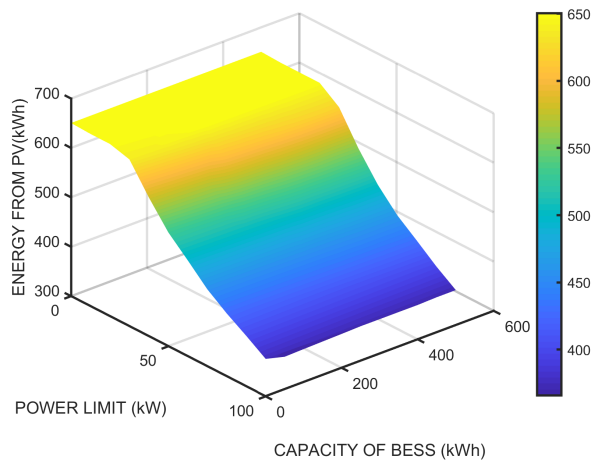
(b) PV energy

Figure 5.9: Sensitivity analysis result of SECP with BESS and PV on 01/01/2019.

Comparing the results of the two dates, we find that PV energy utilization for the SECP system on 01/07/2019 is higher than on 01/01/2019, while the increasing power limit has more negative impact on the PV energy utilization for the SECP. Along with the power limit increases from 0kW to 100kW, the PV energy utilization for the SECP drops by almost 45% on 01/07/2019, and 25% on 01/01/2019.



(a) Average increasing SoC



(b) PV energy

Figure 5.10: Sensitivity analysis result of SECP with BESS and PV on 01/07/2019.

Table 5.11: Sensitivity analysis result: average increasing SoC on 01/01/2019

$SoC_a$ (%) \ $P_L$ (kW)	0	20	40	60	80	100
$E_{cBESS}$ (kWh)						
0	4.02	11.83	19.52	26.94	30.18	31.52
100	5.23	14.36	22.29	29.13	31.27	32.08
200	7.92	16.82	25.16	31.20	32.14	32.41
300	10.58	19.53	27.54	31.99	32.44	32.51
400	13.10	22.41	30.17	32.47	32.52	32.53
500	15.73	25.45	32.49	32.52	32.54	32.59

Table 5.12: Sensitivity analysis result: PV energy utilization on 01/01/2019

$E_{PV}$ (kWh) \ $P_L$ (kW)	0	20	40	60	80	100
$E_{cBESS}$ (kWh)						
0	112.82	112.82	112.82	112.82	106.08	83.55
100	112.82	112.82	112.82	112.82	104.85	81.13
200	112.82	112.82	112.82	112.82	108.30	81.96
300	112.82	112.82	112.82	112.82	109.63	82.57
400	112.82	112.82	112.82	112.82	109.81	82.57
500	112.82	112.82	112.82	112.82	109.99	82.88

Table 5.13: Sensitivity analysis result: average increasing SoC on 01/07/2019

$SoC_a$ (%) \ $P_L$ (kW)	0	20	40	60	80	100
$E_{cBESS}$ (kWh)						
0	16.64	26.08	29.58	30.81	31.47	31.95
100	19.38	28.92	30.63	31.53	32.00	32.24
200	22.26	30.64	31.75	32.04	32.32	32.46
300	25.32	31.55	32.12	32.37	32.48	32.52
400	28.12	32.19	32.42	32.50	32.53	32.55
500	31.02	32.45	32.51	32.53	32.56	32.64

Table 5.14: Sensitivity analysis result: PV energy utilization on 01/07/2019

$E_{PV}$ (kWh) \ $P_L$ (kW)	0	20	40	60	80	100
$E_{cBESS}$ (kWh)						
0	650.42	648.55	580.75	493.99	427.27	375.81
100	650.42	648.57	580.20	483.95	421.66	366.86
200	650.42	648.57	604.89	493.29	426.47	368.74
300	650.42	648.57	611.01	500.24	429.02	369.82
400	650.42	648.57	618.12	501.53	429.02	369.72
500	650.42	648.57	619.50	502.51	430.32	370.94

## 5.4 Conclusion

In this chapter, the BESS and the PV are introduced with both being able to significantly increase the average increasing SoC of EVs. Through a sensitivity analysis we find that compared with BESS size, the power feeder limit has more impact on the PV energy utilization for the SECP. The PV energy utilization for SECP only includes the charging energy for EVs and the BESS, and does not include the energy exported to the grid. It is shown that the PV energy utilization for SECP can be as low as 55%. This is because a larger power feeder limit can provide the higher charging rates required for the EVs, hence the EVs could be fully charged over a shorter duration. This reduces the time window for PV power to charge the EVs and reduces the energy requirement from the BESS leaving it a higher SoC and therefore limited capacity left for storing PV energy, the surplus energy from the PV is then exported to the grid. Increasing the BESS size can improve the PV energy utilization for the SECP as the BESS can store more energy from the PV to prevent the PV energy from being exported to the grid. Hence, improving the PV energy utilization for the SECP and reducing the power demand from the grid could be done by choosing a suitable power limit and capacity of the BESS.

# Chapter 6

## SECP for providing ancillary grid services

### 6.1 Introduction

The previous chapters have proposed solutions to manage the power requirements for EV charging in a SECP through power management methods and the integration of PV and BESS. In this chapter, the investigation focuses on exploring ancillary grid services which the PV-BESS based SECP can provide to gain additional revenue and support the grid.

The grid frequency is not stable, it is determined and controlled by total demand and generation; when demand is higher than the generation, the frequency falls and vice versa. National Grid Electricity System Operator (NGESO), the ESO for GB, has the responsibility of maintaining the frequency of the National Electricity Transmission System within 1% of 50Hz (49.5 to 50.5Hz). Dynamic Fast Frequency Response (DFFR) and Dynamic Containment (DC) services are two grid balancing services offered to generators by NGESO, aiming to overcome the unbalanced grid frequency [78]. The NGESO pays for the DFFR/DC service based on the working period and the available power for frequency response, for example, in March 2021, an average price of £11.2/MW of DFFR/h was paid to service providers based on the post-tender report from [77].

Future car parks will require significant power to support EV charging as there will be both an increase in the penetration of EVs and a higher demand for charging power as battery packs increase in capacity. Effective management of the charging and local battery storage can be installed to help avoid excessive increases in electrical feeder capacity, however, it is inevitable that car parks will attain significant power capability in the future. There is an opportunity therefore for car park owners to utilise this and generate additional revenue by providing frequency response services to the electrical grid. This chapter describes the modelling of a SECP that utilises PV power generation, BESS and EV charging management strategies to provide a grid frequency response service.

Research about EV charging parks and grid frequency response do not consider ancillary service specifications and restrictions enforced by the national ESO. In contrast to other works in this field, a PV-BESS based SECP is introduced in this chapter to provide SEC and the DFFR/DC service. Meanwhile, a novel bi-directional electricity transfer method among EV, Grid, PV, and BESS are presented to construct an SEC system. In the DFFR/DC service, grid frequency is categorized into high-frequency zone (HFZ), dead-band, and Low-frequency zone (LFZ), for each of them, the SECP has the corresponding energy flow strategies. The advantage of the SECP is not only reducing the impact of the increasing penetration of EV chargers on the grid, but also helping the SECP owners to profit from providing the grid service in addition to collecting EV charging fees.

## 6.2 DFFR and DC modelling

Any storage system that provides DFFR must provide a power response as frequency deviates from  $50 \pm 0.015$  Hz. Figure. 6.1 shows the envelope of this response, from the figure, 49.985Hz and 50.015Hz are two trigger points that divide the grid frequency into three zones. The HFZ represents the grid frequency when it is higher than 50.015Hz where the storage system imports electricity from the grid, DFFR power is defined as negative. The LFZ occurs when grid frequency is lower than 49.985Hz, the storage system exports

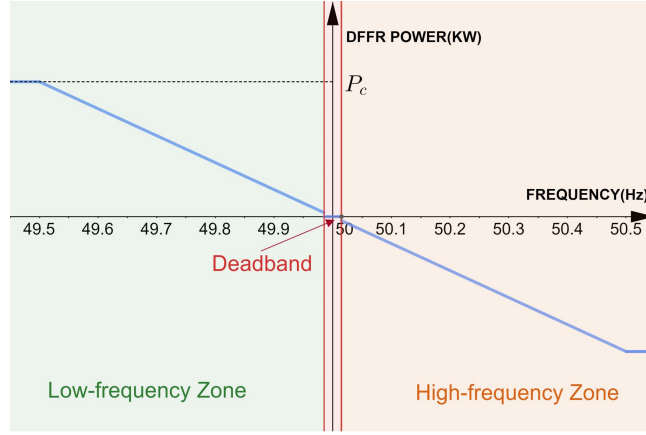


Figure 6.1: DFFR droop curve for a provider (blue line)

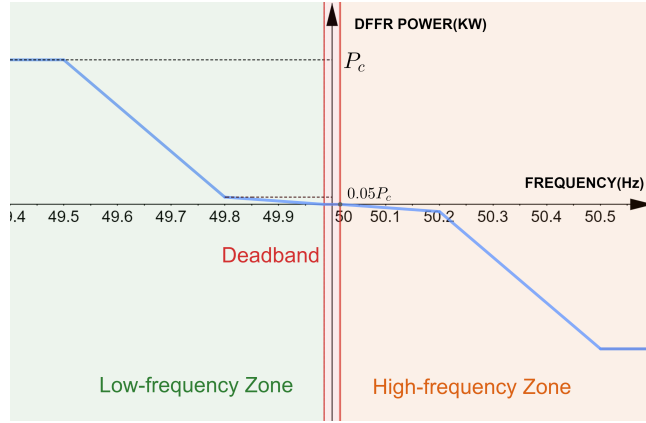


Figure 6.2: DC droop curve for a provider (blue line)

electricity to the grid, DFFR power is defined as positive. The deadband is when the grid frequency is between the 49.985Hz and the 50.015Hz, DFFR power remains at zero. DFFR requires the provider to deliver a minimum of 1MW response power and must sell in 1MW increments for maintaining the grid frequency within 49.5Hz to 50.5Hz, the response power that the provider has tendered is called contracted power ( $P_c$ ). The actual power required by DFFR based on the grid frequency ( $P_{AFR}$ ) is given as:

$$P_{AFR} = -\frac{P_c}{50.5 - 50} * (F(t) - 50)$$

$$50.5 > F(t) > 50.015 \text{ or } 49.5 < F(t) < 49.985 \quad (6.1)$$

$$P_{AFR} = 0 \quad 50.015 \leq F(t) \leq 49.985 \quad (6.2)$$

$$P_{AFR} = -P_c \quad F(t) \geq 50.5 \quad (6.3)$$

$$P_{AFR} = P_c \quad F(t) \leq 49.5 \quad (6.4)$$

where  $F(t)$  is the real-time grid frequency. Positive/Negative  $P_{AFR}$  means providers export/import electricity to/from the grid. The deadband is defined as where the provider must not import or export any power.

Similar to DFFR, but DC further divides the HFZ and LFZ into two parts by knee points (49.8Hz and 50.2Hz) as shown in Figure. 6.2. The actual power required by DC based on the grid frequency ( $P_{ADC}$ ) is given as:

$$P_{ADC} = \left(\frac{19}{6} * (50 - F(t)) - \frac{7}{12}\right) * P_c \quad 49.8 > F(t) > 49.5 \quad (6.5)$$

$$P_{ADC} = \left(\frac{19}{6} * (50 - F(t)) + \frac{7}{12}\right) * P_c \quad 50.5 > F(t) > 50.2 \quad (6.6)$$

$$P_{ADC} = \left(\frac{10}{37} * (50 - F(t)) - \frac{3}{740}\right) * P_c \quad 49.985 > F(t) \geq 49.8 \quad (6.7)$$

$$P_{ADC} = \left(\frac{10}{37} * (50 - F(t)) + \frac{3}{740}\right) * P_c \quad 50.2 \geq F(t) > 50.015 \quad (6.8)$$

$$P_{ADC} = 0 \quad 50.015 \leq F(t) \leq 49.985 \quad (6.9)$$

$$P_{ADC} = -P_c \quad F(t) \geq 50.5 \quad (6.10)$$

$$P_{ADC} = P_c \quad F(t) \leq 49.5 \quad (6.11)$$

Compared with DFFR, DC significantly reduces the response power for the same  $P_c$  between the two knee points, and the response power increases/decreases dramatically from the knee points to  $P_c$ , DFFR curve maintains steady increases/decreases from the trigger points to  $P_c$ . According to the historical grid frequency data provided by NGESO, the grid frequency remains in between the two knees points in most situations, which means DC is less demanding on the capacity of storage facilities for the same  $P_c$  as the response power is less.

SECP can be considered a complex energy storage system that includes many energy storage units represented by the EV batteries and a BESS. These can be used to export/import electricity from the grid and provide

frequency response services. Once SECPs get certification from NGENSO, SECPs can generate additional revenue through the provision of frequency response services in addition to the parking and charging revenue.

In a SECP, exporting electricity from EVs to provide grid services may lead to a lower SoC on departure than the SoC expected by the EV owner. The average daily energy consumption of all annual mileage of EVs is calculated as  $6.72kWh$  based on Table 3.1, In order to ensure EVs have enough energy to support costumers' daily driving, the minimum SoC of EV battery ( $SoC_{min}$ ) can be calculated by:

$$SoC_{min} = \frac{6.72}{E_{cev}} \quad (6.12)$$

For a Nissan Leaf 24kWh, Nissan Leaf 30kWh, BMWi3 33kWh, and Volkswagen Golf 26kWh, the minimum SoC is calculated as 28%, 22.4%, 20.4%, 25.9% respectively. This means if the SoC of an EV is lower than the minimum SoC, the EV will not be discharged for grid service or other activities in the SECP.

The power from the SECP might not always meet  $P_{AFR}$ , failure happens when the PV, EVs, and BESS cannot absorb/support the contracted power for DFFR/DC. DFFR/DC availability ( $AVA$ ) is used to evaluate the quality of the delivered DFFR/DC service:

$$AVA = \frac{T_Z - T_F}{T_Z} * 100\% \quad (6.13)$$

$T_F$  is the period when failure occurs, and  $T_Z$  is the period of DFFR/DC. Taking an example of 100 minutes charging, with three minutes of failed service, the availability is calculated as 97%.

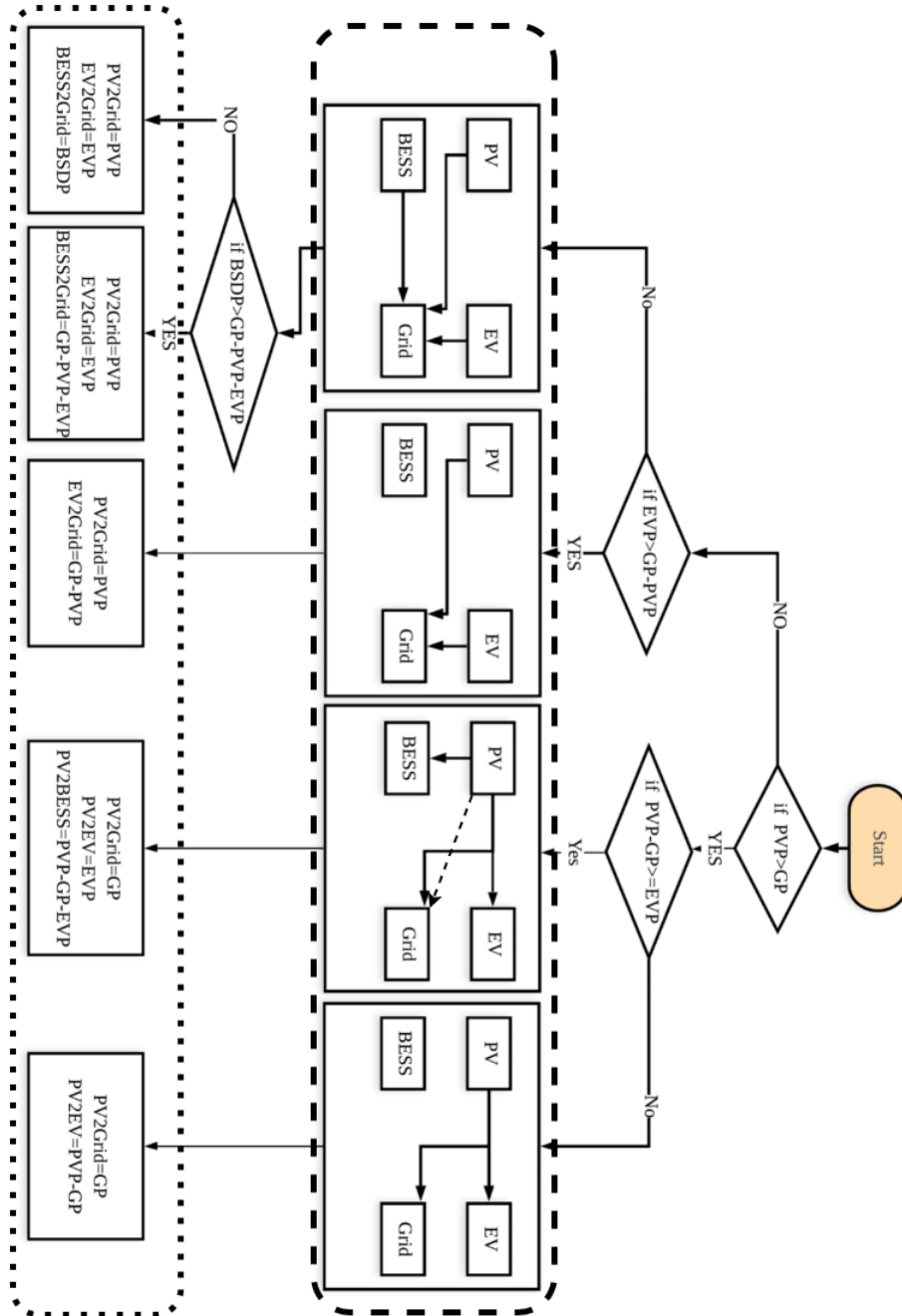


Figure 6.3: The energy flow in the LFZ

## 6.3 Energy flow between the system components

The energy flow in this section is considered for two grid-service scenarios, the DFFR/DC period and the Non-DFFR/DC period. The SECP provides the DFFR/DC service in the DFFR/DC period and non-delivery of the service in the Non-DFFR/DC period. It is possible in the GB electricity market to bid to deliver the DFFR/DC service in timed windows.

In the HFZ, the SECP must import power to support the grid, the energy flow with respect to power from the grid (GP), EVs (EVP) and PV (PVP) is detailed in Figure. 5.6 and has been explained in Chapter 5. The PV is still taken as a priority to charge EVs and the BESS. However, unlike the PV introduced in Chapter 5 where the PV is always on since the PV energy is allowed to be exported back to grid anytime, the PV might be switched off when SECP is in the HFZ of the DFFR/DC service, and EVs and the BESS can not fully store all the energy generated by the PV. This is because providers are strictly required to follow the contracted import/export power envelope. For example, even if there is excess PV power available to be exported, if the service envelope dictates that the ‘asset’ should be importing (HFZ) then no PV power can be exported to grid. The export of PV to the grid, therefore, has to be managed during service provision and cannot simply be equal to the surplus energy in the system. Whilst there may be opportunity to install additional physical metering for surplus PV the regulatory requirements for this scenario, considering the system described in this thesis, are not well defined and is therefore not considered here.

In the LFZ, SECP must export power, in this case, the PV is prioritised to export power to the grid, then the remaining will power the EVs, any further excess power will charge the BESS. As with the HFZ case, any further PV surplus is not considered as it is not possible to export more than the contracted envelope to the grid. EVs are the second priority power source for exporting power when PVP is less than GP. If there is still not enough power, BESS is the last priority power source for LFZ. The service is failed when the total exported power capability cannot meet the contracted power

demand. Figure. 6.3 shows the details of how the system operates for LFZ.

SECP working in the deadband region results in that the only power sources for EV charging are the BESS and PV, and the PV is the priority power source. The excess PV power will be used to charge the BESS, any further excess power will sell to the grid through an addition meter and cables. If both sources cannot supply the required EV charging power, then the EV charging power will be reduced through power management Method 2.

Based on an analysis of past tenders, 11pm to 7am the next day, and 7am to 11pm are commonly tendered periods for DFFR/DC delivery. As there are almost no EVs parking during the overnight period (based on the collected car park data) an SECP is not advantageous overnight (compared to a standalone battery) as EVs cannot support the DFFR service as energy storage units. Therefore the DFFR/DC delivery period is set between 7 am to 11 pm, at other times, the grid connection can be used without restriction as it is not delivering the DFFR/DC service. This is therefore used to manage the SoC of the BESS in preparation for the next day (initial SoC of BESS) since it could help to reduce the BESS size and improve the DFFR/DC service quality. The details about the importance of controlling the SoC of the BESS overnight is discussed below.

In the non-DFFR/DC service period the PV is on all the time and primarily transfers energy to EVs, with a second priority to charge the BESS for the next day (initial SoC of BESS). If the PV cannot provide enough power to the EVs, the GP will support the rest, if there is surplus power generated by PV, this power is export back to the grid as the SECP is not following a contracted power envelope. This non-DFFR/DC period happens from 11pm to 7am the next day, therefore, with PVP being close to zero and most EVs having exited or fully charged, the charge power curve is likely to remain flat, meanwhile, BESS will be charged or discharged to a defined initial SoC of BESS.

Table 6.1: The main parameters of the simulation

Parameters	Details
Traffic Flow	Hainault Station (London)
EV brands	4
$C_m$	80
Simulation date	01/01/2019
Capacity of PV panel	$175Wp/m^2$
Capacity of BESS	2MWh
Initial SoC of BESS	60%
$P_c$	1MW
Simulation time	1 day
$T_Z$	7am to 11pm

## 6.4 DFFR results

This section first tests the SECP aggregated with PV-BESS providing DFFR services to see if the SECP can provide DFFR whilst maintaining the charging of EVs. A real-time charging scenario is provided, Table 6.1 shows the main parameters of the simulation. Here we simulate the model with the lowest tenderable power unit of 1MW; The battery's capacity is set as 2MWh and the simulation period is one day.

The results are shown in Figure. 6.4, the first of five figures show the grid frequency ( $f_G$ ), then the grid power ( $P_{Grid}$ ), negative corresponds to SECP importing energy from the feeder, positive is exporting, the third represents the generated PV power ( $P_{pv}$ ). The last two figures are EVs power demand ( $P_{EV}$ ) and BESS power demand ( $P_{BESS}$ ) respectively, a positive value represents EVs or the BESS charging, and discharging for a negative value. The two red lines represent the trigger points (49.985Hz and 50.015Hz) in the grid frequency graph; four time-points are chosen to refer to the four charging periods (grey lines) with the data shown in Table 6.2. At the first charging point (333 minutes), the system is operating in the non-DFFR period,  $P_{EV}$  is 142kW, and 0kW is from the PV, the rest is from the grid, the BESS is not charging at this period. The second charging point (555 minutes) is in the HFZ, the grid at 50.13Hz demands imported power of 253kW to SECP

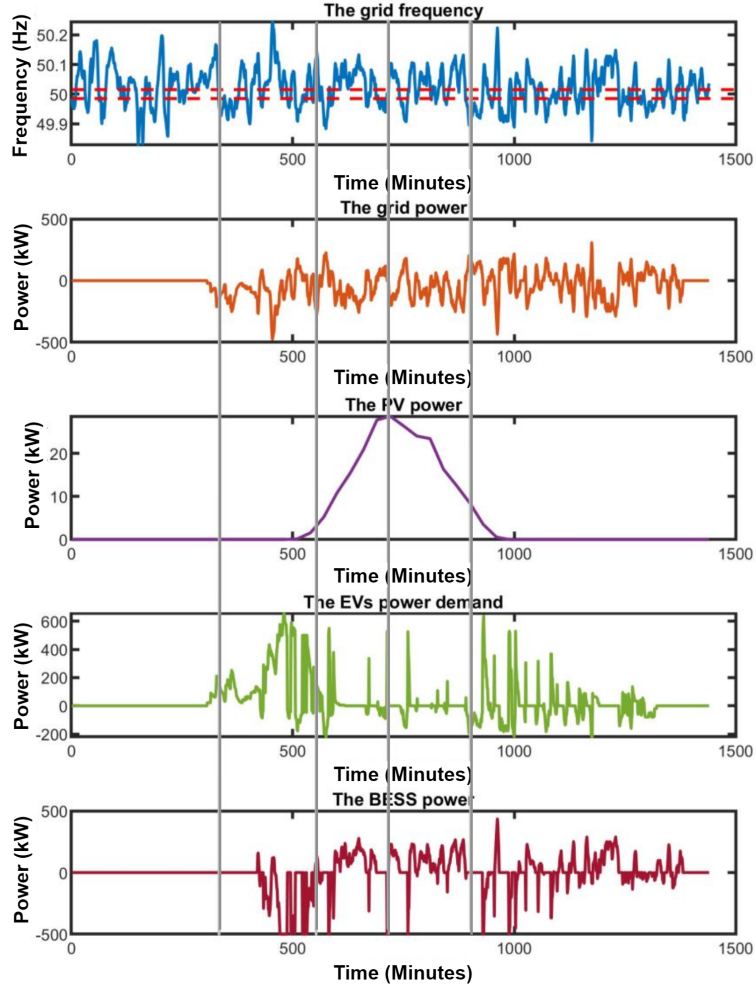
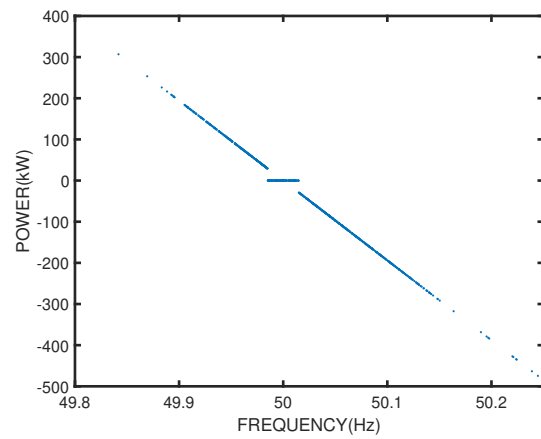


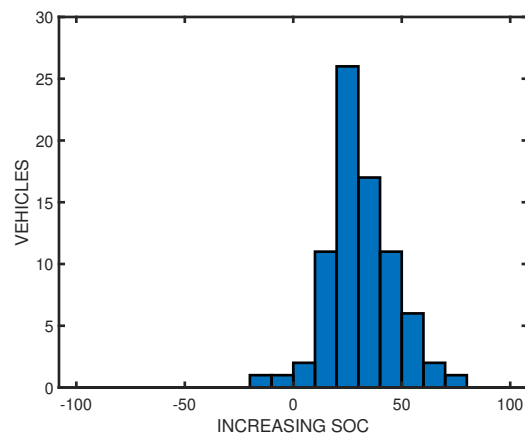
Figure 6.4: System response for DFFR - one day simulation  
Table 6.2: Data points as shown in Figure. 6.4

Time (Min)	$f_G(Hz)$	$P_{Grid}(kW)$	$P_{pv}(kW)$	$P_{EV}(kW)$	$P_{BESS}(kW)$
333	49.97	-142	0	142	0
555	50.13	-253	3.398	134.6	121.8
713	50	0	28.39	528.4	-500
898	49.89	203.7	8.701	-195	0

based on Equation. 6.1, and 3.398kW is generated by the PV, however, at this moment the maximum charging power of all EVs is 134.6kW, so  $P_{pv}$  and 131.2kW of  $P_{Grid}$  is used to support the EV charging, the rest of  $P_{Grid}$



(a) DFFR result showing power vs frequency



(b) Distribution of increase in SoC for EVs

Figure 6.5: Key DFFR operating behaviours during a day

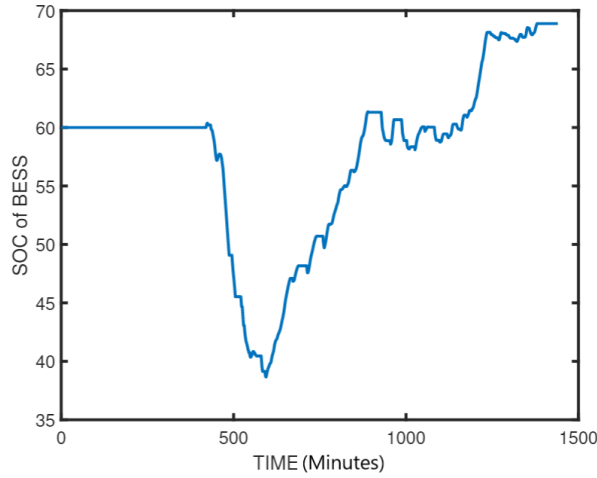


Figure 6.6: The SoC of the BESS for one day DFFR simulation

is allocated to the BESS. The third charging point is during the deadband zone, the system providing the DFFR cannot import or export power from the grid, the demand power from the grid is 0kW,  $P_{pv}$  (28.39kW) and  $P_{BESS}$  (-500kW) is used for EV charging. At the last point, the system is working in the LFZ, depending on Equation. 6.1,  $P_{Grid}$  is 203.7kW, which is from the PV (8.701kW) and the EVs (-195kW). Figure. 6.5a is the DFFR power response, Figure. 6.5b represents the value of increasing SoC referring to the number of EVs,  $AVA$  is 100%. The SoC of BESS is shown in Figure. 6.6. The above results show the PV-BESS integrated SECP can provide a good DFFR service with 100%  $AVA$  and an acceptable EV charging service.

The capacity of the BESS and initial SoC of BESS are variables in the model which can be subjected to a sensitivity analysis. Here are the results based on the traffic flow at Hainault Station (London) to understand the impact of different BESS capacities and the initial SoC of BESS, Table 6.3 shows the main parameters of the simulation. The capacity of BESS are varied in increments of 300kWh starting from 500kWh to 2000kWh.

Table 6.4, Table 6.5, and Table 6.6 are the results of 25%, 50%, and 75% initial SoC of BESS, along with the increasing capacity of BESS, the availability of DFFR, and average increasing SoC of EVs increase with capacity as expected. Compared with the summer season, the average increasing SoC

Table 6.3: The main parameters of the sensitivity analysis for simulating DFFR and DC

Parameters	Details
Traffic Flow	Hainault Station (London)
EV brands	4
$C_m$	80
Simulation date	Summer season (01/07/2019-07/07/2019) Winter season (01/01/2019-07/01/2019)
Capacity of PV panel	$175Wp/m^2$
Capacity of BESS	2MWh
$P_c$	1MW
Simulation time	7 days
$T_Z$	7am to 11pm

is always lower in winter regardless of how the capacity of BESS changes. The higher initial SoC of BESS causes lower availability in the summer. The availability is 100% when the capacity of the BESS is 2000kWh with 25% initial SoC in summer, and 99.48% when the capacity of BESS is 2000kWh with 50% initial SoC in winter, both of them achieve the acceptable average increasing SoC (29.54% and 28.65% in order).

Combined with the energy flow from Figure. 5.6 and Figure. 6.3, the lower average increasing SoC in winter can be explained with the following reasons:

- In the summer season, PV in this season can provide high amounts of energy to support EVs.
- In the winter season, without too much PV power, the total EV energy demand is mainly supplied by the grid and the BESS, but the BESS might store very limited energy from the PV.
- EVs must supply energy to the grid to provide a high availability of service.

The same is observed in winter, the BESS with a 75% initial SoC can provide more energy to EVs than at 25%, hence the average increasing SoC

Table 6.4: Analysis with 25% initial SoC of BESS for DFFR

Capacity of BESS (kWh)	Winter (01/01-07/01)		Summer (01/07-07/07)	
	Availability (%)	Average increasing SoC of EVs (%)	Availability (%)	Average increasing SoC of EVs (%)
500	93.03	12.90	88.90	27.60
800	96.14	15.20	94.17	28.86
1100	97.40	17.24	96.77	29.37
1400	97.50	19.30	97.96	29.48
1700	97.55	21.34	99.32	29.52
2000	97.98	23.12	100	29.54

Table 6.5: Analysis with 50% initial SoC of BESS for DFFR

Capacity of BESS (kWh)	Winter (01/01-07/01)		Summer (01/07-07/07)	
	Availability (%)	Average increasing SoC of EVs (%)	Availability (%)	Average increasing SoC of EVs (%)
500	92.48	16.39	86.75	29.06
800	94.93	20.64	91.38	29.40
1100	97.16	23.97	94.32	29.47
1400	99.05	25.81	96.18	29.51
1700	99.38	27.25	97.10	29.52
2000	99.48	28.65	97.83	29.53

Table 6.6: Analysis with 75% initial SoC of BESS for DFFR

Capacity of BESS (kWh)	Winter (01/01-07/01)		Summer (01/07-07/07)	
	Availability (%)	Average increasing SoC of EVs (%)	Availability (%)	Average increasing SoC of EVs (%)
500	90.99	19.76	84.39	29.13
800	95.26	24.51	87.66	29.40
1100	96.41	26.88	89.46	29.47
1400	97.49	28.58	91.13	29.51
1700	97.89	28.67	92.09	29.52
2000	98.31	28.72	93.49	29.53

of EVs at 75% is higher. The average increasing SoC in summer is very close with different initial SoC values of the BESS since EVs have been fully charged with the available PV power.

The reason the availability decreases in the summer with a higher initial SoC is that sufficient PV power has almost fully charged the BESS and supported the EV charging every day, there is no capacity left in the system to import energy from the grid in the HFZ. This result is based on 100% PV utilisation whereas it would be possible to curtail this power if required.

The results reveal that for different seasons, adjusting suitable initial SoC of battery helps reduce the capacity of the BESS, hence reducing the initial cost associated with the capacity of the BESS. A 2MWh BESS, with a 50% initial SoC in winter and 25% initial SoC in summer is a good choice for the parameters of this SECP providing DFFR service, this conclusion is based on the condition that the SECP manages the SoC of BESS every day.

## 6.5 DC results

The same parameters of the DFFR simulation are used to analyse the DC service. The results are shown in Figure. 6.7, the two red lines still represent the trigger points (49.985Hz and 50.015Hz), the two green lines represent the knee points of DC, the working principle are the same with DFFR, only two time-points are chosen, one is outside the knee points (454 minutes), and the other is between the knee points (649 minutes). The data is listed in Table 6.7, At the first charging point (454 minutes), the grid frequency is 50.24Hz, the imported power is 185.6kW based on Equation. 6.6, the power from the grid and the BESS (170kW) are both used to support EV charging (355.6kW). The second charging point (649 minutes) is still in the HFZ, the imported power is 30.92kW based on Equation. 6.8. The power from the grid and the PV are used to charge the BESS since there is no power demand from the EVs.

Figure. 6.8a shows the DC power response, frequency is not outside the two knee points in LFZ for the simulation period, *AVA* is 100%., Figure. 6.8b represents the value of increasing SoC of the EVs. The SoC of the BESS is

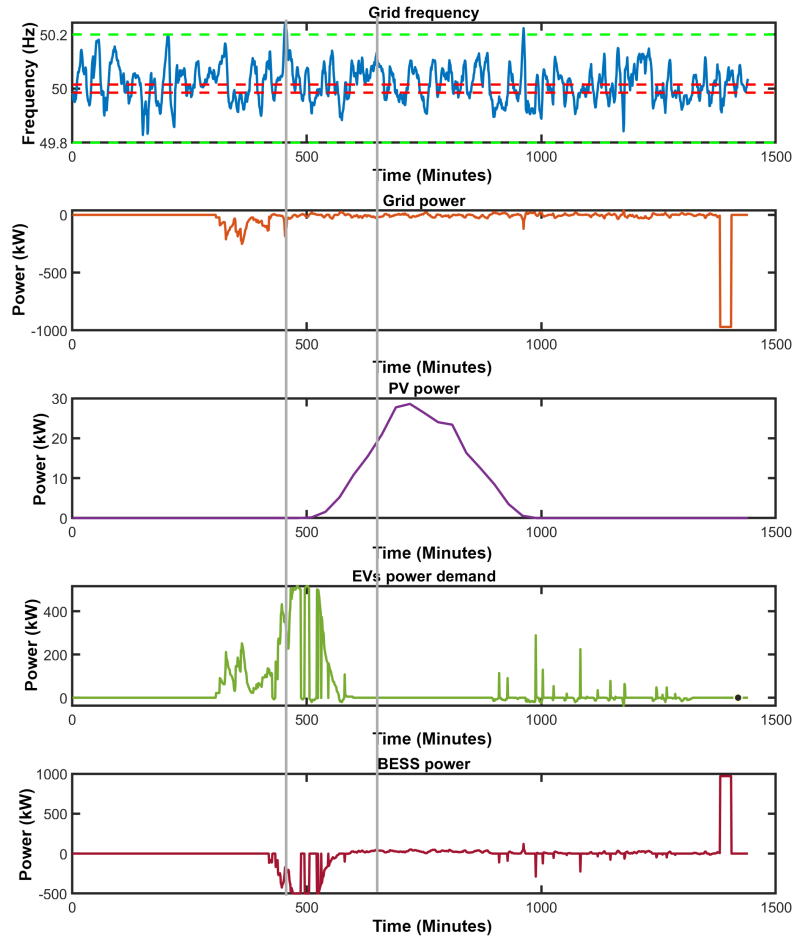
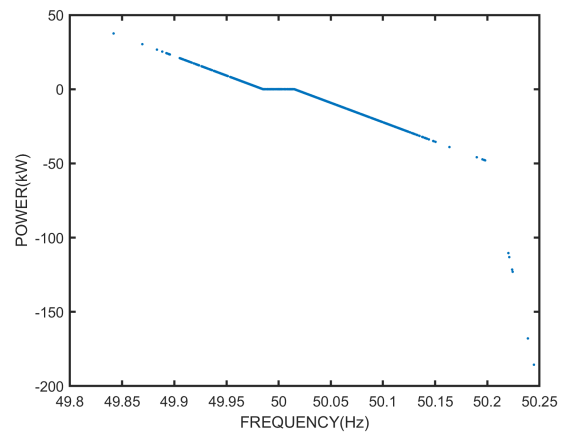


Figure 6.7: System response for DC - one day simulation

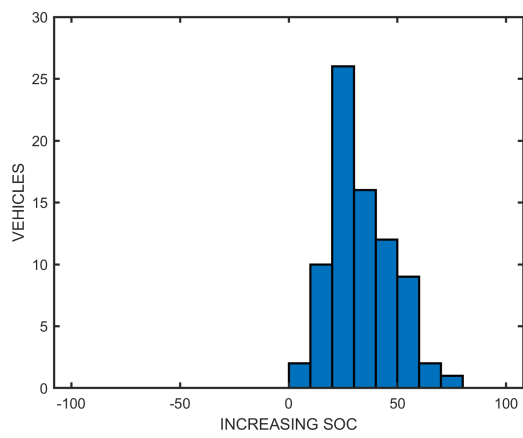
Table 6.7: Data points as shown in Figure. 6.7

Time (Min)	$f_G(Hz)$	$P_{Grid}(kW)$	$P_{pv}(kW)$	$P_{EV}(kW)$	$P_{BESS}(kW)$
454	50.24	-185.6	0	355.6	-170
649	50.13	-30.92	18.92	0	49.84

shown in Figure. 6.9, DC reduces the response power compared with DFFR in the frequency range between the two knee points, hence, the system might require more energy from the BESS to charge the EVs. The above results



(a) DC result showing power vs frequency



(b) Distribution of increase in SoC for EVs

Figure 6.8: Key DC operating behaviours during a day

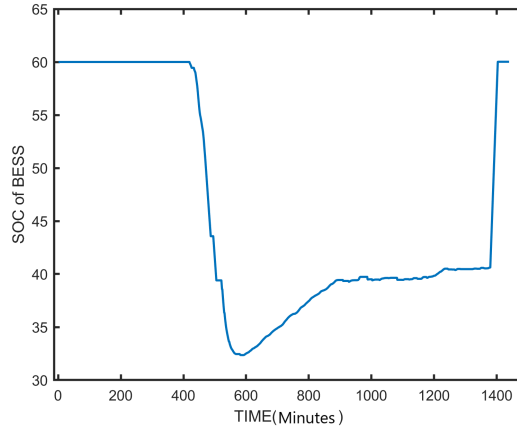


Figure 6.9: The SoC of BESS for one day DC simulation

Table 6.8: Analysis with 25% initial SoC of BESS for DC

Capacity of BESS (kWh)	Winter (01/01-07/01)		Summer (01/07-07/07)	
	Availability (%)	Average increasing SoC of EVs (%)	Availability (%)	Average increasing SoC of EVs (%)
500	99.12	16.19	96.34	31.91
800	99.12	19.78	99.73	32.18
1100	99.15	23.27	100	32.37
1400	99.34	26.33	100	32.40
1700	99.36	28.35	100	32.41
2000	99.93	29.59	100	32.41

show the PV-BESS integrated SECP can provide a good DC service with 100% *AVA* and an acceptable EV charging service.

To analyse the impact of the capacity of the BESS and initial SoC of the BESS, a sensitivity analysis for DC is carried out using the same parameters as the DFFR analysis. Table 6.8, Table 6.9, and Table 6.10 shows the analysis results, overall, the trends are the same as with the DFFR service, where, as the capacity of the BESS and initial SoC of the BESS rises, the average increasing SoC increases; and the availability gradually increases proportionally with the capacity of the BESS. Compared with DFFR, DC can achieve 100% availability with only a 1100 kWh BESS and 25% initial

Table 6.9: Analysis with 50% initial SoC of BESS for DC

Capacity of BESS (kWh)	Winter (01/01-07/01)		Summer (01/07-07/07)	
	Availability (%)	Average increasing SoC of EVs (%)	Availability (%)	Average increasing SoC of EVs (%)
500	99.15	20.97	93.91	32.33
800	99.27	26.67	97.01	32.38
1100	99.38	29.66	99.20	32.39
1400	99.93	30.74	100	32.40
1700	99.93	31.33	100	32.41
2000	100	32.02	100	32.41

Table 6.10: Analysis with 75% initial SoC of BESS for DC

Capacity of BESS (kWh)	Winter (01/01-07/01)		Summer (01/07-07/07)	
	Availability (%)	Average increasing SoC of EVs (%)	Availability (%)	Average increasing SoC of EVs (%)
500	99.14	25.86	90.26	32.33
800	99.38	30.01	92.82	32.38
1100	99.93	31.33	94.43	32.39
1400	100	31.99	96.08	32.40
1700	100	32.01	97.41	32.41
2000	100	32.02	98.83	32.41

SoC in summer, and 1400 kWh with 75% target SoC of BESS in winter, meanwhile DC also achieves good average increasing SoC in the two conditions with 32.37% and 31.99% respectively. This can be explained in that DC has less requirement for response power between the two knee points and the frequency tends to remain in that range.

## **6.6 The Pareto front of availability vs average increasing SoC of EVs based on GA optimisation**

Most DFFR/DC tenders are made up of an availability fee (£/h). The terms of service impose a penalty of non-payment should the performance not meet a threshold for a given 30 minute period. The penalty is not only applied to the failed period but the entire tendered time-window. SECP owners should therefore aim to keep the system working at 100% availability during the entire operation. It has been shown already in this chapter that the capacity of the BESS and the initial SoC of BESS are important factors to achieve 100% availability, meanwhile SECP owners will also want to minimise the capacity of the BESS to reduce their capital investment. For example, both 1500kWh with 50% SoC and 1200kWh with 30% SoC could achieve 100% availability of DFFR, therefore considering investment costs, the SECP owner may choose a 1200kWh BESS. There is therefore a need to optimize the initial SoC of the BESS and its capacity. This section uses a GA to minimise the capacity of the BESS that could provide 100% availability whilst delivering the DFFR/DC services based on the ABM of a PV-BESS based SECP.

GAs are an excellent mathematical tool for searching for an optimal, or at least a suitable, solution among the space of all possible solutions. It is based on the process of biological evolution and mimics the Darwinian theory of survival of the fittest in nature. It is a population-based search method that employs the survival of the fittest principle. New populations are created by the repeated application of genetic operators to existing individuals in a population. The fundamental parts of a GA include population size, selec-

Table 6.11: GA settings for 100% availability

Parameter	Value
Generation	50
Population	20
Fitness Function	ABM of SECP
Input	Initial SoC of BESS & Capacity of BESS
Output	Availability & Capacity of BESS
Input Bounds	[0 100]-[0 2000]
Selection	Tournament (default)
Reproduction	0.8 (default)
Mutation	Constraint dependent (default)
Crossover function	Intermediate 1.0 (default)

Table 6.12: GA results for 100% availability

Service	Season	$C_{mBESS}$ (kWh)	$SoC_{BESSi}$ (%)
DFFR	Summer	1879.3	25.6
	Winter	1938.4	66.7
DC	Summer	644.9	1.7
	Winter	1041.6	88.9

tion, crossover, mutation, and fitness function [129, 130]. In this work, the capacity of the BESS and the initial SoC of BESS are selected by a GA using gamultiobj which is a Matlab optimization tool (the detail of gamultiobj is illustrated in [131]). The GA settings are presented in Table. 6.11. Note that the values of the generation and population are not unique and they are selected by the author's experience based on computation time and trial and error.

The minimum capacities of BESS ( $C_{mBESS}$ ) and corresponding initial SoC of BESS ( $SoC_{BESSi}$ ) for DFFR and DC in winter and summer to achieve 100% availability are shown in Table. 6.12,

If a SECP could not provide a BESS with the minimum capacity to achieve 100% availability, a high initial SoC of BESS could increase average increasing SoC, but less energy storage capacity remains for importing energy

from the grid, hence the availability will decrease. In this situation, the SECP owner has to decide what level of the initial SoC of BESS is a good balance for this system. There is no correct answer to the question of what the perfect initial SoC of BESS level is. The SECP owner has to choose it based on the availability that the local feeder could tolerate and user satisfaction for their increasing SoC. To make a choice, the changes in the availability and the capacity of BESS based on  $SoC_{BESSi}$  need to be plotted, however, plotting the whole range of solutions requires massive computational ability.

The multi-objective Pareto front is defined as a set of non-inferior solutions in the objective space defining a boundary beyond which none of the objectives can be improved without sacrificing at least one of the other objectives. Taking an example of the parameters of the SECP Figure. 6.10, a point from Parato front represents 97.32% availability and 31.74% average increasing SoC of EVs, if the system wants to increase availability to 98.94% by adjusting the  $SoC_{BESSi}$ , the average increasing SoC of EVs must be 31.14%, which is lower than 31.74%.

The Pareto front can be plotted using gamultiobj from the Matlab optimization tool. A 500kWh BESS is employed to observe the Pareto front since the SECP with a 500kWh BESS can never achieve 100% availability for proving DC service. The GA parameters are shown in the Table. 6.13. Note that these are the same as with the GA in Table. 6.11 where the values of the generation and population are not unique and selected by the author's experience based on the computation time and trial and error. Figure. 6.10 and Figure. 6.11 show the Pareto fronts of SECP with a 500kWh BESS in summer and winter, respectively. The results are all negative since gamultiobj could only calculate the minimum value, hence we transfer the output functions to negative to get the maximum value. The points of them are shown in Table. 6.14 for summer and Table. 6.15 for winter.

## 6.7 Conclusion

In this chapter, the SECP is demonstrated to provide the DFFR and the DC grid frequency response services. The energy flow strategies for the different

Table 6.13: GA parameters for the Pareto front of a 500kW BESS for providing DC service

Parameter	Value
Generation	30
Population	10
Fitness Function	ABM of SECP
Input	Initial SoC of BESS
Output	Availability & Capacity of BESS
Input Bounds	0-100
Selection	Tournament (default)
Reproduction	0.8 (default)
Mutation	Constraint dependent (default)
Crossover function	Intermediate 1.0 (default)

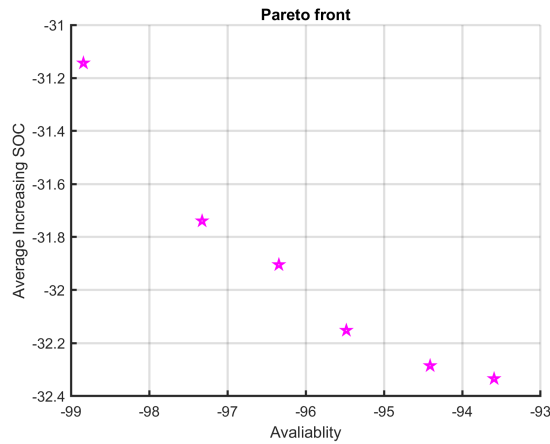


Figure 6.10: The Pareto fronts of SECP with a 500kW BESS in summer

frequency zones are developed and results show that 100% availability is achievable. By optimising the initial SoC of the BESS and the capacity of the BESS, it is possible to reduce the capital investment and achieve improved performance for both the average increasing SoC of EVs and the availability of the frequency response service.

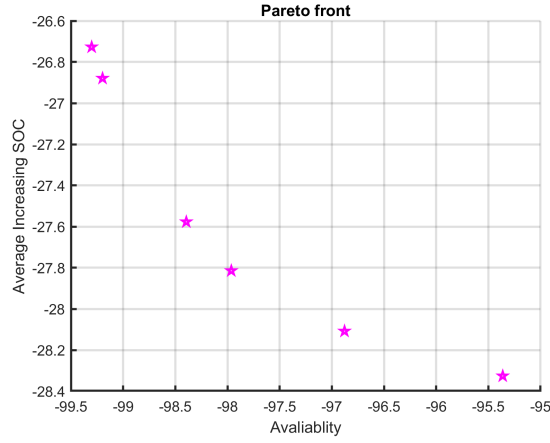


Figure 6.11: The Pareto fronts of SECP with a 500kW BESS in winter

Table 6.14: The points from Pareto fronts from summer simulation

$SoC_{BESSi}$	Availability (%)	Average Increasing SoC (%)
0.25	-98.94	-31.14
52.30	-93.59	-32.33
15.91	-97.32	-31.74
45.24	-94.41	-32.29
24.97	-96.34	-31.90
34.81	-95.48	-32.15

Table 6.15: The points from Pareto fronts from winter simulation

$SoC_{BESSi}$	Availability (%)	Average Increasing SoC (%)
80.99	-99.30	-26.73
87.44	-98.39	-27.58
93.50	-96.88	-28.11
90.13	-97.96	-27.81
97.44	-95.36	-28.33
81.99	-99.20	-26.88

# Chapter 7

## Conclusions & Further Work

### 7.1 Conclusions

This thesis presents the work carried out to analyse, design and evaluate the EV charging park. The results generated by this process have extended the existing state of knowledge in this area and have prompted proposals for methods by which some of these issues may be overcome. In addition, some work has considered how the different charging management methods and different power flows can be applied to EV car parks to provide ancillary grid services. Furthermore, the preliminary investigation of the BESS and its SoC in the SECP is introduced to improve the EV charging park behaviour for both EV charging and providing grid ancillary services.

The chapter 2 undertook a detailed review of the literature surrounding EVs, EV charging, and EV charging parks. The literature review highlighted that as more attention has focused on EVs by people and countries, EV sales and the number of EV charging facilities have increased significantly. With the improvement of EV batteries and EV charging infrastructure, EV charging power demand will definitely be a burden on the grid in the future and therefore smart EV charging is required and has recently been introduced in UK government policy.

In order to achieve smart EV charging for an EV charging park, which is also the aim of this thesis, the literature review investigates the previous

work on the EV charging load modelling, and the optimizations of EV car parks. Existing EV charging load modelling research includes queuing theory, Poisson process application, neural network and deep learning, Markov Chain and ABM. Most of the work is concentrated on estimating EV load by analysing the holistic data of the whole EV station, ignoring the load changes in a single EV, which makes further research on EV charging behaviour very difficult to carry out, hence ABM is the method for the load modelling in this thesis.

For the optimization of EV charging parks, EV charging is managed through the decentralized and centralized methods. The two methods mainly concentrate on the Valley filled by shifting EV charging to off peak period, thus reducing the EV load impact on the grid. However, shifting EV charging may affect customer satisfaction, since the SoC of some EVs can not meet the customer requirement. The PV and BESS based EV parks are introduced to achieve better charging satisfaction for customers and also reduce the power feeder requirement from the grid.

At the end of the literature review, we explore V2G services and use EV charging parks to provide frequency regulation services to the grid. We find that the current research does not well consider the frequency regulation from both grid perspective and EV owners perspective.

Together, this gives a clear direction to strands of the research: firstly, to build an EV load model of EV charging parks which allows us to analyse results from a single EV perspective as agents, secondly, to optimize the EV charging park with power management method by integrating PV and BESS in to this model, and further to explore the use of EV car parks to provide grid frequency response services.

The chapter 3 presents the modelling methodology and describes a detailed investigation into the parameters that determine the total EV power load of an SECP. The ABM approach is introduced with the agents such as the EVs, PV and BESS, having independent decisions based on a set of rules. The parameters and behaviours of the agents are described and source data introduced such as EV model parameters, methods to calculate the arrival initial SoC and charging power rates. EV charging periods are

also introduced and are based on the real-world traffic flow of a car park located in London by using PDFs and CDFs. With the model, the EV load can be calculated by summing the power demand of all EVs, where each EV power demand is independent and calculated by using the rules acquired by analyzing historical data. A sensitivity analysis using different penetrations of slow and fast charging is presented, where each simulation period is a week. The results reveal that the maximum total EV power load in the EV charging park can reach very high levels without a power management method, and that whilst increasing penetration of fast charging leads to high average increasing of SoC, this requires increasingly significant power feeder capacities.

The chapter 4 focuses on charging optimization to constrain the peak power requirements. First, three power management methods based on the different EV power demands and EV SoC are introduced. Different from methods introduced in the literature review, which directly stop the charging of EVs and coordinate new time slots to continue charging, the three methods presented here allocate the available power to all EVs using a sharing methodology. These methods extend the charging time, but each EV is always charging and whenever they leave, the SoC of that EV is always higher than on arrival. The first method allocates a power limit based on the power demand of each EV, the second and third allocate the power based on the SoC of the EV battery.

The evaluation parameter, average SoC variance, is employed to analyse if all the charging EVs are to charge to the same SoC. A smaller SoC variance means load sharing between EVs is more equal, and the system allocates more power to low SoC EVs. As the number of low SoC EVs decreases, if EVs are providing V2G service, more EVs are available to provide higher instantaneous power. Based on the evaluation parameter, a fourth method is introduced that can further reduce the SoC variance.

A sensitive analysis based on the model presented in Chapter 3 is undertaken to evaluate the four methods' behaviours on charging EVs. The input is the power limit from the local power feeder, the output is the average increasing SoC, and the result reveals that Method 1, 3 and 4 have higher

average increasing SoC for lower power limits, whereas Method 2 has better behaviour with higher power limits.

The methods presented in the chapter 4 are shown to successfully constrain the power requirements for the SECP, however, this results in undesirable small increases in SoC for some EVs. In chapter 5, the SECP is improved by integrating BESS and PV into the system to increase the available EV charging power and hence improve the charging behaviour.

The newly integrated BESS in the system stores energy and supplies it back when required, the aggregator collects information from all the system elements and controls the power flow based on the processed information. Based on the new structure, a cases study based on the provided ABM of SECP is analysed, and shows that a BESS could improve the utilization rate of a limited power feeder to increase peak powers available for EV charging. A sensitive analysis on the impact of different capacities of BESS and power feeder limits is carried out for the four proposed power management methods with a conclusion that for most methods, the increasing capacity of BESS could significantly increase the EVs SoC when the power feeder for the SECP is constrained.

PV is then introduced to the BESS based SECP to further improve the charging behaviour with a new PV and BESS based SECP structure. A PV model is integrated based on the UK PV historical data. A case study is presented based on the new structure of the ABM of SECP, results shows that PV power can be efficiently utilised for the SECP most of period. Compared with a BESS based SECP where the power feeder is always under full-power operation, a PV and BESS based SECP allows power feeder utilisation to be reduced offering the possibility to avoid costly on-peak periods. In order to observe the impact of the BESS, PV and the power feeder a sensitivity analysis is carried out. The results reveal that improving the PV energy utilization for the SECP and reducing the power demand from the grid could be done by choosing a suitable power limit and capacity of the BESS.

The previous chapters have already achieved a well-constructed EV charging system for a SECP. In the chapter 6, the research focuses on utilizing this SECP to provide ancillary grid services for additional revenue generation

and to support the grid. The EVs in the SECP can be considered as energy storage units which store energy from the grid and export it when the grid requires, this is also known as V2G technology. Different energy flow strategies are presented to enable a reliable service to be provided where both an availability of 100% is achieved whilst providing an acceptable EV charging service. Case studies are used to demonstrate the service delivery for both DFFR and DC with the impacts under different conditions being analysed. The results of the case studies show that the SECP can provide long-term stable and continuous DFFR and DC service by managing the power flows between the BESS and the PV, and using the charging power management methods presented previously.

An analysis investigating the impact of different seasons is conducted with capacity of BESS and initial SoC of BESS considered as variables. The results reveal that for different seasons, optimising the initial SoC of BESS enables a reduction in capacity of the BESS, hence reducing the capital cost of the BESS. Finally, a GA is proposed and demonstrated to show how it can be used by owners of an SECP to minimise the capacity of a BESS through optimising its SoC management. It is apparent from the results that the target values for the SoC management of the BESS would need to dynamically change throughout the year or perhaps consider weather conditions that would affect the solar irradiance.

This thesis presents the work carried out to analyse, design and evaluate the EV charging park. The results generated by this process have extended the existing state of knowledge in this area and have prompted proposals for methods by which some of these issues may be overcome. In addition, some work has considered how the different charging management methods and different power flows can be applied to EV car parks to provide ancillary grid services. Furthermore, the preliminary investigation of the BESS and its SoC in the SECP is introduced to improve the EV charging park behaviour for both EV charging and providing grid ancillary services.

Overall, this research introduces the question of how a SECP could transfer massive EVs charging power demand from a burden on the grid to the benefits for SECP owner, EV charging customers, and the grid. The benefits

include reducing the EV charging park investment in terms of power feed reinforcement, potential savings on costs passed onto EV charging customers, minimising the EVs charging power demand on the grid, and the ability to support the balancing of the grid through frequency response services. The simulation results demonstrate that the ABM of an SECP can calculate the EV load and provide a centralised command-based control structure for system power management. The four EV charging power management methods based on the ABM of SECP can flatten EV charging peak loads over longer time periods to minimise grid power local feeder requirements. A methodology of controlling the power flow and the integration with the suitable sizing of the BESS and PV, the SECP is shown to further reduce the power demand from the local feeder. Finally, the effective power flow strategies are presented that can enable a PV-BESS based SECP to achieve 100% availability for DC/DFFR services offered by NGENSO by optimizing the size of the BESS and its SoC management strategy.

## **7.2 Further Work**

### **7.2.1 Improvements of the ABM of SECP**

#### **7.2.1.1 SECP modelling**

The traffic flow data in this thesis is collected from a London car park located in a commercial area. More representative traffic flow could be collected from other areas, such as shopping centres, train stations, residential areas. For different areas, the results might be different. Meanwhile, more EV brands and relevant parameters could be uploaded to make the model more closer to real-world behaviour.

#### **7.2.1.2 Power management method**

In this thesis, the SECP did not give customers a chance to decide how urgent their EV charging requirements are, in reality, some EV users might want to pay more and get their EV charged with priority. By adjusting the

parameters in method 4 and developing relevant electricity fee strategies this would allow customers to choose their own charging preference. Collecting and analysing EV users preferences for this SECP can further improve fee strategies.

### **7.2.1.3 Other improvements**

This thesis has developed two grid frequency services, there are many grid services that require BESS, more grid services could be explored based on the SECP. This SECP only has a single floor, the PV canopy is over the car park spaces, hence the area of PV equals to the parking spaces. Future work could investigate multi-floor SECP, hence the PV power is different. This thesis mainly focuses on the exploration of the possibility of future development of SECP. Future work should introduce facilities cost and consider financial optimization.

## **7.2.2 Research on hardware aspects**

In the literature review, AC-connected system and DC-connected system are introduced on Figure. 2.7. The AC-connected system is employed as the power conversion system for the SECP where each EV charger and PV and BESS are equipped with a separate AC/DC conversion system. The AC-connected system has the advantages of availability and maturity for a power conversion technology, with protective devices, and well-established standards and practices for the AC power distribution systems [50]. However, compared with DC-connected system, the AC-connected system requires more conversion steps, and hence increases the system complexity, cost and decreases the system efficiency [50]. The DC-connected system reduces the conversion steps with only a DC/DC between the facilities, hence reducing the cost and the complexity, but the DC-connected system does not have well-established standards since most state of the art EV charging stations are AC-connected system. The future work could focus on developing a DC-connected system, it should also include the DC protection [132, 133] and DC metering.

### **7.2.3 A remote centralized management system for multi-locations EV charging**

The power management system between the PV, the BESS and EVs in this thesis is developed for a single SECP, however, the separated chargers are distributed everywhere, such as in residents' homes or on the side of the road. A remote centralized management system could be developed to control all EV chargers, renewable energy sources and available BESSs for an area such as a city to further reduce the impact of EV charging and improve the quality of grid services. The management system should have more efficient and closer communication with the grid. Meanwhile, nearby EV chargers could be collated into a subsystem with a sub-manager such as a SECP introduced in this thesis to create 'autonomous' virtual SECPs and reduce the amount of centralized communication that would otherwise be needed to process and improve the system reliability. More comprehensive EV charging habits need to be investigated, for example, people might prefer to charge their EVs in a public area at work or at their home while sleeping. The high-speed data transfer is also necessary since it might directly impact the response time of the grid services.

# References

- [1] “Trends and developments in electric vehicle markets.” Global EV Outlook 2021. [Online] <https://www.iea.org/reports/global-ev-outlook-2021/trends-and-developments-in-electric-vehicle-markets>.
- [2] “Deployment of vehicle-charging infrastructure.” Global EV Outlook 2021. [Online] <https://www.iea.org/reports/global-ev-outlook-2021/trends-and-developments-in-electric-vehicle-markets#deployment-of-vehicle-charging-infrastructure>.
- [3] Y. Wang and D. Infield, “Markov chain monte carlo simulation of electric vehicle use for network integration studies,” *International Journal of Electrical Power & Energy Systems*, vol. 99, pp. 85–94, 2018.
- [4] H. Das, M. Rahman, S. Li, and C. Tan, “Electric vehicles standards, charging infrastructure, and impact on grid integration: A technological review,” *Renewable and Sustainable Energy Reviews*, vol. 120, p. 109618, 2020.
- [5] “Bu-216: Summary table of lithium-based batteries.” BATTERY UNIVERSITY. [Online] <https://batteryuniversity.com/article/bu-216-summary-table-of-lithium-based-batteries>.
- [6] “Transport and technology: Public attitudes tracker.” Department for Transport. [Online] <https://assets.publishing.service.gov.uk/government/>

uploads/system/uploads/attachment\_data/file/803347/  
transport-and-transport-technology-public-attitudes-tracker-wave-3-report.  
pdf.

- [7] Y. Hori, “Future vehicle driven by electricity and control-research on four wheel motored” uot electric march ii”, in *7th International Workshop on Advanced Motion Control. Proceedings (Cat. No. 02TH8623)*, pp. 1–14, IEEE, 2002.
- [8] “Electric vehicle smart charging: government response.” Department for Transport, HM Government. *[Online]* <https://www.gov.uk/government/consultations/electric-vehicle-smart-charging>.
- [9] “Ev30@30 campaign.” Clean Energy Ministerial. *[Online]* [https://iea.blob.core.windows.net/assets/8cbeac6e-50e5-4a50-909c-24108adaf603/CampaignDocumentupdate\\_2020.pdf](https://iea.blob.core.windows.net/assets/8cbeac6e-50e5-4a50-909c-24108adaf603/CampaignDocumentupdate_2020.pdf).
- [10] “Electric vehicle charging device statistics october 2019.” Department for Transport. *[Online]* [https://assets.publishing.service.gov.uk/government/uploads/system/uploads/attachment\\_data/file/850417/electric-vehicle-charging-device-statistics-october-2019.pdf](https://assets.publishing.service.gov.uk/government/uploads/system/uploads/attachment_data/file/850417/electric-vehicle-charging-device-statistics-october-2019.pdf).
- [11] V. M. Iyer, S. Guler, G. Gohil, and S. Bhattacharya, “Extreme fast charging station architecture for electric vehicles with partial power processing,” in *2018 IEEE Applied Power Electronics Conference and Exposition (APEC)*, pp. 659–665, IEEE, 2018.
- [12] B. Chokkalingam, S. Padmanaban, P. Siano, R. Krishnamoorthy, and R. Selvaraj, “Real-time forecasting of ev charging station scheduling for smart energy systems,” *Energies*, vol. 10, no. 3, p. 377, 2017.
- [13] N. Kularatna, “Rechargeable battery technologies: An electronic engineer’s view point,” *Energy Storage Devices for Electronic Systems: Rechargeable Batteries and Supercapacitors*, Elsevier, pp. 29–61, 2014.

- [14] “How to measure state-of-charge.” Battery University. [Online] <https://batteryuniversity.com/article/bu-903-how-to-measure-state-of-charge>.
- [15] M. Charkhgard and M. Farrokhi, “State-of-charge estimation for lithium-ion batteries using neural networks and ekf,” *IEEE transactions on industrial electronics*, vol. 57, no. 12, pp. 4178–4187, 2010.
- [16] P. Shrivastava, T. K. Soon, M. Y. I. B. Idris, and S. Mekhilef, “Overview of model-based online state-of-charge estimation using kalman filter family for lithium-ion batteries,” *Renewable and Sustainable Energy Reviews*, vol. 113, p. 109233, 2019.
- [17] J. Peng, J. Luo, H. He, and B. Lu, “An improved state of charge estimation method based on cubature kalman filter for lithium-ion batteries,” *Applied energy*, vol. 253, p. 113520, 2019.
- [18] C. Chen, R. Xiong, R. Yang, W. Shen, and F. Sun, “State-of-charge estimation of lithium-ion battery using an improved neural network model and extended kalman filter,” *Journal of Cleaner Production*, vol. 234, pp. 1153–1164, 2019.
- [19] L. Kang, X. Zhao, and J. Ma, “A new neural network model for the state-of-charge estimation in the battery degradation process,” *Applied Energy*, vol. 121, pp. 20–27, 2014.
- [20] S. Tong, J. H. Lacap, and J. W. Park, “Battery state of charge estimation using a load-classifying neural network,” *Journal of Energy Storage*, vol. 7, pp. 236–243, 2016.
- [21] F. Yang, W. Li, C. Li, and Q. Miao, “State-of-charge estimation of lithium-ion batteries based on gated recurrent neural network,” *Energy*, vol. 175, pp. 66–75, 2019.
- [22] W. Zheng, B. Xia, W. Wang, Y. Lai, M. Wang, and H. Wang, “State of charge estimation for power lithium-ion battery using a fuzzy logic sliding mode observer,” *Energies*, vol. 12, no. 13, p. 2491, 2019.

- [23] C. Lin, A. Tang, and W. Wang, “A review of soh estimation methods in lithium-ion batteries for electric vehicle applications,” *Energy Procedia*, vol. 75, pp. 1920–1925, 2015.
- [24] M. H. Lipu, M. Hannan, A. Hussain, M. Hoque, P. J. Ker, M. M. Saad, and A. Ayob, “A review of state of health and remaining useful life estimation methods for lithium-ion battery in electric vehicles: Challenges and recommendations,” *Journal of cleaner production*, vol. 205, pp. 115–133, 2018.
- [25] K. B. Hatzell, A. Sharma, and H. K. Fathy, “A survey of long-term health modeling, estimation, and control of lithium-ion batteries: Challenges and opportunities,” in *2012 American Control Conference (ACC)*, pp. 584–591, IEEE, 2012.
- [26] P. A. Topan, M. N. Ramadan, G. Fathoni, A. I. Cahyadi, and O. Wahyunggoro, “State of charge (soc) and state of health (soh) estimation on lithium polymer battery via kalman filter,” in *2016 2nd International Conference on Science and Technology-Computer (ICST)*, pp. 93–96, IEEE, 2016.
- [27] N. A. Azis, E. Joelianto, and A. Widyotriatmo, “State of charge (soc) and state of health (soh) estimation of lithium-ion battery using dual extended kalman filter based on polynomial battery model,” in *2019 6th International Conference on Instrumentation, Control, and Automation (ICA)*, pp. 88–93, IEEE, 2019.
- [28] Y. Song, D. Liu, and Y. Peng, “Fpga-based implementation of lithium-ion battery soh estimator using particle filter,” in *2020 IEEE International Instrumentation and Measurement Technology Conference (I2MTC)*, pp. 1–6, IEEE, 2020.
- [29] J. Wei, G. Dong, and Z. Chen, “Remaining useful life prediction and state of health diagnosis for lithium-ion batteries using particle filter and support vector regression,” *IEEE Transactions on Industrial Electronics*, vol. 65, no. 7, pp. 5634–5643, 2017.

- [30] P. Singh, S. Kaneria, J. Broadhead, X. Wang, and J. Burdick, “Fuzzy logic estimation of soh of 125ah vrla batteries,” in *INTELEC 2004. 26th Annual International Telecommunications Energy Conference*, pp. 524–531, IEEE, 2004.
- [31] A. Zenati, P. Desprez, H. Razik, and S. Rael, “Impedance measurements combined with the fuzzy logic methodology to assess the soc and soh of lithium-ion cells,” in *2010 IEEE Vehicle Power and Propulsion Conference*, pp. 1–6, IEEE, 2010.
- [32] H.-T. Lin, T.-J. Liang, and S.-M. Chen, “Estimation of battery state of health using probabilistic neural network,” *IEEE transactions on industrial informatics*, vol. 9, no. 2, pp. 679–685, 2012.
- [33] D. Yang, Y. Wang, R. Pan, R. Chen, and Z. Chen, “A neural network based state-of-health estimation of lithium-ion battery in electric vehicles,” *Energy Procedia*, vol. 105, pp. 2059–2064, 2017.
- [34] S. Habib, M. M. Khan, F. Abbas, and H. Tang, “Assessment of electric vehicles concerning impacts, charging infrastructure with unidirectional and bidirectional chargers, and power flow comparisons,” *International Journal of Energy Research*, vol. 42, no. 11, pp. 3416–3441, 2018.
- [35] L. Solero, “Nonconventional on-board charger for electric vehicle propulsion batteries,” *IEEE Transactions on Vehicular Technology*, vol. 50, no. 1, pp. 144–149, 2001.
- [36] S. Habib, M. M. Khan, F. Abbas, and H. Tang, “Assessment of electric vehicles concerning impacts, charging infrastructure with unidirectional and bidirectional chargers, and power flow comparisons,” *International Journal of Energy Research*, vol. 42, no. 11, pp. 3416–3441, 2018.
- [37] B. Li, Q. Li, F. C. Lee, Z. Liu, and Y. Yang, “A high-efficiency high-density wide-bandgap device-based bidirectional on-board charger,”

*IEEE Journal of Emerging and Selected Topics in Power Electronics*, vol. 6, no. 3, pp. 1627–1636, 2018.

- [38] N. Wong and M. Kazerani, “A review of bidirectional on-board charger topologies for plugin vehicles,” in *2012 25th IEEE Canadian Conference on Electrical and Computer Engineering (CCECE)*, pp. 1–6, IEEE, 2012.
- [39] H. Li, L. Bai, Z. Zhang, S. Wang, J. Tang, X. Ren, and J. Li, “A 6.6 kw sic bidirectional on-board charger,” in *2018 IEEE Applied Power Electronics Conference and Exposition (APEC)*, pp. 1171–1178, IEEE, 2018.
- [40] R. K. Lenka, A. K. Panda, A. R. Dash, N. N. Venkataramana, and N. Tiwary, “Reactive power compensation using vehicle-to-grid enabled bidirectional off-board ev battery charger,” in *2021 1st International Conference on Power Electronics and Energy (ICPEE)*, pp. 1–6, IEEE, 2021.
- [41] V. Monteiro, J. C. Ferreira, A. A. N. Melendez, J. A. Afonso, C. Couto, and J. L. Afonso, “Experimental validation of a bidirectional three-level dc-dc converter for on-board or off-board ev battery chargers,” in *IECON 2019-45th Annual Conference of the IEEE Industrial Electronics Society*, vol. 1, pp. 3468–3473, IEEE, 2019.
- [42] “Porsche installs first 350-kw electric car charging station in berlin.” MOTORAUTHORITY. [Online] [https://www.motorauthority.com/news/1111866\\_porsche-installs-first-prototype-350-kw-electric-car-charging-station-in-berlin](https://www.motorauthority.com/news/1111866_porsche-installs-first-prototype-350-kw-electric-car-charging-station-in-berlin)
- [43] “Uk’s first 350kw ev charging station opens in kent.” Auto EXPRESS. [Online] <https://www.autoexpress.co.uk/car-news/101586/uk-s-first-350kw-ev-charging-station-opens-in-kent>.
- [44] “Fastcharge consortium presents prototype for 450 kw charging station; porsche research vehicle charges at 400 kw.” Green Car

- Congress. [Online] <https://www.greencarcongress.com/2018/12/20181213-fastcharge.html>.
- [45] “China and japan push for a global charging standard for evs.” IEEE Spectrum. [Online] <https://spectrum.ieee.org/a-global-charging-standard-for-evs>.
- [46] C. Botsford and A. Szczepanek, “Fast charging vs. slow charging: Pros and cons for the new age of electric vehicles,” in *International Battery Hybrid Fuel Cell Electric Vehicle Symposium*, pp. 1–9, Citeseer, 2009.
- [47] A. Tomaszewska, Z. Chu, X. Feng, S. O’Kane, X. Liu, J. Chen, C. Ji, E. Endler, R. Li, L. Liu, *et al.*, “Lithium-ion battery fast charging: A review,” *ETransportation*, vol. 1, p. 100011, 2019.
- [48] H. Tu, H. Feng, S. Srdic, and S. Lukic, “Extreme fast charging of electric vehicles: A technology overview,” *IEEE Transactions on Transportation Electrification*, vol. 5, no. 4, pp. 861–878, 2019.
- [49] R. Collin, Y. Miao, A. Yokochi, P. Enjeti, and A. Von Jouanne, “Advanced electric vehicle fast-charging technologies,” *Energies*, vol. 12, no. 10, p. 1839, 2019.
- [50] H. Tu, H. Feng, S. Srdic, and S. Lukic, “Extreme fast charging of electric vehicles: A technology overview,” *IEEE Transactions on Transportation Electrification*, vol. 5, no. 4, pp. 861–878, 2019.
- [51] B. Singh and R. Kushwaha, “A pfc based ev battery charger using a bridgeless isolated sepic converter,” *IEEE Transactions on Industry applications*, vol. 56, no. 1, pp. 477–487, 2019.
- [52] R. Kushwaha and B. Singh, “Power factor improvement in modified bridgeless landsman converter fed ev battery charger,” *IEEE transactions on Vehicular technology*, vol. 68, no. 4, pp. 3325–3336, 2019.
- [53] B. Singh and R. Kushwaha, “Ev battery charger with non-inverting output voltage-based bridgeless pfc cuk converter,” *IET Power Electronics*, vol. 12, no. 13, pp. 3359–3368, 2019.

- [54] C. Iclodean, B. Varga, N. Burnete, D. Cimerdean, and B. Jurchiş, “Comparison of different battery types for electric vehicles,” in *IOP conference series: materials science and engineering*, vol. 252, p. 012058, IOP Publishing, 2017.
- [55] M.-K. Tran, A. DaCosta, A. Mevawalla, S. Panchal, and M. Fowler, “Comparative study of equivalent circuit models performance in four common lithium-ion batteries: Lfp, nmc, lmo, nca,” *Batteries*, vol. 7, no. 3, p. 51, 2021.
- [56] “Nmc vs lfp – let’s talk about it..” SOLTARO. [Online] <https://soltaro.com/soltaro-batteries-news-archives/nmc-vs-lfp-advantages-disadvantages>.
- [57] “Solar photovoltaics deployment.” Department for Business, Energy Industrial Strategy, HM Government. [Online] <https://www.gov.uk/government/statistics/solar-photovoltaics-deployment>.
- [58] I. De la Parra, M. Muñoz, E. Lorenzo, M. García, J. Marcos, and F. Martínez-Moreno, “Pv performance modelling: A review in the light of quality assurance for large pv plants,” *Renewable and Sustainable Energy Reviews*, vol. 78, pp. 780–797, 2017.
- [59] K. Chaudhari, N. K. Kandasamy, A. Krishnan, A. Ukil, and H. B. Gooi, “Agent-based aggregated behavior modeling for electric vehicle charging load,” *IEEE Transactions on Industrial Informatics*, vol. 15, no. 2, pp. 856–868, 2018.
- [60] T. Gnann, S. Funke, N. Jakobsson, P. Plötz, F. Sprei, and A. Bennehag, “Fast charging infrastructure for electric vehicles: Today’s situation and future needs,” *Transportation Research Part D: Transport and Environment*, vol. 62, pp. 314–329, 2018.
- [61] “The potential impact of electric vehicles on global energy systems.” McKinseyCompany. [Online] <https://www.mckinsey.com/industries/automotive-and-assembly/our-insights/the-potential-impact-of-electric-vehicles-on-global-energy-systems>.

- [62] “Global ev outlook 2019.” IEA. [Online] <https://www.iea.org/reports/global-ev-outlook-2019>.
- [63] M. A. Awadallah, B. N. Singh, and B. Venkatesh, “Impact of ev charger load on distribution network capacity: A case study in toronto,” *Canadian Journal of Electrical and Computer Engineering*, vol. 39, no. 4, pp. 268–273, 2016.
- [64] A. D. Hilshey, P. Rezaei, P. D. Hines, and J. Frolik, “Electric vehicle charging: Transformer impacts and smart, decentralized solutions,” in *2012 IEEE Power and Energy Society General Meeting*, pp. 1–8, IEEE, 2012.
- [65] S. Panich and J. G. Singh, “Impact of plug-in electric vehicles on voltage unbalance in distribution systems,” *International journal of engineering, science and technology*, vol. 7, no. 3, pp. 76–93, 2015.
- [66] F. Shahnia, A. Ghosh, G. Ledwich, and F. Zare, “Predicting voltage unbalance impacts of plug-in electric vehicles penetration in residential low-voltage distribution networks,” *Electric Power Components and Systems*, vol. 41, no. 16, pp. 1594–1616, 2013.
- [67] T. Antić, T. Capuder, and M. Bolfek, “A comprehensive analysis of the voltage unbalance factor in pv and ev rich non-synthetic low voltage distribution networks,” *Energies*, vol. 14, no. 1, p. 117, 2021.
- [68] I. F II, “Ieee recommended practices and requirements for harmonic control in electrical power systems,” *New York, NY, USA*, pp. 1–1, 1993.
- [69] R. Bass, R. Harley, F. Lambert, V. Rajasekaran, and J. Pierce, “Residential harmonic loads and ev charging,” in *2001 IEEE Power Engineering Society Winter Meeting. Conference Proceedings (Cat. No. 01CH37194)*, vol. 2, pp. 803–808, IEEE, 2001.
- [70] S. Pirouzi, J. Aghaei, T. Niknam, H. Farahmand, and M. Korpås, “Proactive operation of electric vehicles in harmonic polluted smart

- distribution networks,” *IET Generation, Transmission & Distribution*, vol. 12, no. 4, pp. 967–975, 2018.
- [71] A. Ul-Haq, C. Cecati, A. Ehsan, and K. Strunz, “Impact of electric vehicles on voltage profile and harmonics in a distribution network,” in *2015 First Workshop on Smart Grid and Renewable Energy (SGRE)*, pp. 1–6, IEEE, 2015.
- [72] L. P. Fernandez, T. G. San Román, R. Cossent, C. M. Domingo, and P. Frias, “Assessment of the impact of plug-in electric vehicles on distribution networks,” *IEEE transactions on power systems*, vol. 26, no. 1, pp. 206–213, 2010.
- [73] C. Dharmakeerthi, N. Mithulananthan, and T. Saha, “Impact of electric vehicle fast charging on power system voltage stability,” *International Journal of Electrical Power & Energy Systems*, vol. 57, pp. 241–249, 2014.
- [74] Y. Xiang, S. Hu, Y. Liu, X. Zhang, and J. Liu, “Electric vehicles in smart grid: a survey on charging load modelling,” *IET Smart Grid*, vol. 2, no. 1, pp. 25–33, 2019.
- [75] J. Brownlee, “A gentle introduction to probability density estimation.” Machine Learning Mastery. [Online] <https://machinelearningmastery.com/probability-density-estimation/>.
- [76] J. S. Arora, “Chapter 20: Additional topics on optimum design,” 1989.
- [77] Y. Zhang, P. You, and L. Cai, “Optimal charging scheduling by pricing for ev charging station with dual charging modes,” *IEEE Transactions on Intelligent Transportation Systems*, vol. 20, no. 9, pp. 3386–3396, 2018.
- [78] M. Alizadeh, A. Scaglione, J. Davies, and K. S. Kurani, “A scalable stochastic model for the electricity demand of electric and plug-in hy-

- brid vehicles,” *IEEE Transactions on Smart Grid*, vol. 5, no. 2, pp. 848–860, 2014.
- [79] G. Li and X.-P. Zhang, “Modeling of plug-in hybrid electric vehicle charging demand in probabilistic power flow calculations,” *IEEE Transactions on Smart Grid*, vol. 3, no. 1, pp. 492–499, 2012.
- [80] X. Zhang, K. W. Chan, H. Li, H. Wang, J. Qiu, and G. Wang, “Deep-learning-based probabilistic forecasting of electric vehicle charging load with a novel queuing model,” *IEEE Transactions on Cybernetics*, vol. 51, no. 6, pp. 3157–3170, 2021.
- [81] F. Xie, M. Huang, W. Zhang, and J. Li, “Research on electric vehicle charging station load forecasting,” in *2011 International Conference on Advanced Power System Automation and Protection*, vol. 3, pp. 2055–2060, 2011.
- [82] J. Zhu, Z. Yang, M. Mourshed, Y. Guo, Y. Zhou, Y. Chang, Y. Wei, and S. Feng, “Electric vehicle charging load forecasting: A comparative study of deep learning approaches,” *Energies*, vol. 12, no. 14, p. 2692, 2019.
- [83] D. L. Marino, K. Amarasinghe, and M. Manic, “Building energy load forecasting using deep neural networks,” in *IECON 2016-42nd Annual Conference of the IEEE Industrial Electronics Society*, pp. 7046–7051, IEEE, 2016.
- [84] X. Wei, L. Lin, X. Yue, H. Yuan, and L. Yuanxi, “Optimal allocation for charging piles in multi-areas considering charging load forecasting based on markov chain,” in *2016 China International Conference on Electricity Distribution (CICED)*, pp. 1–7, IEEE, 2016.
- [85] P. Olivella-Rosell, R. Villafafila-Robles, A. Sumper, and J. Bergas-Jané, “Probabilistic agent-based model of electric vehicle charging demand to analyse the impact on distribution networks,” *Energies*, vol. 8, no. 5, pp. 4160–4187, 2015.

- [86] M. Liu, P. K. Phanivong, Y. Shi, and D. S. Callaway, “Decentralized charging control of electric vehicles in residential distribution networks,” *IEEE Transactions on Control Systems Technology*, vol. 27, no. 1, pp. 266–281, 2017.
- [87] Z. Yi, D. Scofield, J. Smart, A. Meintz, M. Jun, M. Mohanpurkar, and A. Medam, “A highly efficient control framework for centralized residential charging coordination of large electric vehicle populations,” *International Journal of Electrical Power & Energy Systems*, vol. 117, p. 105661, 2020.
- [88] N. Daina, A. Sivakumar, and J. W. Polak, “Electric vehicle charging choices: Modelling and implications for smart charging services,” *Transportation Research Part C: Emerging Technologies*, vol. 81, pp. 36–56, 2017.
- [89] M. Liu, P. K. Phanivong, Y. Shi, and D. S. Callaway, “Decentralized charging control of electric vehicles in residential distribution networks,” *IEEE Transactions on Control Systems Technology*, vol. 27, no. 1, pp. 266–281, 2017.
- [90] T.-H. Chang, A. Nedić, and A. Scaglione, “Distributed constrained optimization by consensus-based primal-dual perturbation method,” *IEEE Transactions on Automatic Control*, vol. 59, no. 6, pp. 1524–1538, 2014.
- [91] L. Zhang, V. Kekatos, and G. B. Giannakis, “Scalable electric vehicle charging protocols,” *IEEE Transactions on Power Systems*, vol. 32, no. 2, pp. 1451–1462, 2016.
- [92] K. Zhan, Z. Hu, Y. Song, N. Lu, Z. Xu, and L. Jia, “A probability transition matrix based decentralized electric vehicle charging method for load valley filling,” *Electric Power Systems Research*, vol. 125, pp. 1–7, 2015.

- [93] C.-K. Wen, J.-C. Chen, J.-H. Teng, and P. Ting, “Decentralized plug-in electric vehicle charging selection algorithm in power systems,” *IEEE Transactions on Smart Grid*, vol. 3, no. 4, pp. 1779–1789, 2012.
- [94] W. Zhang, D. Zhang, B. Mu, L. Y. Wang, Y. Bao, J. Jiang, H. Morais, *et al.*, “Decentralized electric vehicle charging strategies for reduced load variation and guaranteed charge completion in regional distribution grids,” *Energies*, vol. 10, no. 2, p. 147, 2017.
- [95] Z. Ma, D. Callaway, and I. Hiskens, “Decentralized charging control for large populations of plug-in electric vehicles: Application of the nash certainty equivalence principle,” in *2010 IEEE International Conference on Control Applications*, pp. 191–195, IEEE, 2010.
- [96] L. Gan, U. Topcu, and S. H. Low, “Optimal decentralized protocol for electric vehicle charging,” *IEEE Transactions on Power Systems*, vol. 28, no. 2, pp. 940–951, 2012.
- [97] J. Kang, S. J. Duncan, and D. N. Mavris, “Real-time scheduling techniques for electric vehicle charging in support of frequency regulation,” *Procedia Computer Science*, vol. 16, pp. 767–775, 2013.
- [98] H. Liu, Z. Hu, Y. Song, and J. Lin, “Decentralized vehicle-to-grid control for primary frequency regulation considering charging demands,” *IEEE Transactions on Power Systems*, vol. 28, no. 3, pp. 3480–3489, 2013.
- [99] L. Chen, Y. Jiang, X. Li, L. Yao, X. Xu, and T. Geng, “Frequency regulation strategy for decentralized v2g control,” in *2015 5th International Conference on Electric Utility Deregulation and Restructuring and Power Technologies (DRPT)*, pp. 2626–2629, IEEE, 2015.
- [100] M. Lempriere, “Leeds opens uk’s first solar-power park and ride.” SOLAR POWER PORTAL. *[Online]* [https://www.solarpowerportal.co.uk/news/leeds\\_opens\\_uks\\_first\\_solar\\_power\\_park\\_and\\_ride](https://www.solarpowerportal.co.uk/news/leeds_opens_uks_first_solar_power_park_and_ride).

- [101] A. J. Cheng, B. Tarroja, B. Shaffer, and S. Samuelsen, “Comparing the emissions benefits of centralized vs. decentralized electric vehicle smart charging approaches: A case study of the year 2030 california electric grid,” *Journal of Power Sources*, vol. 401, pp. 175–185, 2018.
- [102] L. Jian, X. Zhu, Z. Shao, S. Niu, and C. Chan, “A scenario of vehicle-to-grid implementation and its double-layer optimal charging strategy for minimizing load variance within regional smart grids,” *Energy conversion and management*, vol. 78, pp. 508–517, 2014.
- [103] Z. Yi, D. Scofield, J. Smart, A. Meintz, M. Jun, M. Mohanpurkar, and A. Medam, “A highly efficient control framework for centralized residential charging coordination of large electric vehicle populations,” *International Journal of Electrical Power & Energy Systems*, vol. 117, p. 105661, 2020.
- [104] Z. Wei, Y. Li, Y. Zhang, and L. Cai, “Intelligent parking garage ev charging scheduling considering battery charging characteristic,” *IEEE transactions on industrial electronics*, vol. 65, no. 3, pp. 2806–2816, 2017.
- [105] A. Khaksari, G. Tsaousoglou, P. Makris, K. Steriotis, N. Efthymiopoulos, and E. Varvarigos, “Sizing of electric vehicle charging stations with smart charging capabilities and quality of service requirements,” *Sustainable Cities and Society*, vol. 70, p. 102872, 2021.
- [106] R. Fachrizal and J. Munkhammar, “Improved photovoltaic self-consumption in residential buildings with distributed and centralized smart charging of electric vehicles,” *Energies*, vol. 13, no. 5, p. 1153, 2020.
- [107] K. Zhang, Y. Mao, S. Leng, Y. Zhang, S. Gjessing, and D. H. Tsang, “Platoon-based electric vehicles charging with renewable energy supply: A queuing analytical model,” in *2016 IEEE International Conference on Communications (ICC)*, pp. 1–6, IEEE, 2016.

- [108] Y. Zhang, J. He, and D. M. Ionel, “Modeling and control of a multiport converter based ev charging station with pv and battery,” in *2019 IEEE Transportation Electrification Conference and Expo (ITEC)*, pp. 1–5, IEEE, 2019.
- [109] K. Chaudhari, A. Ukil, K. N. Kumar, U. Manandhar, and S. K. Kollimalla, “Hybrid optimization for economic deployment of ess in pv-integrated ev charging stations,” *IEEE Transactions on Industrial Informatics*, vol. 14, no. 1, pp. 106–116, 2017.
- [110] P. Bastida-Molina, E. Hurtado-Pérez, M. C. M. Gómez, and C. Vargas-Salgado, “Multicriteria power generation planning and experimental verification of hybrid renewable energy systems for fast electric vehicle charging stations,” *Renewable Energy*, vol. 179, pp. 737–755, 2021.
- [111] D. B. Richardson, “Electric vehicles and the electric grid: A review of modeling approaches, impacts, and renewable energy integration,” *Renewable and Sustainable Energy Reviews*, vol. 19, pp. 247–254, 2013.
- [112] K. M. Tan, V. K. Ramachandaramurthy, and J. Y. Yong, “Integration of electric vehicles in smart grid: A review on vehicle to grid technologies and optimization techniques,” *Renewable and Sustainable Energy Reviews*, vol. 53, pp. 720–732, 2016.
- [113] K. Clement-Nyns, E. Haesen, and J. Driesen, “The impact of vehicle-to-grid on the distribution grid,” *Electric Power Systems Research*, vol. 81, no. 1, pp. 185–192, 2011.
- [114] L. Noel, G. Z. de Rubens, J. Kester, and B. K. Sovacool, “Beyond emissions and economics: Rethinking the co-benefits of electric vehicles (evs) and vehicle-to-grid (v2g),” *Transport Policy*, vol. 71, pp. 130–137, 2018.
- [115] S. B. Peterson, J. Whitacre, and J. Apt, “The economics of using plug-in hybrid electric vehicle battery packs for grid storage,” *Journal of Power Sources*, vol. 195, no. 8, pp. 2377–2384, 2010.

- [116] G. M. Freeman, T. E. Drennen, and A. D. White, “Can parked cars and carbon taxes create a profit? the economics of vehicle-to-grid energy storage for peak reduction,” *Energy Policy*, vol. 106, pp. 183–190, 2017.
- [117] M. Wang, Y. Mu, Q. Shi, H. Jia, and F. Li, “Electric vehicle aggregator modeling and control for frequency regulation considering progressive state recovery,” *IEEE Transactions on Smart Grid*, vol. 11, no. 5, pp. 4176–4189, 2020.
- [118] J. Meng, Y. Mu, H. Jia, J. Wu, X. Yu, and B. Qu, “Dynamic frequency response from electric vehicles considering travelling behavior in the great britain power system,” *Applied energy*, vol. 162, pp. 966–979, 2016.
- [119] A. Bampoulas and A. Karlis, “Provision of frequency regulation by a residential microgrid integrating pvs, energy storage and electric vehicle,” in *2017 IEEE International Conference on Environment and Electrical Engineering and 2017 IEEE Industrial and Commercial Power Systems Europe (EEEIC/I&CPS Europe)*, pp. 1–6, IEEE, 2017.
- [120] E. Bonabeau, “Agent-based modeling: Methods and techniques for simulating human systems,” *Proceedings of the national academy of sciences*, vol. 99, no. suppl 3, pp. 7280–7287, 2002.
- [121] “Vehicle licensing statistics:annual 2019.” Department for Transport. [Online] [https://assets.publishing.service.gov.uk/government/uploads/system/uploads/attachment\\_data/file/882196/vehicle-licensing-statistics-2019.pdf](https://assets.publishing.service.gov.uk/government/uploads/system/uploads/attachment_data/file/882196/vehicle-licensing-statistics-2019.pdf).
- [122] “Let’s look at fast charging curves for popular electric cars.” INSIDEEVs. [Online] <https://insideevs.com/news/338777/lets-look-at-fast-charging-curves-for-popular-electric-cars/>.
- [123] M. Kane, “Vw id.4 amazes with dc fast charging consistency.” INSIDEEVs. [Online] <https://insideevs.com/news/495561/volkswagen-id4-dc-fast-charging-consistency-amazes/>

?fbclid=IwAR3CT0UfIfyPJKUNB0tr\_IA20kcWog3CRtmyIkLLW7eDb\_7erymoz\_xKQU.

- [124] Y. Cao, S. Tang, C. Li, P. Zhang, Y. Tan, Z. Zhang, and J. Li, “An optimized ev charging model considering tou price and soc curve,” *IEEE Transactions on Smart Grid*, vol. 3, no. 1, pp. 388–393, 2011.
- [125] Y. Gao, J. Jiang, C. Zhang, W. Zhang, Z. Ma, and Y. Jiang, “Lithium-ion battery aging mechanisms and life model under different charging stresses,” *Journal of Power Sources*, vol. 356, pp. 103–114, 2017.
- [126] “Smart export guarantee (seg).” ofgem. [Online] <https://www.ofgem.gov.uk/environmental-and-social-schemes/smart-export-guarantee-seg>.
- [127] “How much electricity can i generate with solar panels?.” The eco experts. [Online] <https://www.theecoexperts.co.uk/solar-panels/how-much-electricity#:~:text=The%20standard%20solar%20panel%20has,150%2D200W%20in%20good%20sunlight>.
- [128] “Live pv generation.” National Grid ESO. [Online] <https://www.solar.sheffield.ac.uk/pvlive/>.
- [129] S. Sivanandam and S. Deepa, “Genetic algorithms,” in *Introduction to genetic algorithms*, pp. 15–37, Springer, 2008.
- [130] S. Katoch, S. S. Chauhan, and V. Kumar, “A review on genetic algorithm: past, present, and future,” *Multimedia Tools and Applications*, pp. 1–36, 2020.
- [131] “gamultiobj algorithm.” Mathworks. [Online] <https://uk.mathworks.com/help/gads/gamultiobj-algorithm.html#brjtxfv-1>.
- [132] D. Salomonsson, L. Soder, and A. Sannino, “Protection of low-voltage dc microgrids,” *IEEE Transactions on power delivery*, vol. 24, no. 3, pp. 1045–1053, 2009.

- [133] W. Javed and D. Chen, “Low voltage dc microgrid protection system- a review,” in *2018 53rd International Universities Power Engineering Conference (UPEC)*, pp. 1–6, IEEE, 2018.